A Hybrid Modeling Workflow for Performing Finite Element Analyses Under *In-Vivo* Conditions

Camille Chartrand

Thesis submitted to the University of Ottawa

in partial Fulfillment of the requirements for the

Master of Applied Science in Biomedical Engineering

Ottawa-Carleton Institute of Biomedical Engineering (OCIBME)

Faculty of Engineering

University of Ottawa

ABSTRACT

Computational models are commonly used to evaluate spinal loads due to difficulties associated with acquiring *in-vivo* measurements. Musculoskeletal (MSK) models can be used for performing simulations of movement by considering active structures such as muscles and simplified representations of joint structures. Finite element (FE) models are rather actuated with simplified loading conditions determined from *in vitro* studies and consider detailed representations of tissues and joint structures, making them suitable to evaluate stresses and strains within the spine. This work was done in collaboration with Numalogics Inc., where a hybrid modeling workflow was developed to combine MSK and FE modeling methods to be able to evaluate stresses and strains within spinal instrumentation devices under the influence of *in-vivo* loading conditions, i.e., muscle forces. A previously validated fully articulated thoracolumbar spine MSK model was selected, simplified, and replicated exactly in Ansys, the FE modeling platform. The sensitivity of the compressive joint loads to the modifications brought to the original model was evaluated for static flexion poses. Then, two hybrid simulation workflows were developed. Version I consisted of performing a static optimization analysis using the MSK model to calculate muscle forces that satisfy equilibrium constraints. Version II consisted of performing a stability-constrained static optimization analysis to calculate muscle forces and stiffnesses that satisfy equilibrium and stability constraints in the MSK model. The forces and moments calculated from the MSK model were then transferred to the FE model as loading conditions. Validation studies were performed for both simulation workflows by comparing the kinematics and compressive joint loads in the MSK and FE models under identical loading conditions, for various static flexion poses and for six scaled models. Version I could not be validated due to convergence issues and large discrepancies between model outputs. Version II was successfully validated, with negligible kinematic and joint load differences between models across different ranges of motion. Very strong to perfect correlations were observed between model kinematics and joint loads, respectively, over all simulations performed. Overall, it was found that the consideration of stability constraints is essential for successfully performing FE analyses of the entire thoracolumbar spine under *in-vivo* loading conditions over physiological ranges of motion. In this work, no soft tissue deformations nor stresses were evaluated with the FE model. However, with the developed workflow, Numalogics will be equipped with a framework for their future works,

including the comparison of stress distributions in spinal instrumentation devices when applying *in vitro* versus *in-vivo* loading conditions to their FE models.

ACKNOWLEDGEMENTS

I would like to express my gratitude to my supervisor, Dr. Ryan Graham, for giving me the opportunity to join his laboratory, for his continued support, and for providing me with all the resources that I needed to complete this research project. I would also like to thank my colleagues, members of the Movement Biomechanics and Analytics Laboratory, with a special regard to Dr. Mohammad Akhavanfar, for his time and guidance throughout the completion of this project. The knowledge and experience that he passed down to me was invaluable and I am forever grateful for the hours that he spent with me troubleshooting because of convergence issues or other modeling difficulties.

I would like to thank the members of the Numalogics team, Dr. Julien Clin, Dr. Franck LeNaveaux, Loïc Degueldre, and Pierre Legay, for collaborating with me in defining a project that aligned perfectly with my interests and for all their ongoing support. A special thank you goes to Loïc for his immense help in the progression of this project by automating the modeling workflow in Ansys.

I would also like to thank my thesis evaluation committee, Dr. Thomas Uchida and Dr. Eng Kuan Moo for their time spent reviewing my thesis and for their valuable comments. A special thanks to Dr. Uchida for introducing me to OpenSim and for providing support when needed.

Thank you to the University of Ottawa, the Ontario Graduate Scholarship (OGS), the Natural Sciences and Engineering Research Council of Canada (NSERC) and Mitacs for providing me with financial support throughout my graduate studies.

Finally, a very special and heartfelt thank you to my parents for their ongoing support and encouragement throughout my academic studies, and for being my personal cheerleading squad. Last but certainly not least, thank you to my partner and best friend, Léo, for always being there for me, for supporting me in so many ways, and for offering to be “house husband” and taking care of dinner when I was focused on my work. Your love and support were essential in the completion of this project.

CONTRIBUTIONS

The work presented in this thesis was done in collaboration with Numalogics Inc., specifically with members Dr. Julien Clin, Dr. Franck LeNaveaux, Loïc Degueldre, and Pierre Legay. The author of this thesis, Camille Chartrand, was responsible for the design, testing, and implementation of the methodology, the analysis and interpretation of the data, the writing of all texts related to this work, including this thesis, and the preparation and leading of all meetings executed with Numalogics in relation to the project.

The members of the Numalogics team participated in the definition of the objectives of the project, introduced Camille Chartrand to their softwares and current modeling methods, and assisted in troubleshooting when issues occurred with the development of the methods described in this thesis.

Loïc Degueldre, an expert in automation, significantly contributed to the work in writing scripts for the automation of the modeling methods designed and tested by Camille Chartrand. More specifically, all modeling procedures in Ansys, namely the building and setup of the model and the application of the loading conditions to perform FE simulations were developed and tested by Camille Chartrand. After the testing of the modeling process, Loïc Degueldre built an automated script for the creation and definition of the models in Ansys and the application of loading conditions, based on user inputs. This script was essential for the work described in this thesis, significantly reducing the time required to perform the simulation workflow.

TABLE OF CONTENTS

LIST OF FIGURES

LIST OF TABLES

ACRONYMS

API	Application programming interface
BC	Boundary condition
BW	Body weight
COM	Centre of mass
CS	Coordinate system
DOF	Degrees of freedom
EMG	Electromyography
EW	External work
FATLS	Fully articulated thoracolumbar spine
FE	Finite element
FL	Follower load
FLV	Force-length-velocity
GS	Geometric stability
GUI	Graphical user interface
ID	Inverse dynamics
IDP	Intradiscal pressure
IVD	Intervertebral disk
IVJ	Intervertebral joint
JRA	Joint reaction analysis
LBP	Low back pain
MA	Muscle analysis
MAPD	Mean absolute percent differences
MRI	Magnetic resonance imaging
MSK	Musculoskeletal
ROM	Range of motion
SCSO	Stability-constrained static optimization
SD	Standard deviation
SO	Static optimization
VPN	Virtual Private Network

1. INTRODUCTION

1.1. Background

The spine is a complex structure comprising many articulating bodies and joints and is surrounded by an even larger number of ligaments and muscles. As such, the spine is subjected to various types of loading throughout an individual's lifetime, making it susceptible to injuries and deformities. For example, low back pain (LBP) has an annual prevalence of 10-30% in the adult population and up to 80% of adults will experience LBP in their lifetime [1-2]. Most options for treating LBP revolve around pain management instead of targeting the root cause as the mechanisms involved in LBP are poorly understood and findings from the literature are inconsistent [1]. In some cases, LBP has been linked to degenerative changes in intervertebral disks (IVDs) and injuries such as disc herniation and spondylolisthesis [2]. Contrarily, a study investigating irregularities in IVDs through magnetic resonance imaging (MRI) found that disc herniation was not always associated with LBP [3].

Difficulties in defining the root causes of LBP, along with the investigation of other spine injuries and deformities, come in part from the testing and measurement methods. Common methods for investigating the etiology of spine injuries involve the analysis of joint loads determined through cadaver studies [4]. Cadaver studies are usually performed on the cadavers of older adults that do not accurately represent the entirety of the population [5-6]. These studies employ simplified loading conditions that may not be representative of physiological loading of the spine from muscle forces and analyses are usually performed on a single spinal level and not in a holistic manner [7]. Moreover, the observations made in cadaver studies are highly dependent on external factors such as specimen storage and testing environment, which can alter the specimen's mechanical properties [5].

Another method utilized to investigate spinal loads consists of collecting *in-vivo* measurements of joint loads acquired through implanted devices or pressure sensors. This method poses problems as it is highly invasive and usually provides data pertaining to a single spinal level and not the entirety of the spine [8-11]. Due to the difficulty in implementation and invasiveness of these

methods, computational models have gained popularity for the estimation and quantification of *in-vivo* joint loads in the spine.

In fact, computational models of the spine are not only beneficial for our understanding of joint loads and the mechanisms involved in LBP, spine injuries, and deformities, but also in the estimation of muscle forces generated during movements, and in the evaluation of stresses and strains occurring in medical instrumentation devices. For instance, multiple groups have developed computational spine models of varying complexities for the estimation of intervertebral forces during daily movements, during lifting tasks, or during work-related tasks, which can provide insight on the mechanisms involved in injuries and, in turn, injury prevention [12-13]. Other groups have used models for surgical planning, implant design optimization, and medical device performance [14-15].

These examples of computational models can be broadly classified into two categories: multibody models, often referred to as musculoskeletal (MSK) models, and finite element (FE) models. MSK models are useful for performing simulations of movement through inverse or forward dynamic approaches, estimating muscle forces required to produce movement, and estimating internal joint loads. Biofidelic spine MSK models effectively represent the role of active structures, i.e. muscles, in human movements. However, these models use ideal mechanical joints, such as pin or spherical joints, to represent the degrees of freedom (DOF) and passive stiffness properties of IVDs. Other passive structures such as ligaments are often not explicitly modeled. Therefore, MSK models are well-suited to investigate internal joint loads on a macroscopic scale but are not used for detailed examination of structural behaviour nor for analyzing strain and stress distributions within the different components of the spine [13, 16].

FE models of the spine, on the other hand, often consider detailed geometries and nonlinear material properties of tissues, making them suitable for gaining insights into the microstructural and complex deformations of IVDs and other passive tissues. However, FE models often do not explicitly calculate the muscle forces acting on the skeletal system due to high computational costs and challenges associated with the redundancy of muscles surrounding the skeletal system. A well-established method for simulating spinal motions is to apply a pure moment to the superior vertebra of the model while fixing the inferior vertebra or pelvis in space. Follower loads (FLs), which induce compressive loads at each intervertebral joint (IVJ) that are tangent to the curvature of the

spine, are implemented to represent the compression of the spine produced by body weight and muscle forces. These boundary conditions (BCs) applied in FE models are designed to replicate *in vitro* conditions from experiments carried out on cadaver specimens but are not necessarily biofidelic representations of the physiological loads acting on the spine [7, 15-18].

To consider the mechanical properties of both active and passive spinal structures on internal joint loads, hybrid modeling, also known as coupled modeling or co-simulation, has been presented as an effective means for combining the strengths of both MSK and FE models. The most common hybrid modeling approach involves performing an inverse dynamics-based analysis on a MSK model to compute muscle forces acting on the skeletal system during a specified motion or static pose. These forces are subsequently used as loading conditions in a FE model, which is then employed to estimate stresses and strains in the spine or in spinal implants [16]. This approach allows for the analysis of deformations and stresses in the spine in a holistic manner while considering the kinematics and kinetics of the whole spine [16].

The work described in this thesis was developed in collaboration with Numalogics Inc., a company based in Montreal, Quebec, Canada, that specializes in the use of FE models for computer modeling and simulation consulting services. Their services span the areas of healthcare, defense, and sports through design optimization of medical devices, personal protective equipment, and sports equipment, respectively. Numalogics specifically has expertise in FE modeling of the spine for testing the capabilities of spinal implants such as bone screws and vertebral body tethering devices used to correct scoliotic deformities [18-20]. Numalogics currently uses *in vitro* loading conditions including pure moment loads and FLs to induce flexion in the different planes of motion of their spine models. They desire to assess whether these loading conditions are representative of *in-vivo* loading conditions in the evaluation of load distributions in spinal instrumentation devices, and whether this modeling choice has a significant impact on the conclusions drawn from their FE simulations.

1.2. Objectives

To be able to answer Numalogics' questions, a method for applying *in-vivo* loading conditions to FE models of the whole thoracolumbar spine was first required. Therefore, the objective of this

project was to create a hybrid modeling workflow to determine *in-vivo* loading conditions, namely muscle forces, that can be used to simulate functional range of motion (ROM) flexion poses in a FE model of the whole spine. More specifically, this objective can be divided into the three following goals:

1. To replicate a validated MSK model of a fully articulated thoracolumbar spine in Ansys, the FE modeling software used by Numalogics.
2. To determine muscle forces and other BCs required to produce static simulations of spinal flexion in Ansys.
3. To validate the modeling workflow by comparing simulation outputs between the FE and MSK models, such as joint kinematics and joint loads. This is essential to evaluate how well a MSK simulation can be reproduced in a FE model of the spine.

In developing this simulation workflow, we will be providing Numalogics with a framework for answering their research questions; for example, comparing joint loads or spinal implant stress distributions when using *in vitro* versus *in-vivo* loading conditions.

1.3. Outline

This thesis contains six Chapters. Chapter 2 contains an in-depth review of the literature of the anatomy of the spine and on MSK, FE, and hybrid models of the spine. For each type of model, common modeling choices are listed, such as the definition of joint stiffnesses, muscle modeling, and material models typically employed. Recent developments in each type of modeling are also reviewed.

Chapter 3 presents the developed modeling and simulation workflow and details the methodology required to produce simulations of static flexion poses in Ansys with *in-vivo* loading conditions.

Chapter 4 presents the results of the simulations performed for comparing joint kinematics and loads between the MSK and FE models.

Chapter 5 provides an in-depth analysis of the results presented in Chapter 4 along with implications of these results and limitations of the workflow developed.

Lastly, Chapter 6 summarizes the thesis and introduces ideas for future developments of this work.

2. LITERATURE REVIEW

2.1. Anatomy of the Spine

In this section, an overview of the anatomy of the spine will be presented, focusing on the thoracic and lumbar regions, with emphasis on key structures relevant for the biomechanical modeling methods used in this thesis.

2.1.1. Overview of the Spinal Structures

The human spine is composed of three regions, namely the cervical, thoracic, and lumbar regions (Figure 1a). The cervical spine, composed of seven vertebrae (C1 to C7) and defined by its lordotic or inward curve, connects the head to the trunk and its articulation permits complex movements of the neck [21-22]. The thoracic spine, composed of 12 vertebrae (T1 to T12) and defined by its kyphotic or outward curve, connects the superior and inferior regions of the spine and serves as attachment sites for the rib cage [21, 23]. The rib cage is composed of 12 pairs of ribs (Figure 1b). The seven superior pairs are named fixed ribs as they are connected to the sternum via costal cartilage. Ribs 8 to 10 are connected to adjacent superior ribs via costal cartilage and are identified as floating ribs. The last two pairs of ribs are known as false ribs as they are not connected to structures other than the thoracic vertebrae. The rib cage serves as a protective structure for internal organs, and the stiffening properties of the connections between the ribs and the sternum via costal cartilage provide a stabilizing effect on the thoracic spine [23]. The lumbar spine, composed of five vertebrae (L1 to L5) and defined by its lordotic or inward curve, connects the thoracic spine to the sacrum (S1). The lumbar vertebrae are larger than the other vertebrae of the spine, and as a result can withstand increased compressive loads acting on the lumbar spine [21, 24].

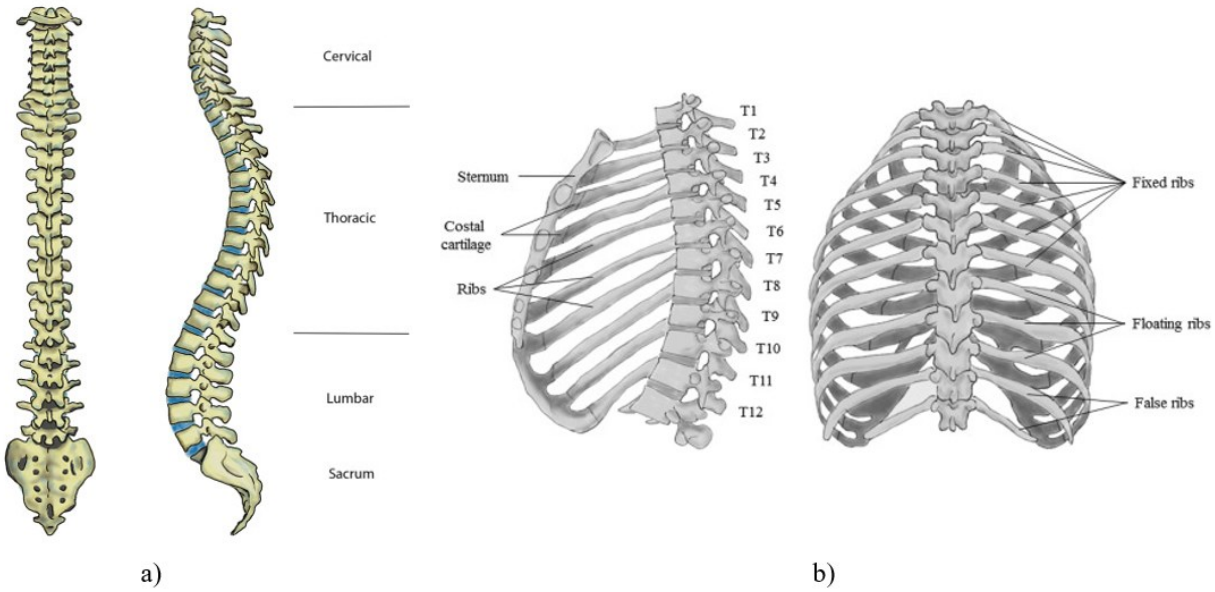

Figure 1: a) The three regions of the lumbar spine [21], and b) the components of the rib cage [23].

2.1.2. Intervertebral Joints

The articulation between adjacent vertebrae consists of various structures composing the IVJ. Each IVJ has six DOF, allowing rotations and small translations in the three planes of motion [25-26]. The structures composing the IVJ, namely the ligaments, facet joints, and IVDs, define the allowed movements between adjacent vertebrae and contribute to load transmission throughout the spine [23-24].

The ligaments have stabilizing functions and limit excessive movements of the joints (Figure 2a). The anterior and posterior longitudinal ligaments limit excessive extension and flexion movements, respectively. The ligamentum flavum limits joint distraction while also limiting movements in flexion, extension, and axial rotation. The intertransverse ligaments resist movements in lateral bending and axial rotation. The interspinous and supraspinous ligaments prevent hyperflexion of the spine and the costotransverse ligaments contribute to spinal stabilization provided by the rib cage [23].

The facet joint consists of bilateral articular surfaces with cartilaginous tissue. This joint influences the motions of the IVJ by limiting the allowable motion in flexion, extension, and axial rotation. Furthermore, it resists anteroposterior translation of the vertebrae and contribute to the transfer of compressive loads from the superior to inferior vertebra (Figure 2b) [22-23].

The IVD is composed of cartilaginous endplates, the nucleus pulposus, and the annulus fibrosis (Figure 2b). The cartilaginous endplates are rigid cartilaginous structures at the interface between the bone and IVD. The nucleus pulposus, located at the centre of the IVD, is mainly composed of water, with proteoglycans and collagen. Like a viscous fluid, it provides viscoelastic properties to the IVD and gives it shock absorbing properties. The nucleus pulposus is surrounded by the annulus fibrosis, which consists of collagen fibres organized in parallel concentric layers, called lamellae. The overall structure of the IVD allows it to transmit large compressive loads throughout the spine while avoiding damage to other spinal tissues [27].

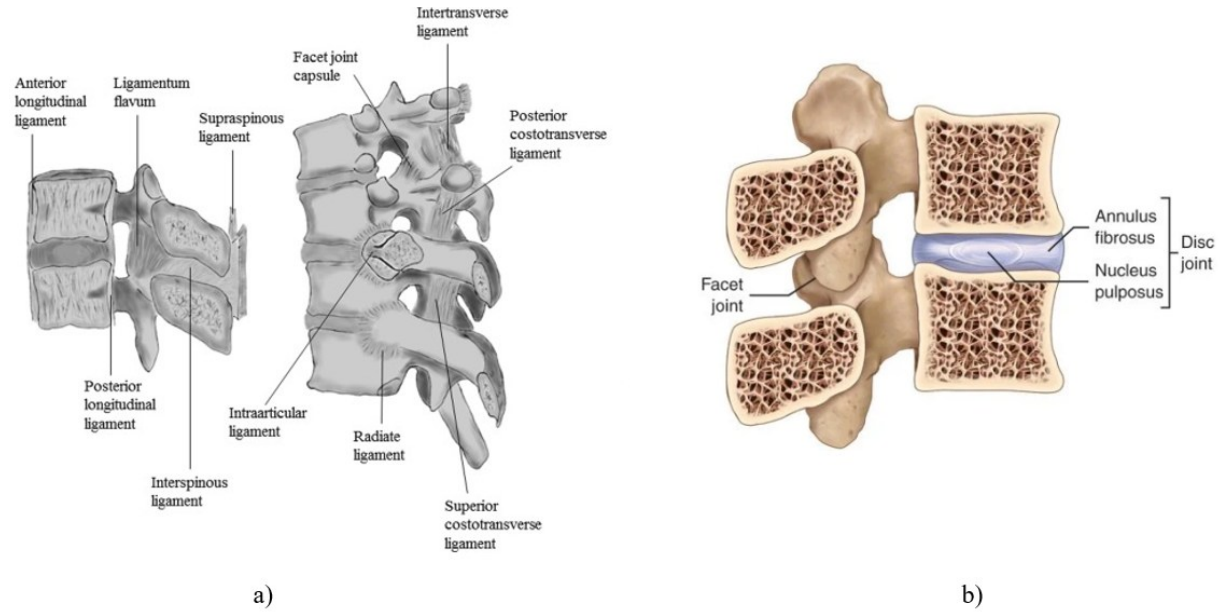

Figure 2: a) Ligaments surrounding the IVJs [23] and b) the components of the IVJ, namely the facet joint and IVD [28].

2.1.3. Spinal Musculature

The spine is surrounded by multiple muscle groups which both enable movement of the spine and act as stabilizers. Large posterior muscle groups also enable the movement of the upper limbs, like for example the trapezius and latissimus dorsi muscles, however these will not be detailed in this section. Only the key muscle groups that were considered in the modeling framework detailed in this thesis will be presented, along with their principal functions.

The main extensors of the spine are the erector spinae, which include the spinalis, longissimus, and iliocostalis muscles (Figure 3a). These muscles also co-activate during flexion

movements, acting as antagonist muscles. When contracted unilaterally, they produce lateral bending of the spine. These muscles have several fascicles spanning the lumbar, thoracic, and cervical regions. The multifidus is composed of several short intersegmental fascicles, spanning two to four spinal levels each (Figure 3a). Running through all spinal regions, the multifidus primarily extends the spine but is also considered a stabilizer of the spine [29].

The iliac muscles, including the quadratus lumborum, iliacus, psoas major, and psoas minor, are deep muscles that enable movement between the lumbar spine and the hips. Of interest are the psoas major and quadratus lumborum, which have attachments to the lumbar vertebrae and the pelvis (Figure 3b). More specifically, the psoas major allows both hip flexion and spinal flexion, and it has been suggested that it constitutes a stabilizer of the lumbar spine in upright positions. The quadratus lumborum on the other hand has several functions, such as decompressing the lower ribs, lateral bending, and extension of the lumbar spine [29].

The abdominal muscles (Figure 3c) are the main flexors of the spine. In various layers, these muscles connect the thorax to the pelvis, assist in respiration, and maintain intra-abdominal pressure. Specifically, the external obliques produce lateral bending and axial rotation of the spine, the rectus abdominus produces flexion of the spine with respect to the pelvis, the internal obliques produce lateral flexion and axial rotation of the spine in conjunction with the external obliques, and the transverse abdominis contributes to spinal stability [29].

Lastly, the neck is surrounded by several short muscles that allow for complex movements. For instance, the flexion of the neck is produced by the action of the sternocleidomastoid, the scalene anterior, (Figure 3d), and the longus colli (Figure 3e). Extension of the neck is produced by the posterior muscles, such as the semispinalis (Figure 3a), the splenius (Figure 3d), and the cervical erector spinae. The sternocleidomastoid, scalene muscles, semispinalis, and splenius are also involved in lateral bending and axial rotation of the neck [22].

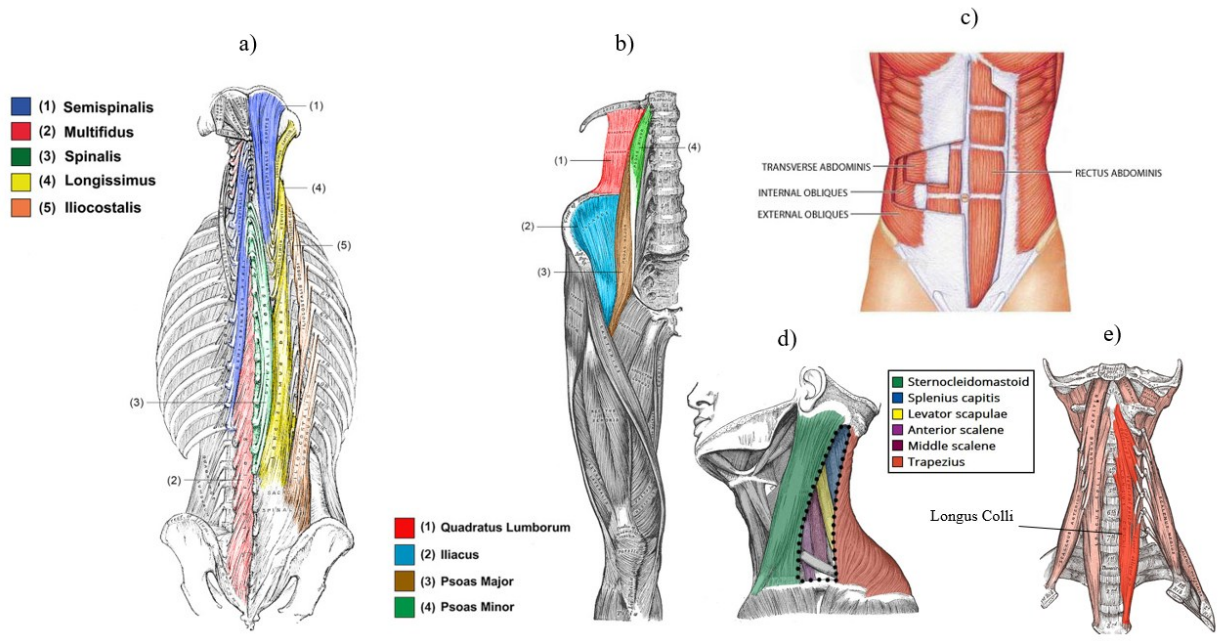

Figure 3: Identification of a) the posterior spinal muscles [29], b) the iliac muscles [29], c) the abdominal muscles [30], d) the lateral and posterior cervical muscles [31], and e) the anterior cervical muscles [32].

2.2. Musculoskeletal Modeling of the Spine

2.2.1. Overview of Musculoskeletal Modeling of the Spine

MSK models of the spine offer a macroscopic representation of the mechanical components of the MSK spine to analyze the kinematics and kinetics of the system. These models generally include a large number of articulating rigid bodies, i.e. bones, that are connected by joints. The IVJs are either modeled as spherical joints, with three rotational DOF between adjacent vertebrae [33-37], or as joints with six DOF, representing the relative rotations and translations occurring between vertebrae during movements [38-41]. Soft tissue structures such as IVDs, ligaments, and cartilage are rarely explicitly modeled. Early models of the spine omitted the mechanical considerations of these passive tissues [33, 35]. More recent models rather included them as simplified passive mechanical components such as springs, beams, and bushings [12, 34, 37-41]. The kinematics of the models are produced by musculotendon actuators, and/or idealized force and torque producing actuators. As many muscle groups surrounding the spine span large areas, these muscles are represented by several distinct fascicles with respective origin and attachment sites. The mechanical properties of the passive components and muscle actuators are incorporated

from experimental measurements and medical imaging techniques, and bone geometry is usually obtained from medical imaging techniques as well [13, 16].

In sum, the simplified representation of the mechanical components of the spine and the rigid behaviour assumption of the skeletal system allow for increased computational efficiency during simulations, and for the consideration of the spine mechanics on a macroscopic level. This has been shown to be effective in the evaluation of joint loads, muscle forces, and muscle activation patterns during movements and static positions, for both healthy and pathological spines. Thus, the use of MSK models of the spine has gained popularity to study the etiology and mechanisms behind injuries and deformities in the spine, and in turn injury prevention and rehabilitation strategies [13, 16].

2.2.2. Muscle Modeling

One of the key components of MSK models is the detailed mechanical description of the musculotendon actuators. The most widely adopted muscle model is the Hill-type musculotendon model, which describes the mechanical action of the muscle-tendon unit as analogous to mechanical elastic elements like springs and dampers [42]. Zajac has enhanced this model to describe it using four normalized curves and five muscle-specific parameters which are commonly used in computer simulations of muscles. The enhanced model will be summarized in the following paragraphs [43].

The active force that can be generated by a muscle fibre depends on its length, contraction velocity, and activation level. The maximum force that can be produced by a muscle occurs at its optimal fibre length (1st muscle-specific parameter). Moreover, the force that can be produced decreases as the contraction velocity increases and increases during eccentric contractions, in comparison to the force generated in an isometric contraction. The contraction velocity at which the muscle can no longer generate force occurs at the maximum contraction velocity (2nd muscle-specific parameter). Lastly, the activation level of a muscle, controlled by the central nervous system, dictates the amplitude of the muscle force being generated. Hence, the maximum isometric muscle force (3rd muscle-specific parameter) corresponds to the maximal force that can be produced by a muscle when it is maximally activated and held in an isometric contraction, at its

optimal fibre length. Muscles also generate passive forces, which occur when the muscle fibre is stretched beyond its resting length, which also corresponds to the optimal fibre length.

The forces transmitted to the skeletal system depend on characteristics of the tendon. For instance, the muscle force transmitted to the tendon depends on the pennation angle (4^{th} muscle-specific parameter), which is the angle at which the muscle fibres attach to the tendon. Hence, the muscle force transmitted to the tendon is expressed as

$$F_T = F_M \cos(\varphi) \qquad \text{Eq. 1}$$

where F_T is the tendon force, F_M the muscle fibre force, and φ the pennation angle. Lastly, the forces transmitted to the skeletal system also depend on the compliance of the tendon and its resting length, which is called the tendon slack length (5^{th} muscle-specific parameter) [44].

Figure 4 illustrates the mechanical representation of the Hill-type model (A), with parallel spring and damper elements representing the passive and active muscle forces, respectively, and another spring element representing the tendon force. The muscle spring and damper elements are connected to the tendon at the pennation angle (φ). The curves illustrated are the muscle force-velocity curve (B), describing the muscle force produced as a function of contraction velocity, the tendon force-length curve (C), describing the tendon force produced as a function of its length, and the active (green) and passive (yellow) muscle force-length curves (D), describing the muscle force produced as a function of the fibre length. Each of these curves is scaled for specific muscles based on the muscle-specific parameters, namely maximum contraction velocity, tendon slack length, and optimal fibre length, respectively. The y-axis on each curve for muscle force is scaled by the maximum isometric force [44].

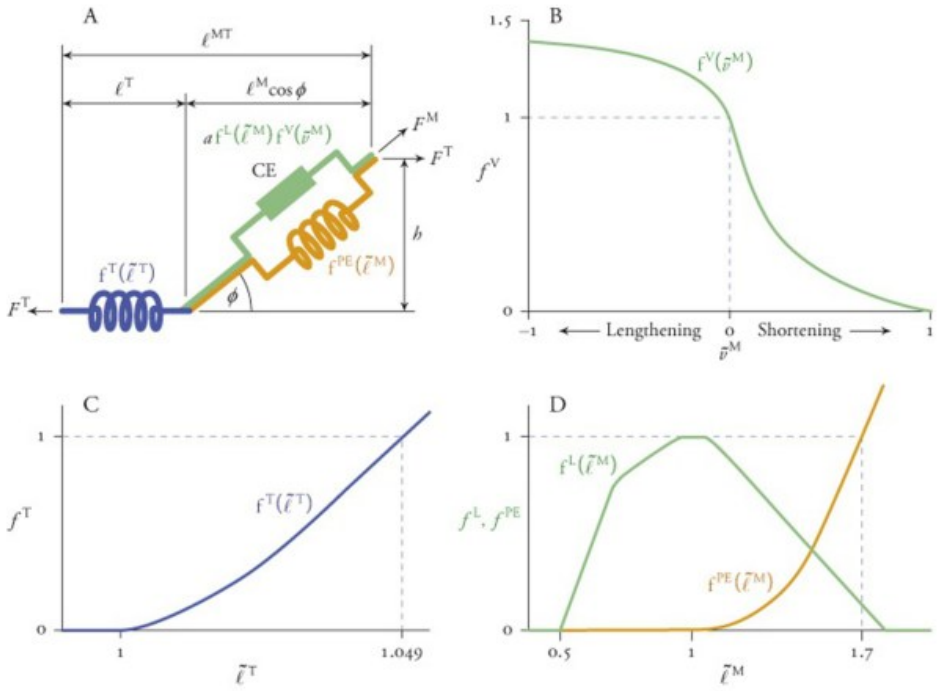

Figure 4: (A) A mechanical representation of the Hill-type muscle model, (B) force-velocity curve, (C) tendon force-length curve, and (D) active (green) and passive (yellow) muscle force-length curves. Diagram from Biomechanics of Movement: The Science of Sports, Robotics, and Rehabilitation [44].

The 5 muscle-specific parameters, namely, maximum isometric force, optimal fibre length, maximum contraction velocity, tendon slack length, and pennation angle, are generally obtained from experimental measurements or medical imaging techniques such as MRI [44].

2.2.3. Musculoskeletal Modeling Analyses

The two most common MSK modeling platforms are AnyBody (AnyBody Technology, Aalbrog, Denmark), a commercially available software package, and OpenSim (SimTK, Stanford, United States), an open-source software package [45]. Both offer an extensive set of tools that can be used to perform various types of analyses involving the kinematics and kinetics of models. The most common modeling approach consists of the inverse dynamics (ID) method. Kinematics, either measured through experimental methods like motion capture, or manually specified, are determined for each of the generalized coordinates of the model. An ID analysis is then performed, which determines the net joint forces and moments that produce said kinematics, using Newton's second law. Then, a static optimization (SO) algorithm is employed to estimate muscle forces that produce joint moments which, when summed with those produced by external forces (ground reaction forces, weights, etc.), correspond to the ID results. The MSK system is redundant,

meaning that there are more muscles actuating the skeletal system than there are DOF, hence there is an infinite number of possible solutions for muscle forces that could satisfy the model equilibrium equations. Therefore, the SO algorithm finds muscle forces which minimize an objective function, subject to a set of constraints [44]. Common objective functions include minimizing the sum of muscle activations or stresses to a given power [12, 46-48]. Constraints include the determination of muscle forces that remain within physiological bounds and the maintenance of dynamic equilibrium equations at each instant in time [46].

A limitation of the SO approach is the lack of physiological accuracy in muscle force predictions as this method computes solutions at each independent step in time without considering the studied motion as a whole. Furthermore, SO has been shown to penalize activation of antagonist muscles and co-contraction during movements [46].

Other methods have been employed to estimate muscle forces, such as electromyography (EMG) -based modeling approaches, although these methods have been associated with limitations and challenges, such as the complex nature of EMG signal processing [46].

2.2.4. Recent Advancements in Musculoskeletal Modeling of the Spine

Many MSK spine models have been developed in the last decade to investigate muscle activation patterns and joint loads during spine movements and static poses. Most studies reused a few base models and enhanced them based on recent technical advancements or knowledge obtained from the literature. Moreover, most models include a detailed representation of the lumbar spine DOF with a rigid thorax, although recent models have started to include a holistic representation of the spine kinematics.

For instance, Christophy *et al.* developed a MSK model of the thoracolumbar spine in OpenSim [33]. The model featured a rigid pelvis, sacrum, 5 lumbar vertebrae articulated with 3-DOF spherical joints, and a rigid torso consisting of the lumped thoracic vertebrae and the ribcage. The model featured key muscle groups such as the erector spinae, abdominal muscles, and stabilizer muscle groups. The model was validated by comparing muscle moment arms during flexion-extension tasks with anatomical measurements. Since then, this model was enhanced by combining it with models of the neck and upper limbs and by modeling translational DOF in the lumbar spine along with joint stiffness properties [36, 38]. These models were validated against

in-vivo measurements of intradiscal pressure (IDP) and joint loads from vertebral body replacements during static poses [38], and against EMG measurements during jogging [36]. Another group also used this model to propose a force-dependent kinematics method to model secondary kinematics, which determines smaller motions, such as rotations and translations in secondary planes of motion, that are dependent on joint stiffness properties and input kinematics of the overall lumbar spine [39].

Ignasiak *et al.* developed a model of the thoracolumbar spine, in Anybody, with articulation of all vertebrae from T1 to S1, and of the ribcage [40]. IVJs and joints between the ribs and sternum were modeled with 6-DOF, and costovertebral joints were modeled as pin joints. Stiffness properties of the IVJ passive structures were modeled as linear functions of angular joint displacements. The joint kinematics were computed based on the force-dependent kinematics algorithm developed by Meng *et al.* [39]. All key muscle groups, namely the back, abdominal, stabilizer muscles, and intercostal muscles, were included. The model was validated against IDP measurements during dynamic spine movements in the sagittal plane. Through this model, they determined that the modeling of a flexible thoracic spine was necessary for estimating joint loads in the upper lumbar and thoracic spine [49], and that the inclusion of the ribcage had significant effects on model predictions in the thoracic spine, suggesting that the ribcage has a stabilizing role on the spine [40].

Similarly, Bruno *et al*. developed a fully articulated thoracolumbar spine (FATLS) model, in OpenSim, with articulation of all vertebrae and of the ribcage [35]. The IVJs were modeled with three rotational DOF, and the costovertebral joints as pin joints. Force actuators were implemented between the ribs and sternum, and between adjacent ribs, to represent forces transmitted by costal cartilage. The model also incorporated articulated upper limbs and a lumped body for the head and neck, to allow the model to be used in simulations of lifting tasks. All major muscle groups, including the back, abdominal, stabilizer, intercostal, and upper limb muscles were incorporated. The sensitivity of the model outputs was evaluated by varying parameters such as maximum muscle stress (which relates to the maximum isometric muscle force), optimal forces of the rib actuators, and locations of the IVJs. Furthermore, the model was validated by comparing compressive loads of various IVJs to IDP measurements and by comparing the muscle activations of the erector spinae to EMG measurements during multiple static poses and lifting tasks [35]. This

same group then used this model to generate subject-specific models by adjusting muscle properties and the spine curvature based on CT scans of individuals [50]. Schmid *et al*. adapted the model to create models for children and adolescents [51] and Wang *et al*. enhanced it through the implementation of 6-DOF IVJs with nonlinear stiffness properties [41]. Since then, multiple groups have extended the validation of this model. For instance, the model was validated against EMG measurements for static and dynamic tasks in older adults [52]. Akhavanfar *et al.* enhanced the model by considering the passive stiffness functions defined by Weng *et al.* for the rotational DOF and linearizing them to be able to simulate the full rotational ROM of the spine. Moreover, they removed the costovertebral DOF and defined the movement of the abdomen as a function of L5S1 kinematics so that the model kinematics could be defined from optical motion capture methods. They also incorporated lower limbs to the model to be able to couple motion capture with ground reaction force measurements. With these additions, the model joint loads at the L1L2 level were validated against vertebral implant measurements for various dynamic lifting tasks [12].

Other models have been developed in recent years and validated against both EMG and vertebral load measurements, but none to the extent of the FATLS model [37, 48, 53]. In addition, with the many enhancements brought to the FATLS model, it is well suited to perform analyses for a large portion of the population, from children and adolescents to the elderly population, and for person-specific modeling.

2.2.5. Stability Considerations

As previously mentioned, SO algorithms for estimating muscle forces by minimizing muscle effort have been shown to penalize activation of antagonist muscles and co-contraction during movements when comparing model predicted activations to EMG measurements [46]. One reason for this is that most SO algorithms estimate muscle forces required to maintain equilibrium of the system, but do not consider the mechanical stability of the model. The concept of mechanical stability in MSK modeling has been defined in various ways. For instance, the mechanical stability of a system in static equilibrium has been defined as its ability to return to its equilibrium state after a small perturbation. A critical load, causing the system to become unstable, would lead to structural buckling [54-55]. Mathematically, the concept of stability has been defined through the energy criterion, which states that a system is stable when the potential energy of the system is at a relative minimum. This occurs when the second derivative of the system potential energy has a

positive value, or when the Hessian matrix of potential energy is positive definite at the equilibrium position. The Hessian matrix is a square matrix containing the second-order partial derivatives of the potential energy of the system with respect to the system's coordinates (DOF). It is positive definite when its determinant is positive, or when all of its eigenvalues are positive [55-56].

Bergmark determined that muscles can contribute to the potential energy of the spine by storing energy when being stretched, like a mechanical spring would, based on their stiffness [54]. They defined the muscle stiffness as being proportional to the muscle force and inversely proportional to its length:

$$k = q\frac{F}{L} \qquad \text{Eq. 2}$$

where k is the stiffness, F the muscle force, L the muscle length, and q a muscle proportionality constant which is assumed to be the same for all skeletal muscles [54]. A physiological value for q has not yet been determined, as estimates from the literature have ranged between 0.5 and 42, with a mean value of 10 [56].

It is clear that the musculature and other structures surrounding the spine contribute to stability, as it has been shown that the spine buckles under loads of 20 N and 90 N on the thoracolumbar and lumbar spines, respectively, although the human spine is subjected to loads surpassing 6000 N during everyday activities [56-57]. In fact, increased activities in trunk antagonists, such as the abdominal muscles, have been associated with higher levels of spinal stability [55, 58-61]. Moreover, considering stability constraints in the estimation of muscle forces has resulted in better correlation of abdominal muscle activations to EMG measurements [59-60].

Although the consideration of stability in spine modeling has been shown to improve the realism of model estimates, this concept is not yet widely adopted in MSK modeling of the spine due to the complex nature of the mathematics involved and associated increased computational expenditure. Cholewicki and McGill defined the potential energy of the spine as a combination of the elastic energy stored in muscles and tendons (i.e., springs) with the elastic energy stored in passive joint elements, namely the IVDs and ligaments (i.e., torsional springs), minus the external work done:

$$V = U_L + U_T - W \quad \text{Eq. 3}$$

where V is the total potential energy, U_L the potential energy stored in muscles, U_T the elastic energy stored in passive joint properties, and W the external work [57]. Potvin and Brown derived a simplified equation for Eq. 3 for quantifying stability about one joint, for one rotational DOF. Their equation takes as inputs the muscle origin and insertion points (or nodes) with respect to the joint, muscle force, and muscle stiffness (based on Eq. 2). The potential energy of muscles is quantified from the geometry of muscles, i.e., their length and moment arms with respect to the joints of a model, and their stiffnesses, which they called geometric stability (GS), and muscle forces [62]. Therefore, their simplified equation for stability states that the spinal joint is stable if the potential elastic energy, determined from the GS and muscle forces (F), minus the external work (EW) done on the joint, is greater than or equal to zero:

$$GS \cdot F - EW \geq 0 \quad \text{Eq. 4}$$

In this thesis, the stability of the system will be determined based on the definition of Potvin and Brown, as defined in Eq. 4. Recently, Akhavanfar *et al.* used this simplified equation to develop an open-access MATLAB script for computing muscle forces using the OpenSim SO algorithm, while also considering stability constraints, which was called the stability-constrained static optimization (SCSO) framework. The script can be used for complete spine models containing multiple joints and DOF [63]. A limitation of this script is that it does not consider the passive joint properties (term U_T in Eq. 3). Barrett *et al.* have developed a custom script using similar methods, while also considering passive stiffness contributions to the stability of the system, but have not made this accessible to the public [64].

2.2.6. Limitations of Musculoskeletal Modeling

In sum, MSK models of the spine have commonly been used to evaluate spinal loads during both static and dynamic everyday and lifting tasks. Multiple models have been developed and validated to great extents against *in-vivo* measurements such as IDP and joint loads from vertebral implants as well as EMG. However, this modeling method comes with several limitations. These include the inability of SO methods to accurately predict co-activation of antagonist muscles and the difficulty of implementing stability considerations, although simplified methods for calculating

stability have started to emerge. Other limitations include the inability to evaluate microstructural deformations and stresses as all vertebral structures are modeled with rigid behaviour and passive joint properties are not explicitly modeled. Many models only consider three rotational DOF in the IVJs of the spine, which may impact model predictions. Lastly, because of limited information on biological and mechanical properties of the spine, due to difficulties in performing *in-vivo* measurements, it is difficult to build fully person-specific models [13, 46].

2.3. Finite Element Modeling of the Spine

2.3.1. Overview of Finite Element Modeling of the Spine

FE analysis functions by discretizing the geometry of the model into a finite number of elements, each of which is associated with material properties. The elements are interconnected through nodes, and their mechanical behaviour is determined by governing differential equations and applied boundary conditions (BCs). BCs are composed of constraints applied to the system and loading conditions. From these BCs, the FE analysis can calculate nodal displacements, which are used to extract information on stresses, strains, and structural deformations within the system [65-66].

FE models are widely used to evaluate structural deformations and stresses within the spine, as they can explicitly model geometrical and material properties of biological tissues. FE spine models often include vertebral bodies, the sacrum, and the pelvis, all of which are modeled as cancellous bone with an external layer of cortical bone, with elastic material properties. The IVDs can be explicitly modeled with the nucleus pulposus, annulus fibrosis, and cartilaginous endplates. The nucleus pulposus has often been modeled as a fluid-filled cavity or as a hyperelastic material. The annulus fibrosis is modeled as concentric layers of isotropic elastic fibres with a hyperelastic ground substance. Hyperelastic material properties mostly vary in the literature between Mooney-Rivlin and neo-Hookean material models. Cartilaginous endplates are most often modeled as rigid elements. Ligaments are generally represented by truss, spring, or beam elements with tensile-only elastic properties. Lastly, facet joints between vertebral bodies are modeled as contact surfaces. Material properties for each component of the spine are assigned based on cadaveric studies or *in-vivo* measurements and the geometric shape of the spine is obtained from imaging techniques, rendering person-specific models easy to generate [15, 66-67].

In most cases, FE analysis studies perform simulations using BCs mimicking those in *in vitro* studies with cadaver specimens, as measurements taken from cadaver experiments can also be used to validate model outputs and because it is difficult to define realistic physiological BCs [16]. Unlike MSK models, muscles are not often included in FE models due to high computational costs and the difficulty associated with experimentally reconstructing the action of muscle forces [7, 15]. Instead, the concept of the FL has been widely implemented to represent the combined action of gravity and muscle loads on the spine, and is defined as a resultant compressive force, acting on each spinal level, the direction of which follows the curvature of the spine, in order to minimize flexion and anterior shear loads at the IVDs [7, 15]. Mimicking *in vitro* experiments, FE simulations simulate functional movements by pairing the FL with a pure bending moment applied to the superior vertebra in the model and by fixing the sacrum, pelvis, or most inferior vertebra in space [67-68].

Due to the complexity and level of detail included in the modeling of each spinal component, many studies have focused on simulations using a single functional spinal unit or small spinal segments. These models have been used for a variety of analyses, like the investigation of load sharing between the different spinal components, surgical planning, the evaluation of the mechanisms behind disc degeneration, spinal curve correction capabilities of instrumentation devices for the treatment of scoliosis, and implant design and optimization [15, 67, 69].

2.3.2. The Concept of the Follower Load

As previously mentioned, the thoracolumbar and lumbar spines are known to buckle under vertical loads of 20 N and 90 N, respectively. However, through acquisition of *in-vivo* measurements, it was shown that the spine is subjected to compressive loads surpassing 6000 N during everyday activities [56-57]. Therefore, it is evident that the musculature surrounding the spine plays an important role in stabilizing the spine and reducing shear and moment loads that would otherwise cause it to buckle [15]. The implementation of muscle forces in *in vitro* experiments is technically difficult to implement. To circumvent this issue, Patwardhan *et al.* found that the spine could withstand significant compressive loads when the latter were applied along a path that is tangent to the curvature of the spine, which was called the FL [70]. Because the FL is always tangent to the spine, this results in all spinal segments being loaded in pure compression, with no internal shear or bending moments. This group implemented the FL through bilateral

cables attached to the vertebral bodies and were able to apply compressive loads up to 1200 N, the maximum value being limited by the strength of the cables and not the spinal structure itself. Multiple groups have implemented the concept of FLs in FE studies since then. For instance, Rohlmann *et al.* used a FE model of the lumbar spine and recommended a FL of 500 N which produced intervertebral rotations and IDP that matched well with *in-vivo* data for a standing posture [71].

Because FLs can easily be used in both computational and *in vitro* experiments, it has been widely implemented in FE modeling as a loading condition providing a simple representation of gravity and muscle loads. However, whether or not the FL produces an accurate depiction of the action of muscles is controversial. Kim *et al.* implemented 117 pairs of muscle fascicles in a FE model of the lumbar spine and estimated muscle forces using an optimization algorithm with a constraint limiting the shear forces in the spine. They were not able to find a solution for muscle forces within a physiological range that could produce a perfect FL, but were able to find good solutions when shear forces were limited to 20% of the compressive forces, indicating that muscles do in fact produce some level of shear forces [72-73]. On the other hand, Han *et al.* used a lumbar spine model with 232 muscle fascicles to investigate this same issue, and were able to predict muscle forces corresponding to the FL mechanism in a standing posture [74]. Lastly, Shih *et al.* compared FLs and muscle forces on a lumbar spine model during flexion tasks and compared the spinal profiles and stress distribution in the spine between the loading methods. They found that FLs and muscle forces produced similar lumbar profiles but that muscles produced gradual increases in compression, shear, and moments toward the caudal (inferior) levels of the spine, whereas FLs produced no shear, and the compression loads were the same throughout the spine. Moreover, the FL method produced higher motion and stresses at the cephalic (superior) levels than muscle forces, and the inverse at caudal levels, in comparison to muscle forces [7].

2.3.3. Numalogics' Advances in Finite Element Modeling of the Spine

For this project, the base model used was of type MSK, and the methods used consisted of those described for MSK analyses in Chapter 2.2.3. No elastic/hyperelastic material properties were considered in this project, nor the evaluations of stresses and strains as would be in most FE studies. Therefore, only recent work produced by members of the Numalogics team will be

reviewed in this Chapter, to discuss their current methods and provide background information on their needs in relation to this project.

Numalogics has done a lot of research in collaboration with orthopedic surgeons for the evaluation of the scoliotic curve correction capabilities of spinal instrumentation devices such as pedicle screw/rod systems. This work typically involves creating patient-specific models of the whole spine (from T1 to the pelvis) for adolescent idiopathic scoliosis patients from EOS images (low-dose X-ray technology). While the geometry is patient specific, material properties for IVDs and ligaments are taken from the literature. Bones are modeled as rigid bodies as their deformation is minimal during surgery [75]. These models are then used to perform surgical simulations of the pedicle screw/rod system installation to evaluate reaction forces at the screw-vertebra interface [19]. They also use these models to simulate postoperative functional movements such as flexion, extension, lateral bending, and axial rotation. The BCs for these simulations include fixing the pelvis in space and applying bending moments to T1 with compression loads to simulate body weight [20, 76]. Most recently, with similar methods, they developed a patient-specific lumbar spine model for comparing instrumentation devices for lumbar fusion. All non-instrumented vertebrae were modeled as rigid bodies, while instrumented vertebrae were assigned material properties from the literature. Instead of explicitly modeling IVDs, they modeled their stiffness properties through three-dimensional springs (bushings) with a 6x6 stiffness matrix. The BCs for simulating functional spinal movements included fixing the pelvis in space, limiting the motion of L1 to stay within the plane of motion being simulated, applying a FL of 415 N, and applying bending moments of 7.5 N m to L1 [18].

2.3.4. Limitations of Finite Element Modeling

In sum, FE models of the spine are commonly used to perform surgical simulations and to evaluate stresses and strains within the spine or within spinal instrumentation devices. With the capabilities of FE simulations comes many limitations. Due to the difficulty in defining realistic and physiological BCs, most FE models are limited in applying BCs mimicking those from *in vitro* studies [68, 70]. While BCs from *in vitro* studies are simple to implement, with for example FLs, their physiological accuracy has been debated [7, 72-73]. For instance, FLs applied in FE studies are based on experimental studies, where the compressive load is the same at each spinal level and for all functional movements of the spine. However, it has been shown that muscle forces produce

a gradual increase in compressive loads in the caudal levels, while also producing some levels of shear forces [7]. Moreover, *in-vivo* measurements of IDP indicate that compressive loads vary for different functional movements [9, 77]. Therefore, FE models of the spine could benefit from new methods for implementing muscle forces as BCs during functional spinal movements.

2.4. Hybrid Modeling of the Spine

2.4.1. Overview of Hybrid Modeling of the Spine

As described in the previous Chapters, MSK and FE modeling techniques offer comprehensive ways of analyzing the kinematics and kinetics, and stresses and tissue deformations in the spine, respectively. In combining these modeling techniques and their strengths, we can produce simulations evaluating stresses and tissue deformations while considering both the detailed modeling of passive tissues like IVDs and ligaments and *in-vivo* kinematics and kinetics. The coupling of MSK and FE models can be referred to as hybrid modeling or co-simulation. In a review by Nispel *et al.,* co-simulation approaches were separated into two categories: unidirectional and bidirectional approaches [16]. In unidirectional co-simulation approaches, the outputs of one type of simulation are the inputs of the other, and each simulation type is performed consecutively, producing a unidirectional flow of data. In most cases, this involves the use of a MSK model to perform ID analyses with *in-vivo* kinematics for the estimation of muscle forces. Resulting kinematics and/or computed forces and moments are then used as BCs in a FE model for the evaluation of soft tissue deformations and stresses. In bidirectional approaches, there is a constant flow of data between the two types of models. In cases where large deformations are present, this method is useful for iterative data exchanges that consider the changes in kinetics of a MSK model following soft tissue deformations in the FE model. Despite the potential of bidirectional approaches for understanding the mechanics, stresses, and strain distributions of models with time-varying properties, they are less commonly used due to their high computational costs, difficulty of implementation, and challenges associated with simulation convergence [16].

2.4.2. Recent Advances in Hybrid Modeling of the Spine

This Chapter will offer a review of recent advances in hybrid modeling of the spine, focusing on unidirectional approaches, as these methods are most common and correspond best to the

capabilities and methods accessible to Numalogics. As mentioned, unidirectional approaches usually perform MSK analyses first, and transfer either kinematics, forces and moments, or both, as BCs to the FE model. The MSK model typically considers the stiffness properties of passive joint structures as simplified mechanical elements like springs, beams and bushings while the FE model of matching body geometry explicitly models the geometry of these passive structures with nonlinear and hyperelastic material properties [16].

For instance, Henao *et al.* simulated surgical instrumentation steps for scoliosis curve correction on a multibody model of the spine. The vertebral displacements resulting from applied surgical steps were transmitted as BCs to a FE model for the analysis of the local effects of each maneuver on the spinal cord [78].

Most groups, however, use a combination of kinematics and loads determined from a MSK model as BCs to FE models. The research group of Shirazi-Adl *et al*. have developed multiple co-simulation workflows over the years to answer various research questions [79-80]. In one study, they applied *in-vivo* kinematics to a MSK model of the lumbar spine including 46 muscle fascicles and used an optimization algorithm to solve the muscle redundancy problem. In the FE model, muscles were modeled as uniaxial springs with stiffnesses assigned based on a chosen value of the muscle proportionality constant q (see Eq. 2). BCs in the FE model consisted of the pelvis rotation, muscle forces, and gravity loads for a given static pose. Nonlinear structural and stability analyses were carried out. Using this method, they were able to perform static functional poses and lifting tasks [81]. In another study, they used the same workflow, but this time, the FE model consisted of the L4L5 segment only for the evaluation of IDP, ligament forces, and facet joint forces at that level. The BCs of the FE model included the prescribed kinematics of the joint, muscle forces, and gravity loads. Since the muscle forces were computed using a MSK model of the lumbar spine with rigid torso, they combined all gravity and muscle loads with insertion points higher than L4 into one resultant load acting at the center of L4 [82]. The group noted that the resulting kinematics in the FE model differed from the *in-vivo* (MSK) kinematics because of differences in the modeling of passive joint properties between the two types of models. To remedy this, they performed an iterative procedure where they adjusted the passive stiffness properties of the MSK model based on FE model responses to applied muscle loads, recalculated muscle forces, and fed the updated muscle forces back to the FE model as new BCs. The iterative procedure was performed until

matching kinematics were found between the two models [17]. Lastly, to avoid this iterative process, this same group proceeded to develop a coupled MSK-FE model, where both the detailed geometry and musculature were included in one model, and all analyses could be done in a singular platform [83].

Others have performed simulations using similar methods. Honegger *et al.* collected experimental kinematics using motion capture methods and, with a full-body and detailed lumbar spine MSK model, performed a SO analysis to estimate muscle forces at each instant in time during sit-to-stand movements. The time-dependent kinematics and muscle forces were used as inputs to a detailed FE model of the lumbar spine to evaluate time-dependent IDP and facet joint forces during these movements [84].

While most groups have used co-simulation techniques to evaluate load sharing, stresses, and strains within the spine, there has been little research done on the effect of *in-vivo* loading conditions on stresses within spinal instrumentation devices. This is a question of interest for Numalogics because of the work that they do with the design and optimization of spinal instrumentation devices. Panico *et al.* compared stresses in pedicle screws when simulating functional ROM movements using pure moment bending loads versus muscle forces in a lumbar spine model. They found that muscle forces produced larger stresses in the instrumentation devices than *in vitro* loading conditions, but it should be noted that they neglected FLs in their *in vitro* loading conditions [85].

2.4.3. Limitations of Current Hybrid Modeling Strategies

While hybrid modeling strategies have been shown to be extremely beneficial in the evaluation of stresses and strains within spinal components under the action of *in-vivo* loading conditions, the studies listed had many limitations. Many studies used a limited number of muscle fascicles in their analyses (less than 100) or neglected small intersegmental muscles. Moreover, these studies presented the same limitations of most MSK modeling approaches, where the optimization algorithms used for the estimation of muscle forces penalized abdominal co-contraction [17, 79-83]. In cases where passive joint properties are defined differently between MSK and FE models, iteration is required to obtain matching kinematics, which can be a time-consuming process [17]. Lastly, all hybrid models developed thus far have considered the lumbar spine only, or the lumbar

spine with a rigid thorax. No co-simulation workflow has been developed for a fully articulated thoracolumbar spine, even though the motions of the thorax have been shown to influence loads in the lumbar spine [49]. Therefore, additional work should be done to evaluate FE model responses under *in-vivo* loading conditions while considering a comprehensive number of muscles and the entirety of the thoracolumbar DOF.

3. METHODOLOGY

The development of this hybrid modeling workflow involved multiple steps of trial and error to find modeling choices that would produce converging simulations in both the MSK and FE modeling platforms. To demonstrate the effect that some of these modeling choices had on simulation convergence, two versions of the workflow will be presented in this thesis and will be referred to as version I and version II.

3.1. Simulation Workflow – Version I

The workflow developed for this project consists of a unidirectional co-simulation workflow. To avoid the iterative procedure described by some hybrid modeling studies, it was essential to make sure that the MSK and FE models were equivalent in terms of geometry; mass properties; joint positions, orientations, and stiffnesses; joint types and DOF; and muscle stiffnesses and attachment points. Then, MSK modeling methods were used to compute forces which were used as loading conditions to the FE model. The workflow developed can therefore be broken down into the following key steps: (1) utilizing a SO framework to estimate muscle forces required to satisfy equilibrium equations for a static flexion pose in a MSK model, (2) building the MSK model geometry in the FE modeling platform, (3) defining the model structure in the FE modeling platform so that it matches the MSK model structure, (4) applying loading conditions computed from the SO framework to the FE model, and (5) performing the simulation and exporting the desired results. The following Chapters will elaborate on the selection of the MSK model used for the workflow as well as each of the 5 steps listed above. Note that this workflow was designed to perform simulations of static poses only.

3.1.1. Model Selection and Modifications

The FATLS model that was originally developed by Bruno *et al.* and enhanced by other groups was chosen for this project for its high biofidelity in terms of the large number of bodies, DOF, and muscles modeled, and for the multiple validation studies conducted on it for both static and dynamic tasks [12, 35, 52]. The version of the model that was used was the one modified and enhanced by Akhavanfar *et al.,* with the DOF of the ribs removed and passive stiffnesses

considered at the 3 rotational DOF of the IVJs [12]. Modifications were made to the model to simplify the FE modeling process, reduce computing time, and avoid convergence issues. Since the primary focus of this project was to produce simulations of functional ROM poses of the spine, the upper- and lower-limbs were removed from the model, so that the only bodies remaining were those of the pelvis, sacrum, vertebrae, ribs, sternum, and head-neck. All upper-body muscles with attachment points to these removed bodies were also removed. Since the psoas muscles had attachment points on the femurs, those attachment points were removed, and the tendon slack lengths and optimal fibre lengths were modified based on the original publication of the model which did not include the lower limbs. The pelvis DOF were removed by fixing the pelvis to the ground. The model included a body representing the abdomen for the attachment of abdominal muscles, which had three rotational DOF with respect to the sacrum. The movement of the abdomen was designed to better replicate the muscle lines of action during movements and to prevent muscles from going through other bodies in OpenSim [12]. However, no stiffness properties were associated with the abdomen-sacrum joint, which produced convergence issues in Ansys. Therefore, the abdomen-sacrum joint was fixed. The strategy used for modeling muscles in Ansys required muscles to have a straight line of action connecting origin and insertion points. Hence, all intermediate muscle path points defined in the FATLS model were removed, and muscles with a curved line of action, namely the transverse abdominal muscles, were removed from the model. In simplifying the lines of action of the muscles and in removing some of the muscles, changes associated with muscle force production and the moments that are produced about the coordinates of the model may be impacted. To evaluate whether the simplification of the muscles in the model significantly altered key modeling outputs, a sensitivity analysis was performed and will be described in Chapter 3.3. Lastly, as described by Akhavanfar *et al.*, the ribs were welded together because the motion between them cannot be determined using marker motion capture, and we have no metric for accurately describing their motion during spine movements [12]. Therefore, the intercostal muscles, which are responsible for the movement of the ribs relative to each other, were removed from the model. With these modifications, the model had a total of 56 bodies, 51 rotational DOF, and 306 musculotendon actuators (See Appendix A).

3.1.2. Step 1: Static Optimization Framework

As a first step, the FATLS MSK model is used along with OpenSim 4.5 to calculate muscle forces required to satisfy equilibrium equations for a given static pose. The analyses done in OpenSim can be carried out either through the graphical user interface (GUI) or through the application programing interface (API) and are explained in the following paragraphs (Figure 5).

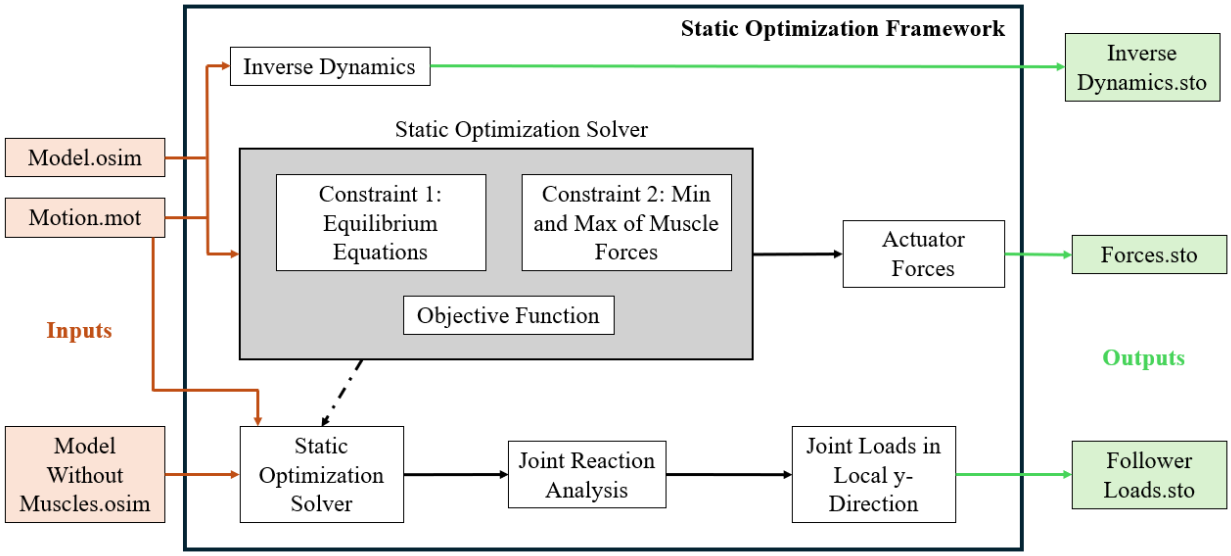

Figure 5: Static optimization framework for version I of the co-simulation workflow

Bruno *et al.* synthesized information from several experimental studies on the percentage of total motion that occurs at individual IVJs during spine movements [35]. This information was taken to generate several motion files corresponding to static forward flexion poses. Static motion files, describing poses ranging from 0 to 100% of the spine ROM in forward flexion, at intervals of 10%, were created. Table 1 lists the total thoracolumbar flexion angles that correspond to each of the percent ROM poses generated. These angles correspond to the sum of all IVJ angles, about the sagittal plane, representing the total flexion angle of the spine. These angles do not include the rotation of the pelvis during flexion. The rotations for each IVJ of each motion file are listed in Appendix B.

Table 1: Flexion angles used to generate motion files

Percent ROM (%)	0	10	20	30	40	50	60	70	80	90	100
Thoracolumbar Flexion (°)	0	10.1	20.0	29.8	39.3	48.5	57.2	65.3	72.4	78.0	81.5

For visualization of the poses simulated, Figure 6 illustrates the static poses in the FATLS model from neutral standing to 100% ROM in flexion, at intervals of 20%.

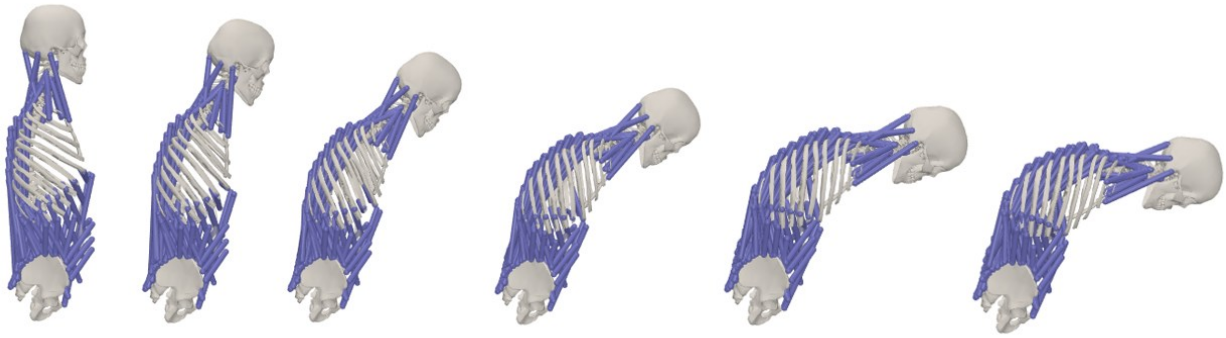

Figure 6: Static flexion poses from neutral standing to 100% ROM, at intervals of 20% ROM

Using the model and one of the motion files, OpenSim is used to perform an ID analysis. This analysis is used to calculate external joint moments required to satisfy equilibrium equations for the given static pose. The ID results are exported to be used as inputs in the FE modeling framework.

SO is then performed to calculate muscle forces required to maintain static equilibrium. The SO solver used by OpenSim uses an objective function which seeks to minimize the sum of squared muscle activations, subjected to two constraints. Constraint 1 requires all model equilibrium equations to be maintained. Constraint 2 requires muscle forces to remain within minimum and maximum bounds, such that muscle activation levels remain between 0 and 1. Muscle forces relate to muscle activation levels through relationships defined by the Millard2012EquilibriumMuscle model in OpenSim that consider force-length-velocity (FLV) relationships. The SO solver outputs a file containing all model forces, which includes active muscle forces, actuator forces, and passive forces produced from the joint bushings, which are then used as inputs in the FE modeling framework. Actuators considered in the model are the rib actuators, as defined by Bruno *et al.* [35],

and coordinate actuators for each DOF that produce joint torques in the event that muscles are not strong enough to maintain model equilibrium.

Lastly, SO is performed a second time, using the model, but without the action of muscle forces. In this case, model equilibrium is completely maintained by the action of coordinate actuators at each DOF. From the SO results, a Joint Reaction Analysis (JRA) is performed on all IVJs to extract joint loads expressed in the joint coordinate systems (CSs). In this case, since no muscle forces are acting on the model, the joint loads determined by the JRA analysis consist of those occurring due to gravity loads alone. By expressing the loads in the joint CSs, the loads in the y-direction correspond to compressive spine loads due to mass properties that are tangent to the curvature of the spine. These joint loads are hence referred to as FLs due to gravity and are used as inputs to the FE modeling framework. In this thesis, the FLs refer to the effect of gravity loads on the spine but do not include the compressive loads produced by muscle forces.

3.1.3. Step 2: Building the Model Geometry in Ansys

To perform co-simulations with MSK and FE models, it is necessary to ensure that the two of models are identical in terms of geometry and model structure. Hence, step 2 of this hybrid modeling framework consists of creating an identical model geometry to the FATLS model in the FE modeling platform. The FE modeling platform used in this project was Ansys, which consists of several software and GUIs for performing different types of engineering simulations. SpaceClaim is Ansys' 3D modeling software for creating, designing, and importing geometry. The FATLS model geometry files, namely the pelvis, sacrum, vertebrae, ribs, and sternum, were converted from *.vtp* to *.stl*, a format that is compatible with SpaceClaim, and imported into the latter. In importing the geometry files into SpaceClaim, the bodies were not positioned nor oriented correctly in space. OpenSim Creator (TU Delft Computational Biomechanics Lab, Delft, Netherlands) was used as an intermediary step to position the geometry correctly in space. This software was useful to easily identify the locations of the centres of mass (COMs) of the geometry meshes, as well as their orientation with respect to the ground frame. These positions and orientations were then used as a guide to reposition the geometry in SpaceClaim (Figure 7).

The head-neck geometry files were not imported into SpaceClaim and were modeled as a single point-mass as their geometry is complex and not required for the analyses performed in this

project. The abdomen bodies were also modeled as point masses. It should be noted that the geometry of the model was positioned correctly in space, but no information on connections and relationships between the bodies was established at this stage.

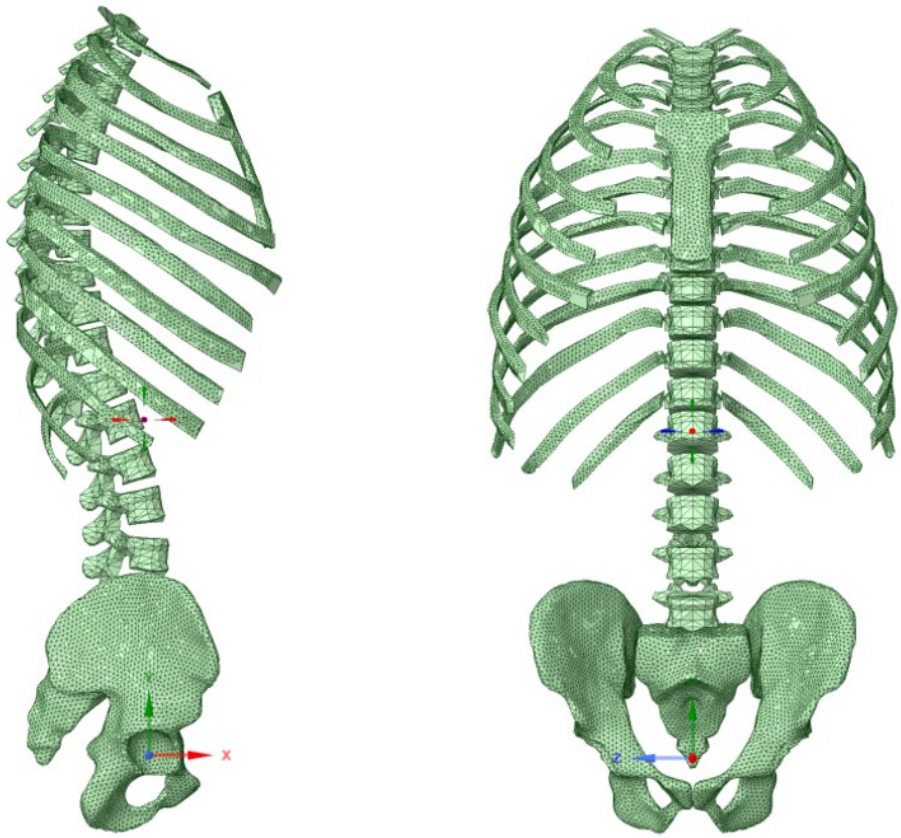

Figure 7: The FATLS model geometry imported and positioned in Ansys SpaceClaim

3.1.4. Steps 3-5: Ansys Model Structure, Loading Conditions, Simulation, and Exporting of Results

The process for generating engineering simulations using Ansys is through the Workbench application, where the user can integrate data from different Ansys softwares. In Workbench, the Static Structural Analysis System was selected, which acts as a template for performing static mechanical simulations. In the Static Structural Analysis System, the SpaceClaim geometry representing the FATLS model was imported. From there, the definition of the model structure and connections between bodies can be established, as well as the setup of boundary and loading conditions, and the execution of the desired simulation. These steps, which correspond to steps 3 to 5 of the co-simulation workflow, are all executed in the Static Structural Analysis System, via

the Ansys Mechanical software, which is used for performing FE analyses of mechanical systems. Steps 3 to 5 were accomplished through an automated scripting workflow, to facilitate the creation of any version of the FATLS model in Ansys. Different versions of the model could include scaled models or models with modifications made to muscles or joint properties for example. The detailed steps followed by the scripting workflow are described in the following paragraphs (Figure 8).

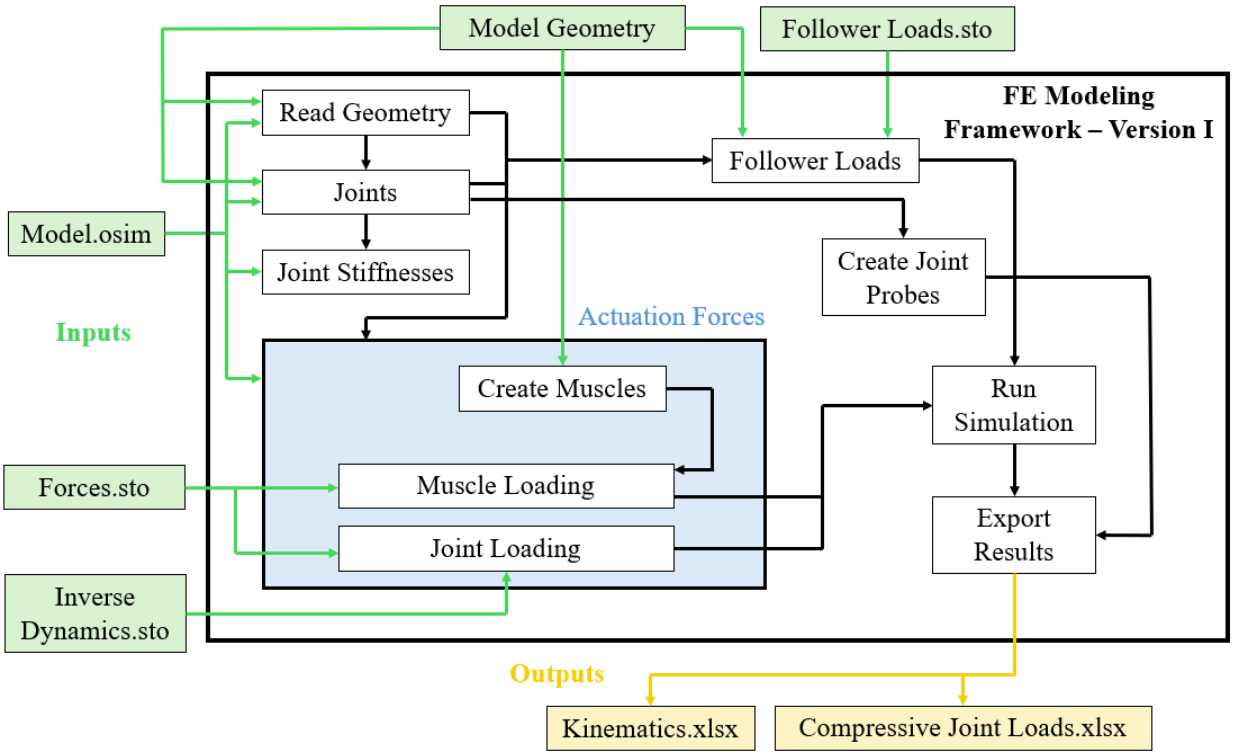

Figure 8: Flow chart for the FE modeling framework - version I

The script goes through a series of steps for reading information from the OpenSim model file and creating an identical model structure in Ansys. First, the geometry, imported from SpaceClaim, is used as a base for defining the model structure and establishing connections between bodies. The bodies' material properties are set to rigid, as all bodies in the MSK model are rigid as well and tissue deformations are not of importance at this stage. The script then performs the Read Geometry function, which scans the model file and extracts information from all the bodies in the model, such as their name, the location of their COM, and whether each body has an associated geometry. In cases where no associated geometry is found for a given body, a point mass is created at the body COM position to represent said body. This is the case for the head-neck and for the abdomen bodies.

The script then performs the Joints function, which extracts information on joints from the model file: joint names, location and orientation of joint CSs, and identification of parent and child bodies (connecting bodies) to each joint. From this information, joints are created in the model through a series of steps. CSs are created for each joint in the model, with positions and orientations matching those from the model file. Then, rigid remote points are created to define the connection between bodies. Remote points are commonly used in Ansys to define the behaviour and kinematics of certain portions of the geometry with a single point. In this model, remote points are used to scope/represent the faces of each body with a single point in space. For each joint, two remote points are created, for scoping the faces of the parent and child bodies. The remote points are both positioned at the origin of the joint CS. Joints are then created between the two remote points and are defined as fixed for all the weld joints in the model file, and as bushings for the IVJs. The definitions of the joint CSs are illustrated in Figure 9, where *A* shows the CS of all IVJs in Ansys, and *B* shows them in the OpenSim model. Their positions and orientations are identical in the two modeling platforms. Furthermore, the definition of the remote points for the L1L2 joint are illustrated as an example. The remote point scoping the faces of L2 (shown in red) is presented in *C,* and the remote point scoping the faces of L1 (also shown in red) is presented in *D*. Both remote points are positioned at the origin of the CS defining the location of the L1L2 joint.

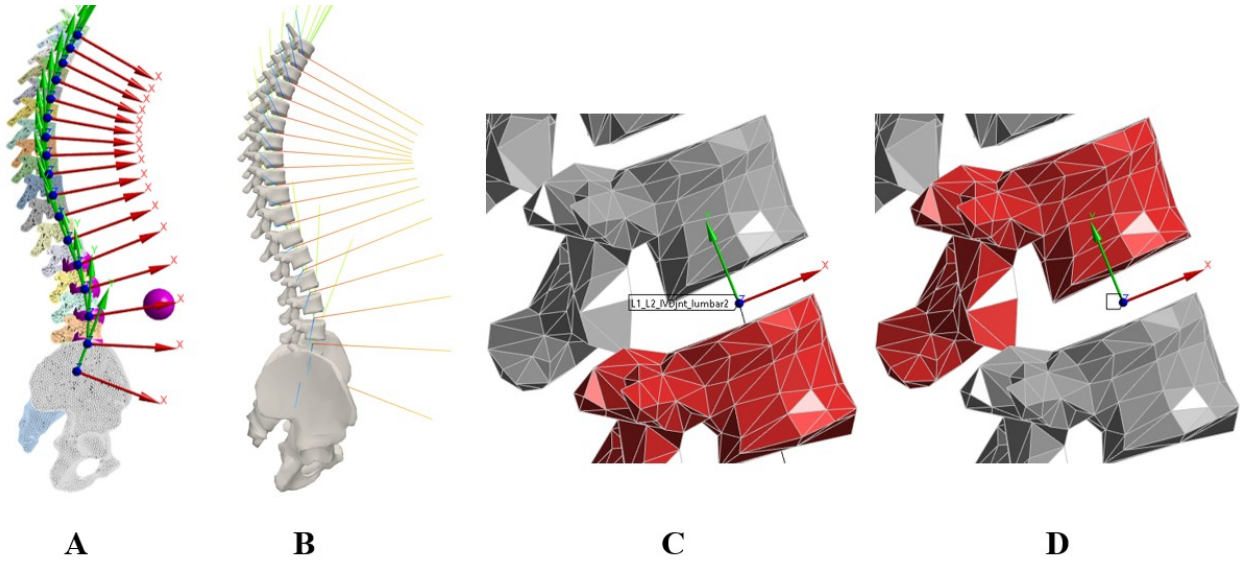

Figure 9: Joint coordinate systems in Ansys (A) and OpenSim (B), and remote points scoping L2 (C) and L1 (D)

For the bushing joints, the script then reads information corresponding to the joint stiffnesses in the model file and assigns the same stiffnesses to each bushing in Ansys.

Next, the script performs the Actuation Forces function, which follows a series of steps. First, it creates all muscles and represents them by uniaxial linear springs. Remote points are created in the locations of the muscle attachment points (origin and insertion), where each remote point scopes the faces of the body to which the muscle is attached. Longitudinal springs are created, connecting the remote points of the origin and insertion points of each muscle. Based on a user input, small spring stiffnesses (range of 1 to 30 N/m) are attributed to all muscles, except the neck muscles which are attributed stiffnesses of 40 N/m. A bit of trial and error is required from the user here to find the smallest stiffnesses attributable to the muscles to obtain simulation convergence. When stiffnesses are too low, the model can "explode", producing highly erroneous kinematics and model deformations, and it becomes impossible to reach convergence. However, large stiffnesses result in discrepancies in muscle modeling between Ansys and OpenSim. When performing a SO analysis in OpenSim, the solver computes active muscle forces specifically but does not consider passive forces or muscle stiffness properties. Hence, spring stiffnesses in Ansys should be minimized. Figure 10 illustrates the matching OpenSim and Ansys models, where the point masses representing the neck-head and abdomen and the muscle springs are visible.

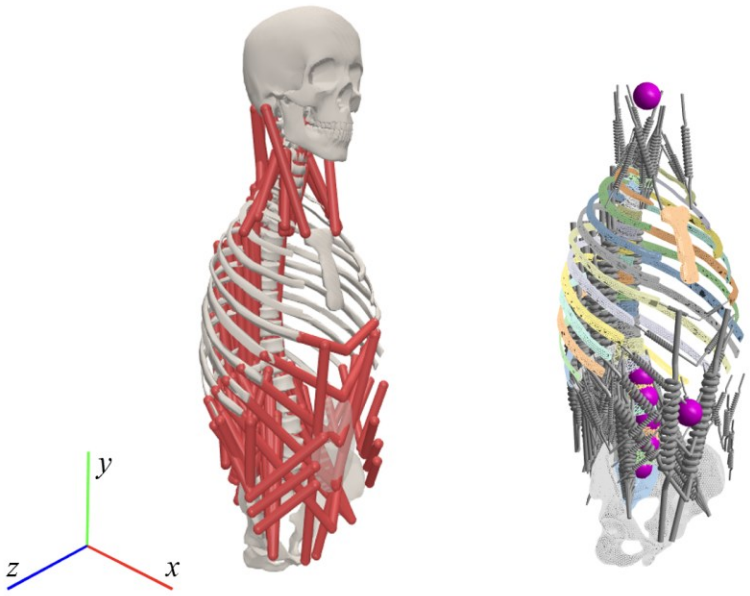

Figure 10: OpenSim FATLS model (left) and matching Ansys FE model (right)

Once the muscles have been created, the forces and ID files exported from the SO framework are read to assign muscle forces and joint loads to the model. The forces file contains values for muscle forces, torques produced by the joint bushings, and torques produced by coordinate

actuators. Forces produced by the rib actuators are ignored because these actuators are not being modeled in Ansys, for simplicity. Muscle forces are directly applied to each respective muscle spring in Ansys. Furthermore, pure moment loads are applied at each IVJ, about the z-axis, representing the combined action of joint moments created by mass properties of the bodies located above each joint, and coordinate actuators. These moment loads are determined from the following:

$$M_{app} = -ID - M_{joint} + M_{CoordAct} \quad \text{Eq. 5}$$

where M_{app} is the moment to apply at a given joint, ID is the moment extracted from the ID file, M_{joint} is the moment produced by the joint bushing, and $M_{CoordAct}$ is the moment produced by the coordinate actuator for the joint in question. Moments are only applied about the z-axis because the development of this workflow was focused on the simulation of static poses in the sagittal plane. Additional information on the derivation of Eq. 5 can be found in Appendix C.

The Follower Loads function is then performed to apply compressive spine loads produced by gravity as FLs at each IVJ. The loading conditions, namely the muscle forces, joint moments, and FLs, are applied to the Ansys model in its undeformed state (neutral spine position). Therefore, separating the gravity loads into joint torques and FLs is necessary to provide a correct representation of the gravity loads which act on the spine in the flexed configuration. A decision was made to omit the representation of shear loads produced by gravity at this stage, to simplifythe modeling process, although they should be considered and implemented in future developments of this work. The gravitational FLs are outputs of the JRA step of the SO framework. They are implemented at each IVJ with the definition of remote points. Let us take the definition of the FL structure of the L1L2 joint, illustrated in Figure 11, as an example. *A* illustrates a remote point scoping the faces of L1 that is created at the origin (0,0,0) of the L1L2 joint CS. *B* illustrates a second remote point scoping the faces of L2 that is positioned at -1 cm in the y-direction (0,-0.01,0) of the L1L2 joint CS. *C* illustrates a linear spring that is created connecting the 2 remote points, with a nominal length of 1 cm and a longitudinal stiffness of 1000 N/m. The FL forces are applied to the springs at each spinal level to create compressive loads. It should be noted that a high spring stiffness is selected for the follower loads because, while compressive loads are applied on the IVJs, the displacement of the springs or joint elements in compression is not the focus of the analyses being performed with this workflow.

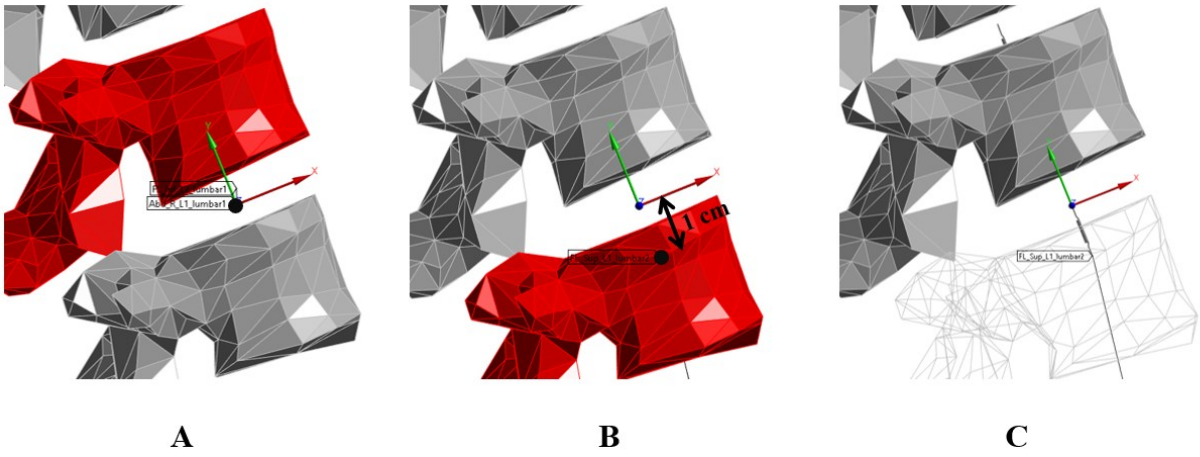

Figure 11: Remote points scoping L1 (A) and L2 (B) connecting the FL spring (C)

To run the simulation, corresponding loads are applied to each FL spring, muscle spring, and joint. The BCs consist of these loading conditions, namely the muscle forces, FLs due to gravity, and joint moments (gravity loads and coordinate actuators), and of the fixed connection between the pelvis and ground. All loading conditions are applied to the model simultaneously, over three load steps, where each load step represents a time interval of one second. Moreover, these loading conditions are applied to the model with the spine in its neutral shape (neutral standing pose). The joint moments applied to the model include moments produced by gravity loads when the spine would otherwise be in the studied flexion pose. Therefore, these drive the model displacement, flexing the spine structure, until static equilibrium is met with the moments produced by muscle forces and joint bushings. In doing so, the static equilibrium position simulated in Ansys should match the flexion pose that was simulated in OpenSim, as described in Chapter 3.1.2. The application of the loading conditions over three load steps was found to be sufficient for the model to reach static equilibrium.

Once the simulation has been performed, the script creates joint probes, which facilitate the monitoring of joint kinematics and compressive loads of the simulation. The joint kinematics being monitored are the relative angles between adjacent vertebral bodies (joint angles) in the sagittal plane. The joint compressive loads are expressed in the direction of the joint CSs so that each load is tangent to the curvature of the spine and corresponds to axial compressive loads. These results are then exported to Excel files. See Appendix D for a detailed schematic of the steps of the simulation workflow, including the calculation of muscle forces and gravity loads, the definition

of the model in Ansys, the application of the loading conditions, and the simulation performed in Ansys.

Lastly, to run multiple simulations on the same model, the script allows the user to input new forces, ID, and FL files onto a model that has already been generated in Ansys. This is useful to perform simulations of various static poses on the same model, without having to create the model every time.

3.2. Simulation Workflow – Version II

As will be discussed in the next Chapters of this thesis, version I of the workflow presented difficulties in producing converging simulations, and the range of flexion poses successfully simulated was very limited. Version II of the co-simulation workflow was developed in an attempt to expand the range of simulations that could be performed successfully in both modeling platforms. Version II follows a similar approach to version I of the workflow, but in this case, the stability of the model is considered in muscle force calculations. The key steps of version II of the workflow are the following: (1) utilizing a stability-constrained static optimization (SCSO) framework to estimate muscle forces required to satisfy equilibrium equations and stability constraints for a given static pose, (2) building the MSK model geometry in the FE modeling platform, (3) defining the model structure in the FE modeling platform to match the structure of the MSK model, (4) applying loading conditions to the FE model, and (5) performing the simulation and exporting desired results. The following Chapters will elaborate on each of these steps and on modifications made to version I of the workflow.

3.2.1. Model Modifications

Version II of the workflow was implemented with the use of the SCSO framework published by Akhavanfar *et al.* for considering stability constraints in the calculation of muscle forces [63]. Further modifications had to be made to the model presented in Chapter 3.1.1 so that it would be compatible for use with the SCSO framework.

The FATLS model included force-producing elements other than muscles, such as coordinate actuators and rib actuators. The SCSO framework does not allow for the consideration of actuators other than muscles when solving the equations of motion as it was developed for models which

are assumed to only require muscular activity to satisfy all constraints. Therefore, these elements were removed from the model. In removing the rib actuators from the model, it was found that the SCSO framework was unable to converge for any of the static poses being simulated. Even though the ribs are fixed, it was thought that the forces being generated by the rib actuators contributed to the equilibrium of the model. To remedy this, the intercostal muscles were added back into the model as a substitute for the rib actuators. In this way, the SCSO framework was able to find solutions for all static poses evaluated. Similar to version I, a sensitivity analysis, as will be detailed in Chapter 3.3, was performed to determine whether these modifications brought to the model significantly affected key modeling outputs. With these modifications, along with those described in Chapter 3.1.1, version II of the model had a total of 56 bodies, 51 DOF, and 458 musculotendon actuators (see Appendix E).

3.2.2. Step 1: Stability-Constrained Static Optimization Framework

As a first step, the FATLS MSK model is used with the MATLAB-based SCSO framework to calculate muscle forces that satisfy equilibrium equations and stability constraints for a given static pose. The framework uses the OpenSim 3.3 API and was adapted for its use with the FATLS model. The key steps taken to calculate muscle forces using this framework, along with modifications made to the published framework, are explained in the following paragraphs, and illustrated in Figure 12. More in-depth information on the processes and equations used in this script can be found in the original publication of the SCSO framework [63].

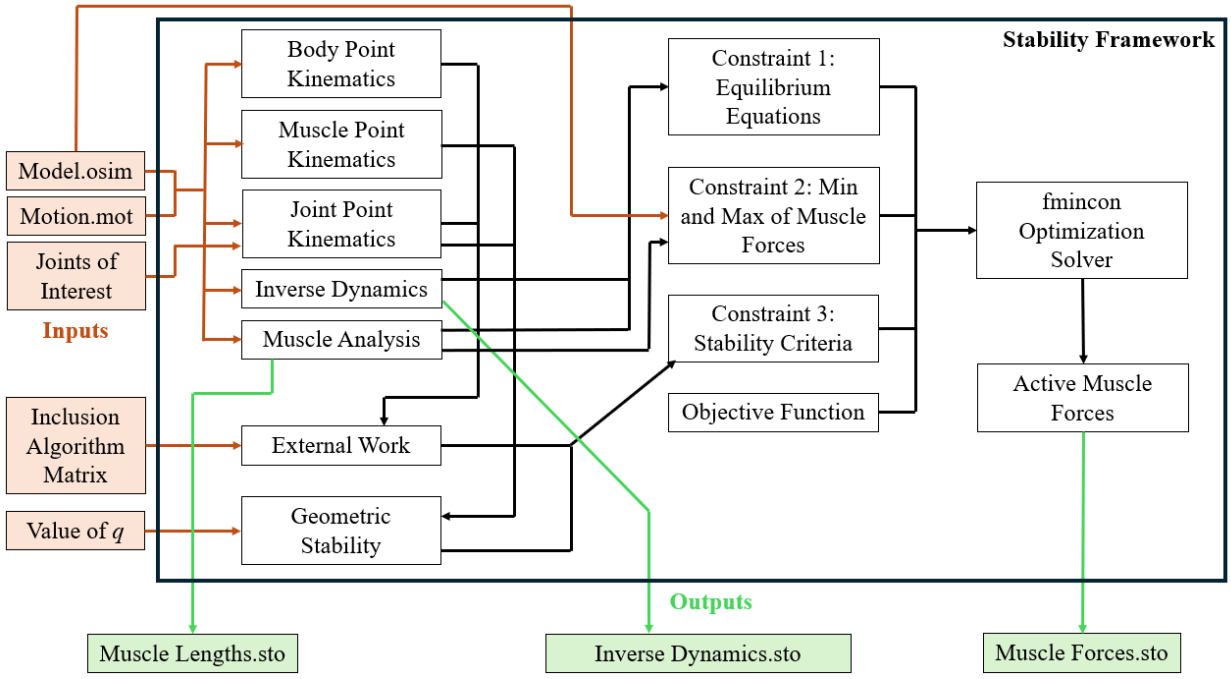

Figure 12: Stability-constrained SO framework flow chart

The model and motion file are used to perform several point kinematics analyses using the OpenSim API. The Body Point Kinematics function finds the location of the body COMs in the global space for the defined motion. The Muscle Point Kinematics function identifies the locations of the muscle origin and insertion points of all muscles in the model. The Joint Point Kinematics function identifies the locations of the Joints of Interest in the model. The Joints of Interest is a matrix manually defined by the user and comprises the identification of the joints for which it is required to satisfy stability constraints. In this case, because the model contains multiple weld joints, the Joints of Interest matrix contains the identification of the IVJs, which are the only joints in the model to have DOF and for which the stability criterion should be satisfied.

Furthermore, using the OpenSim API, the Inverse Dynamics Tool is used to calculate external joint moments required to satisfy equilibrium equations for the given static pose. Then, the Muscle Analysis Tool is used to determine the moment arms of all muscles with respect to each Joint of Interest.

Next, the body COMs and joint locations are used to calculate the external work (EW) on each joint due to mass properties. The original publication of the stability framework also calculated EW due to external loads, but this term was removed because no external loads are considered at

this time. Furthermore, the original publication of the stability framework used an inclusion algorithm to determine which bodies should be considered in the EW calculation. The inclusion of bodies for the calculation of EW at each joint is based on their relative heights, where body COMs located higher than a given joint are considered for EW. In the FATLS model, the ribs and sternum's mass properties are included in the mass properties of the vertebrae. Therefore, the ribs and sternum's masses are listed as zero in the model. Because of this, it was necessary to manually define the inclusion algorithm matrix to only include the vertebrae and head located above the Joints of Interest, and to exclude the ribs and sternum from all EW calculations.

Next, the muscle path points and the joint locations are used to calculate the geometric stability of the model, which quantifies the muscles' contributions to joint stability. To calculate geometric stability, the user must input a value for *q,* representing the muscle proportionality constant which relates muscle force (*F)* and length (*L*) to stiffness (*K*) (see Eq. 2).

Lastly, the framework uses the MATLAB built-in *fmincon* optimization solver to compute muscle forces. The optimization algorithm was designed to match OpenSim's SO solver while adding an additional stability constraint. The optimization algorithm's objective function is to minimize the sum of squared muscle activations, subjected to three constraints. Constraint 1 requires all model equilibrium equations to be maintained, such that forces produced by all muscles generate moments about each joint DOF that correspond to inverse dynamics results. Constraint 2 requires that the muscle forces remain within minimum and maximum bounds, such that muscle activation levels remain between 0 and 1. Muscle forces relate to muscle activation levels by multiplying the muscles' active FLV relationship to the activation level:

$$F = a \cdot e^{-\left(\tilde{L}^M - 1\right)^2/\gamma} \qquad \text{Eq. 6}$$

where *F* is the muscle active force, *a* the activation level, $\tilde{L}^M$ the normalized muscle fibre length, and γ a shape factor of a value of 0.5 which approximates the force-length relationship of individual sarcomeres [86]. The normalized muscle fibre length is extracted from the Muscle Analysis results.

Constraint 3 relates to the mechanical stability of the joints in the sagittal plane (about the z-axis) and requires the Hessian matrix of the potential energy of the model to be positive semi-

definite. To calculate stability, the framework employs the simplified stability equation developed by Potvin and Brown:

$$[GS]_{jm} \cdot [F]_{m1} - [EW]_{j1} \geq 0 \qquad \text{(Eq. 4)}$$

where *GS* is the matrix of geometric stability that each muscle provides to each joint, *F* is a vector of muscle forces, and *EW* is the matrix quantifying the external work about each joint [62-63]. The matrix dimensions j and m represent the number of joints of interest (number of model coordinates for which the stability is being calculated) and the number of muscles in the model, respectively. The geometric stability term, as detailed in Akhavanfar *et al.* [63] and Potvin and Brown [62], is defined as:

$$GS = \frac{A_x B_x + A_y B_y - r_z^2}{l} + \frac{q r_z^2}{L} \qquad \text{Eq. 7}$$

where A_x, B_x, A_y, and B_y are the x and y coordinates of the muscle nodes (attachment points) with respect to a joint of interest, r_z is the functional moment arm of the muscle with respect to the joint of interest, q is the user defined muscle proportionality constant, l is the length of the muscle acting on the joint of interest and represents the distance between the nodes A and B, and L is the total length of the muscle. In this thesis, all muscles are modeled with simple lines of action and only pass through two nodes, therefore l and L have the same value. The term r_z, which represents the functional moment arm of the muscle with respect to the joint of interest, is defined as the moment produced if the muscle exerted a force of 1 N:

$$r_z = \frac{B_x A_y - A_x B_y}{l} \qquad \text{Eq. 8}$$

As mentioned, the muscle nodes and muscle lengths are extracted from the Point Kinematics analyses and the Muscle Analysis functions of the script as detailed in the previous paragraphs, and the muscle proportionality constant is based on a user input value.

The active muscle forces computed from the optimization algorithm are exported to be used as inputs in the FE modeling framework along with the ID results and the muscle lengths for the motion provided.

3.2.3. Step 2: Building the Model Geometry in Ansys

The steps followed for building the model geometry in Ansys were exactly the same as those described in Chapter 3.1.3 for version I of the workflow.

3.2.4. Steps 3-5: Ansys Model Structure, Loading Conditions, Simulation, and Exporting of Results

The process for defining the model structure, loading conditions, producing simulations, and exporting results is very similar to the one described in version I of the workflow. Differences between the workflows occur in the implementation of muscle stiffnesses to satisfy stability requirements. The following paragraphs will elaborate on these differences and on added steps to version I of the workflow. The overall framework is illustrated in Figure 13.

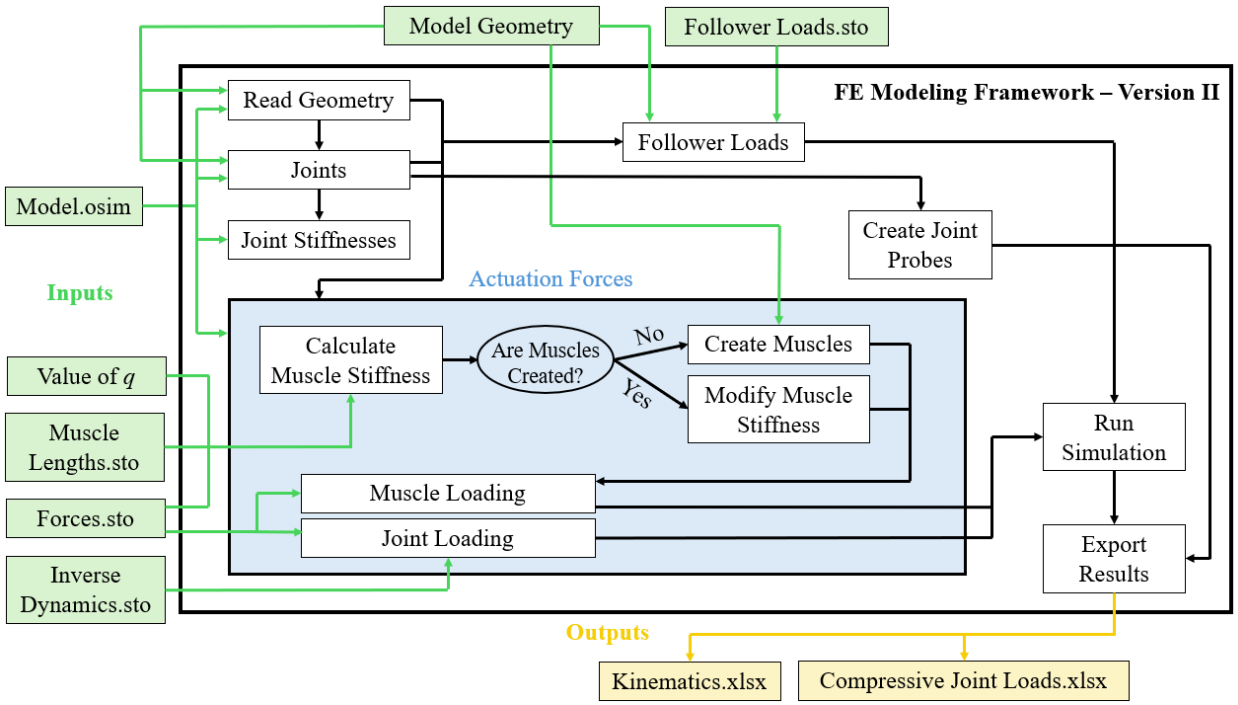

Figure 13: Flow chart of the FE modeling framework – version II

The Read Geometry, Joints, and Joint Stiffnesses functions are executed in the exact same manner as was described in Chapter 3.1.4.

Modifications were brought to the script in the Actuation Forces function. Here, the script begins by computing muscle stiffnesses for each muscle in the model using Eq. 2. The value of q is input by the user and the muscle lengths and forces are outputs of the SCSO framework. The

script then performs a check to determine whether the muscles have already been created in Ansys. This check is useful in the event that the model has already been created, but the user wishes to input new forces files and a new value of q to perform a simulation. In this case, the user would input the correct files and run the Actuation Forces function only instead of running the entire script, and the existing muscles would be assigned the newly calculated stiffnesses. On the other hand, if the model is being built for the first time and the muscles have not yet been created, muscle spring creation is executed in the same fashion as was described for version I of the framework, and the muscle stiffnesses calculated are assigned to each spring, respectively.

Once the muscles have been created, the forces and ID files are used to assign muscle forces and joint loads to the model, in the same way as in version I of the framework. The forces file input by the user must be of the same format as the forces file that is usually output from the SO analysis in OpenSim, containing muscle forces, torques produced by the joint bushings and forces/torques produced by coordinate actuators. The muscle forces are direct outputs from the SCSO framework, and bushing torques, which can easily be obtained from a SO analysis in OpenSim, are added to the muscle forces file by the user. Muscle forces are directly applied to each respective muscle spring in Ansys. Pure moment loads are applied at each IVJ, the values of which are determined by Eq. 5. When using the SCSO framework, coordinate actuators cannot be considered, in which case the $M_{CoordAct}$ term is zero and the moment applied at each joint corresponds only to moments produced by the mass properties of the model.

Lastly, compressive FLs are applied to each IVJ in the same way as in version I of the framework. Because the computation of muscle forces is determined using the SCSO framework which doesn't perform SO via the OpenSim API, the steps for obtaining the FL file were not illustrated in Figure 12. These steps are performed separately by the user, using the OpenSim GUI or API, following the same method as was described in version I of the framework.

To run the simulation, the loading conditions, namely the muscle forces, joint moments, and FLs due to gravity, are simultaneously applied to the model in a neutral spine pose, over three load steps. Similar to version I, these loading conditions drive the flexion of the spine until static equilibrium is met. Results being monitored by the joint probes are exported to Excel files.

3.3. Model Sensitivity Analysis

The original FATLS model was validated extensively for lumbar compressive joint loads, at L1L2 and L4L5 levels specifically, in both static and dynamic tasks, against vertebral implant load and IDP measurements [12, 35]. Modifications, as described in Chapters 3.1.1 and 3.2.1, were brought to the model to simplify its representation in Ansys, to avoid convergence issues, and to make it compatible for use with the SCSO framework. Therefore, a sensitivity analysis was carried out to evaluate the sensitivity of the axial compressive loads on IVJs following each model modification. This was necessary to determine whether the modifications brought to the model had significant impacts on model outputs that were of interest for the co-simulation workflow, and to determine whether compensatory changes should be implemented to account for the simplifications brought to the models.

3.3.1. Sensitivity Analysis – Workflow Version I

The sensitivity of compressive joint loads was evaluated for each of the modifications brought to the model for version I of the co-simulation workflow. Various versions of the model were generated to compare the compressive joint loads after each of the modifications listed in Chapter 3.1.1. The model versions and their modifications are listed in Table 2. Model0 corresponds to the original model, with only the legs removed and pelvis fixed to ground, and serves as the base model for comparing all other model versions.

Table 2: Models used to evaluate the sensitivity of compressive joint loads

Model Version	Modifications from Original Model
Model0	• Legs removed • Pelvis fixed to ground
Model1	• Legs removed • Pelvis fixed to ground • Arms and muscles attaching to the arms removed
Model2	• Legs removed • Pelvis fixed to ground • Arms and muscles attaching to the arms removed • Intercostal muscles removed
Model3	• Legs removed • Pelvis fixed to ground

	• Arms and muscles attaching to the arms removed • Intercostal muscles removed • Rib actuators removed
Model4	• Legs removed • Pelvis fixed to ground • Arms and muscles attaching to the arms removed • Intercostal muscles removed • Abdomen-sacrum joint welded • Muscles were reduced to origin and insertion points only

Compressive joint loads were evaluated by performing SO followed by JRA using OpenSim, for each model version. These analyses were performed for all motion files listed in Table 1, to simulate the entire ROM of the spine in forward flexion. However, only 0 to 60% of the ROM was simulated for Model3, as SO started to fail for larger ROM poses. For Model0, which included the upper limbs, the flexion poses were simulated with the arms always vertically pointing towards the ground.

To assess the sensitivity of the model for each of the key modifications made to it, linear regression was carried out between the compressive joint loads of each model and trunk flexion angle, at the L1L2 and L4L5 levels specifically. To evaluate the strength of the linear relationships between the joint loads of the different model versions over the range of trunk flexion poses simulated, Pearson's correlation coefficients were estimated at the L1L2 and L4L5 levels.

Mean absolute percent differences (MAPD) in joint loads between the different model versions and the original model (Model0) were also evaluated to quantify the magnitude of the variation in joint loads occurring with each modification brought to the original model.

3.3.2. Sensitivity Analysis – Workflow Version II

In version II of the workflow, it was required to remove the rib actuators from the model. In order for the SCSO framework to find convergent solutions, the intercostal muscles were added back into the model. Therefore, a sensitivity analysis was performed to compare joint loads between the original model (Model0) and the model used for version II of the workflow, which will be referred to as Model5. To evaluate the sensitivity of the model, linear regression was carried

out between the compressive joint loads of Model5 and Model0 and trunk flexion angle, at the L1L2 and L4L5 levels specifically. To evaluate the strength of the linear relationships between the joint loads of the two models over the range of trunk flexion poses simulated, Pearson's correlation coefficients were estimated at the L1L2 and L4L5 levels. The MAPD were also calculated between the joint loads of the two models.

3.4. Workflow Verification

A key step to modeling workflows includes their verification, to ensure that the algorithms they contain are implemented correctly [87]. Verification of the SCSO framework was described in its original publication, by checking that muscle forces produced by the algorithm were the same as those produced by OpenSim's SO tool at high values of q ($q > 13$) [63]. The same verification procedure was followed to verify the SCSO framework following the modifications described in Chapter 3.2.2.

Both versions of the hybrid modeling framework were verified by manually inspecting the locations and orientations of joint and body CSs, bushing stiffnesses, locations of muscle attachment points, and muscle stiffnesses in Ansys. Tests were done to ensure that the application of FLs produced the same joint loads as those extracted from OpenSim without the application of muscle forces. Tests were also done to verify that muscle forces were applied to the correct muscle springs and that the correct joint moments were applied at each spinal level in Ansys. Each of these tests was performed for various scaled models.

3.5. Workflow Validation

Another key step in the development of modeling workflows includes their validation. According to the ASME definition, validation is "the process of determining the degree to which a model is an accurate representation of the real world from the perspective of the intended uses of the model" [87]. Therefore, the co-simulation workflow must be validated to ensure that the modeling choices and assumptions made in the definition of the FE model and application of loading conditions accurately reproduce the MSK simulations performed in OpenSim. The FATLS

model was previously validated for lumbar spine joint loads during static and dynamic lifting tasks, which are movements that occur mainly in the sagittal plane. Hence, validation studies comparing the kinematics and joint compressive loads between the FE and MSK models, for static flexion poses, were conducted for both versions of the co-simulation workflow. Moreover, even though the MSK model was validated for lumbar joint loads only, both lumbar and thoracic joint compressive loads will be considered in the validation study, to determine how well the FE model represents the MSK model at all levels.

3.5.1. Validation of the Co-Simulation Workflow – Version I

The generic model was scaled to produce six male models, corresponding to the 10th, 50th, and 90th percentiles for mass and 50th and 90th percentiles for standing height. The models were scaled for mass based on the values published by Cassola *et al.* [88]. The generic FATLS model corresponds to the 50th percentile height, and previously published marker data of a participant representing the 90th percentile height were used to scale the model height [12]. The six models' heights and masses are listed in Table 3, where each model's name reflects its percentile in height (H) and mass (M).

The models were scaled using OpenSim's Scale Tool for analyses performed in the SO and SCSO frameworks. To scale the geometry of the model in Ansys SpaceClaim, a function was added to the automated scripting workflow, which gathers information from the generic and scaled model *.osim* files and scales the geometry accordingly (See Appendix F).

Table 3: Height and mass of the models used for validation of the simulation workflow

	H50_M10	**H50_M50**	**H50_M90**	**H90_M10**	**H90_M50**	**H90_M90**
Height (cm)	175	175	175	185	185	185
Mass (kg)	66	79	98	66	79	98

To validate the co-simulation workflow, the six scaled models were used to simulate the flexion poses listed in Table 1 (Chapter 3.1.2), following the steps of version I of the simulation workflow. As mentioned in Chapter 3.1.4, trial and error were required to find the smallest stiffnesses that could be attributed to the muscles for the simulation to converge in Ansys. Reasonable stiffnesses, ranging between 1 and 30 N/m (and 40 N/m for neck muscles) could be attributed to the models for the poses ranging between 10 and 40% of the ROM. The stiffnesses attributed to the muscles of each model for the simulated poses are listed in Table 4. Neutral spine (0% ROM) and large

flexion poses required significantly larger muscle stiffnesses (stiffness > 100 N/m) for simulations to converge, which did not produce matching kinematics with the OpenSim model. The same outcome was observed for the 40% flexion pose with the H90_M90 model (cell indicated with (-)). Thus, these simulations were not included in the analyses used to validate the simulation workflow.

Table 4: Muscle stiffnesses attributed to models for each flexion pose in Ansys

	Muscle Stiffnesses (N/m)			
	10% ROM	**20% ROM**	**30% ROM**	**40% ROM**
H50_M10	1	1	1	22
H50_M50	4	4	4	18
H50_M90	4	4	4	20
H90_M10	1	1	1	22
H90_M50	1	1	1	27
H90_M90	2	2	2	-

3.5.2. Validation of the Co-Simulation Workflow – Version II

Similarly, the six scaled models of Table 3 were used to simulate the flexion poses listed in Table 1, but this time following the steps of version II of the co-simulation workflow. To use the SCSO framework, the user must input a value for q, the muscle proportionality constant, that is used in stability calculations. During the development of the workflow, it was found that setting q to larger values resulted in larger differences between kinematics obtained in the FE and MSK models. This occurs because the SCSO framework computes muscle forces that will satisfy both equilibrium and stability constraints for a given static flexion pose. In Ansys, the loading conditions are applied to the model in the neutral spine position. The application of the loading conditions perturbs the model which causes the spine to flex forward until equilibrium is met. This equilibrium state corresponds to the flexion pose that was input into the SCSO framework. However, when the parameter q increases in value, so do the stiffnesses associated with the muscle springs in Ansys. Stiff muscles effectively stiffen the model, limiting the flexion of the spine that is observed. Hence, to reduce the kinematic differences between the FE and MSK models, the smallest value of q possible was selected for each model and each simulated pose to achieve convergence in both modeling platforms. The values used for each simulation are listed in Table 5. Cells with (-) are cases where the simulation was not included in the analyses.

Table 5: Muscle proportionality constants, q, required for each simulation

Percent ROM in Flexion (%)	H50_M10	H50_M50	H50_M90	H90_M10	H90_M50	H90_M90
0	1	1	-	2	1	-
10	0.5	0	0.5	0.5	1	2
20	0.5	0	0	0.5	0.5	1
30	0	0	0	0	0	1
40	0	0	0.5	0	0.5	1
50	0	0	0.5	0.5	0.5	1
60	0	0	1	2	2	2
70	0.5	0.5	-	2	2	2
80	0.5	-	-	2	2	-

It was possible to simulate postures ranging from 0 to 80% ROM in flexion using values of q between 0 and 2. While it was possible to achieve convergence for the 90 and 100% ROM poses with higher values of q, these were not included in the analyses as values of q larger than 2 produced models in Ansys that were too stiff to reach the desired kinematics. This was also the case for all cells indicated with (-) in Table 5.

3.5.3. Statistical Analyses

Following all simulations performed for the validation studies, results being tracked by joint probes, namely rotations in the sagittal plane and axial compressive loads at the IVJs, were exported for analysis. The kinematics and joint loads obtained from the simulation in Ansys were compared to those from the OpenSim motion file and from the JRA results, respectively. Comparisons between models were achieved by calculating the absolute differences (Eq. 9) and absolute percent differences (Eq. 10) between corresponding joint kinematics/loads of each model.

$$\text{Absolute Difference} = |AnsysValue - OpenSimValue| \quad \text{Eq. 9}$$

$$\text{Absolute Percent Difference} = \frac{|AnsysValue - OpenSimValue|}{OpenSimValue} * 100\% \quad \text{Eq. 10}$$

The maximum and mean ± standard deviation (SD) differences were calculated over all joints and all six models. Moreover, correlations were estimated between model kinematics and joint loads

as the flexion of the spine increased using Spearman's Rank Order correlation coefficient. This correlation analysis was used with the assumptions that the data are not normally distributed but that there is a monotonic relationship between the variables being compared. The strengths of the correlations were evaluated such that coefficients between 0.70 and 0.89, and between 0.90 and 1.00 indicate strong and very strong correlations, respectively [89].

4. RESULTS

4.1. Model Sensitivity Analysis

4.1.1. Sensitivity Analysis – Workflow Version I

The joint compressive loads at the L4L5 and L1L2 levels are presented in Figure 14 for static poses ranging from 0 to 100% of the spine ROM in forward flexion. All model versions, except for Model3, seem to have similar joint loads in poses from 0 to 70% ROM. In that range, loads from the modified models appear to be less than those in Model0 in standing, and they surpass those of Model0 as the flexion angle increases. From 80 to 100% ROM, larger differences are observed between the joint loads of the different models. In fact, coordinate actuators were included in each model version to assure simulation convergence when performing a SO analysis in the event that the muscles were not strong enough to satisfy equilibrium constraints. Activation of the coordinate actuators in Model0 was near zero for poses in the 0 to 70% ROM range. Their contribution to joint torques started to increase for the 80% ROM pose and exceeded 10% of total joint torques in some joints in the 90-100% ROM poses. This is indicative that the model is not strong enough to satisfy equilibrium constraints in large ROM poses, hence larger discrepancies in joint loads are observed in that range when modifications or simplifications are brought to the model. A significant contribution from coordinate actuators was also observed in that range for Model1 and Model2, but not Model4. As for Model3, joint loads from 0 to 60% of the spine ROM only are presented because, as previously mentioned, SO started to fail in larger flexion poses. Furthermore, Model3 required significant contributions from coordinate actuators for all flexion poses simulated, indicating that the model is not strong enough when rib actuators are not included. Moreover, joint loads increased rapidly as the flexion angle of the spine increased, resulting in large differences with Model0. It is for these reasons that the rib actuators were re-integrated into Model4.

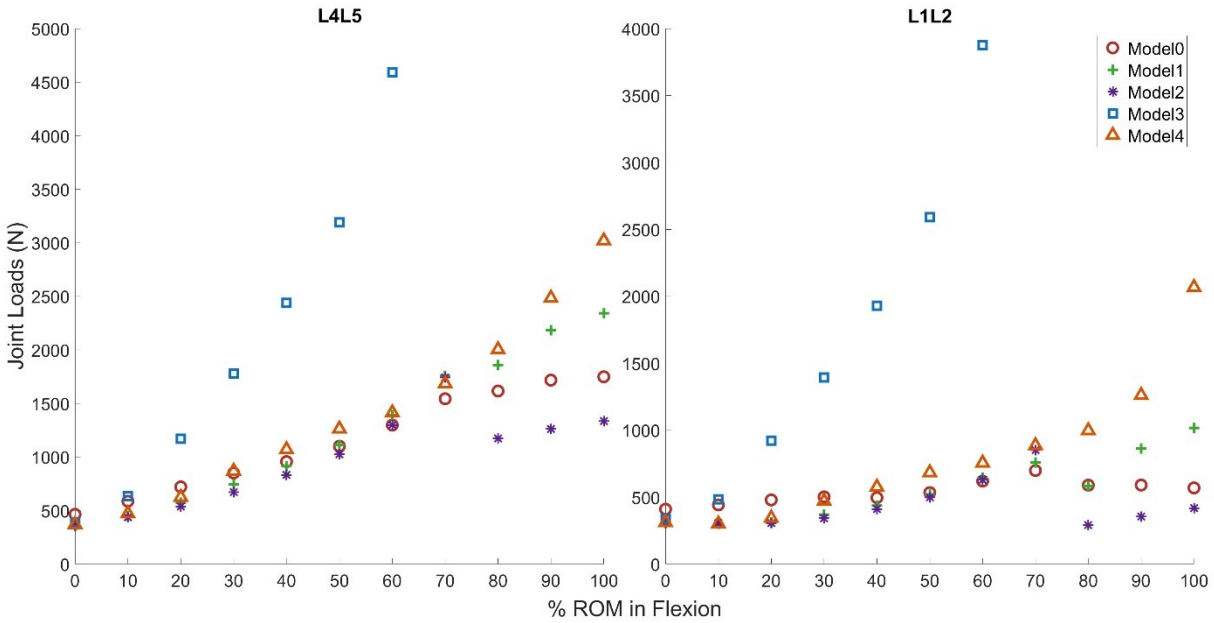

Figure 14: Joint compressive loads for L4L5 and L1L2 – model version 0 to 4

In order to evaluate the linear relationships between each modified model and Model0, linear regressions were performed to determine if joint loads increase proportionally between models as the flexion angle increases. The regression analyses, illustrated in Figure 15 and Figure 16, were performed for the 0 to 70% range of flexion (and 0 to 60% for Model3), only considering the ROM where the models were strong enough to satisfy equilibrium equations. At the L4L5 joint (Figure 15), the linear trend lines show that joint loads in models 1, 2, and 4 increase at 1.33, 1.29, and 1.28 times the rate of Model0 as flexion angle increases, respectively. The relationship between each of these models to Model0 are very similar, suggesting that the modifications made to models 2 and 4 did not produce significant additional changes in joint load patterns following the modifications of Model1. The regression coefficient for Model3 is much larger, indicating that joint loads in Model3 increase 5.09 times more than Model0 as flexion angles increase. This large increase in joint loads is also observed in Figure 14. No comment can be made on the significance of the linear relationships between the joint load patterns of each model as these were evaluated only for the unscaled model and for select flexion angles, resulting in very few data points.

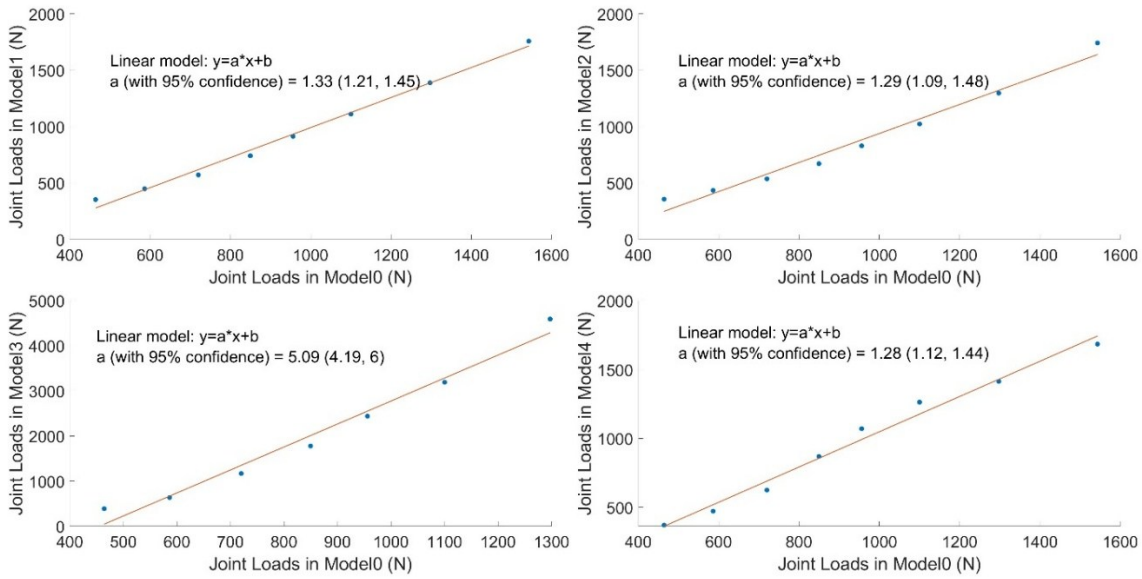

Figure 15: Linear regressions between modified models and Model0 for the L4L5 joint

Similar observations are made considering the relationships between models at the L1L2 joint (Figure 16), but the joint loads appear to increase at larger rates in all models compared to Model0 than at the L4L5 joint. Moreover, the relationships between the models do not appear to be completely linear at the L1L2 joint. There are also larger differences between the coefficient *a* of models 1, 2, and 4 than at the L4L5 joint, indicating that the modifications made to the models had greater repercussions at higher levels of the lumbar spine.

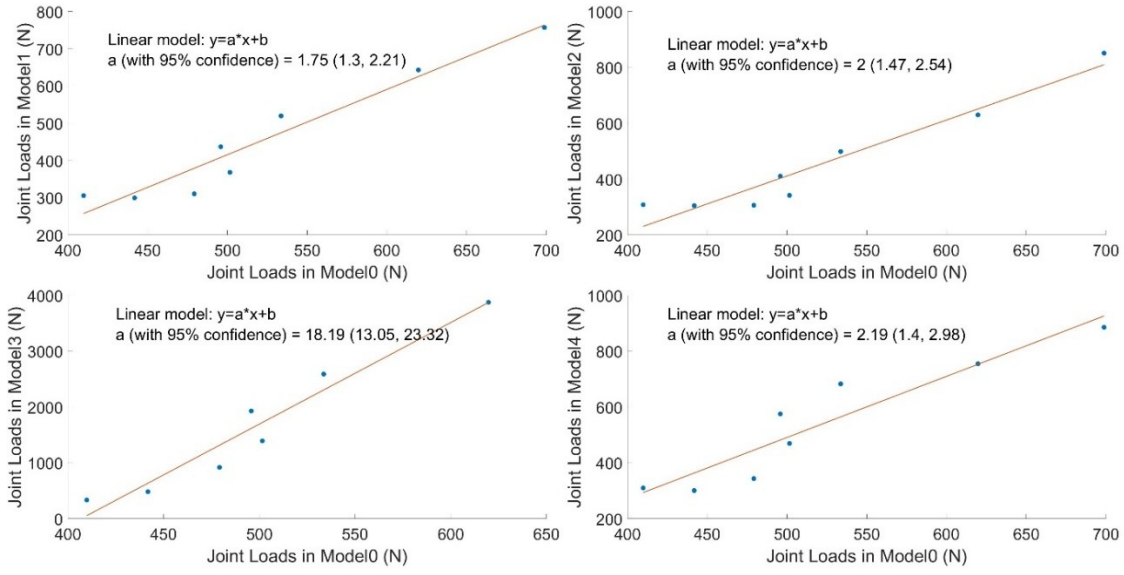

Figure 16: Linear regressions between modified models and Model0 for the L1L2 joint

To evaluate the strength of the linear relationship between the compressive joint loads of each model version to Model0, Pearson's correlation coefficient was estimated over 0 to 70% ROM for models 1, 2, and 4, and over 0 to 60% ROM for Model3. Table 6 presents the correlation coefficients between each model version and Model0. Very strong correlations ($r > 0.90$) were found between each model and Model0 for both L4L5 and L1L2 joints. No comment can be made on the significance of the correlations as the data points were not normally distributed due to a very small sample size. Furthermore, as previously noted, the relationships between the joint loads of the different model versions do not appear to be completely linear at the L1L2 joint, therefore it is expected to find slightly lower correlation coefficients at this spinal level.

Table 6: Correlation coefficients between the joint loads of the modified models and Model0

	Model1 – Model0	**Model2 – Model0**	**Model3 – Model0**	**Model4 – Model0**
L4L5	1.00	0.99	0.99	0.99
L1L2	0.97	0.97	0.97	0.94

Quantifying the magnitude of the absolute differences between the joint loads of each model version can provide additional insight on the effect that each model modification had on joint loads. Therefore, the MAPD were calculated, over 0 to 70% ROM (and over 0 to 60% ROM for Model3), between each model version and Model0 (Table 7). The MAPD between Model1 and Model0 was between 10 and 20%, indicating that removing the arms from the model had a significant impact on joint loads. The MAPD only increased by 2.7% and 3%, at L4L5 and L1L2 respectively, from Model1 to Model2, indicating once again that removing the intercostal muscles caused little change on the joint loads. The MAPD between Model3 and Model0 were greater than 100% and 200% at L4L5 and L1L2, respectively. These differences were visually observed in Figure 14, where it was noted that the action of rib actuators significantly contributed to the strength of the model and to joint loads. Lastly, the MAPD between Model4 and Model0 were comparable to those of Model1 and Model2.

Table 7: Mean absolute percent differences between joint loads of each model version and Model0

IV Joint	**Model1 – Model0**	**Model2 – Model0**	**Model3 – Model0**	**Model4 – Model0**
L4L5	13.3	16.0	113.6	12.5
L1L2	18.3	21.4	214.0	22.9

4.1.2. Sensitivity Analysis – Workflow Version II

In version II of the co-simulation workflow, it was required to remove the rib actuators from the model and reintegrate the intercostal muscles for simulation convergence using the SCSO framework. The joint loads calculated with this version of the model (Model5) are compared with the original model (Model0) in Figure 17. Model4 joint loads are illustrated as well to visualize joint loads in comparison to those obtained in version I of the workflow. Similar to observations made in Chapter 4.1.1, the joint loads in Model5 are lower than those in Model0 in low flexion angles, but they increase to larger values than those in Model0 and Model4 as the flexion angle increases. In model 5, no coordinate actuators were included in the model because these could not be considered in the SCSO framework. As a result, the SO tool failed for the 100% ROM flexion pose, indicating once again that the model is not strong enough to satisfy equilibrium constraints in large flexion poses. However, Model5 did not exhibit large increases in joint loads with flexion angle as was observed with Model3, even though the rib actuators were not included in the model. Moreover, larger contributions of the intercostal muscles were observed in Model5 than in Model0 and Model1, which included them as well, indicating that these muscles are more active in the model when rib actuators are not present.

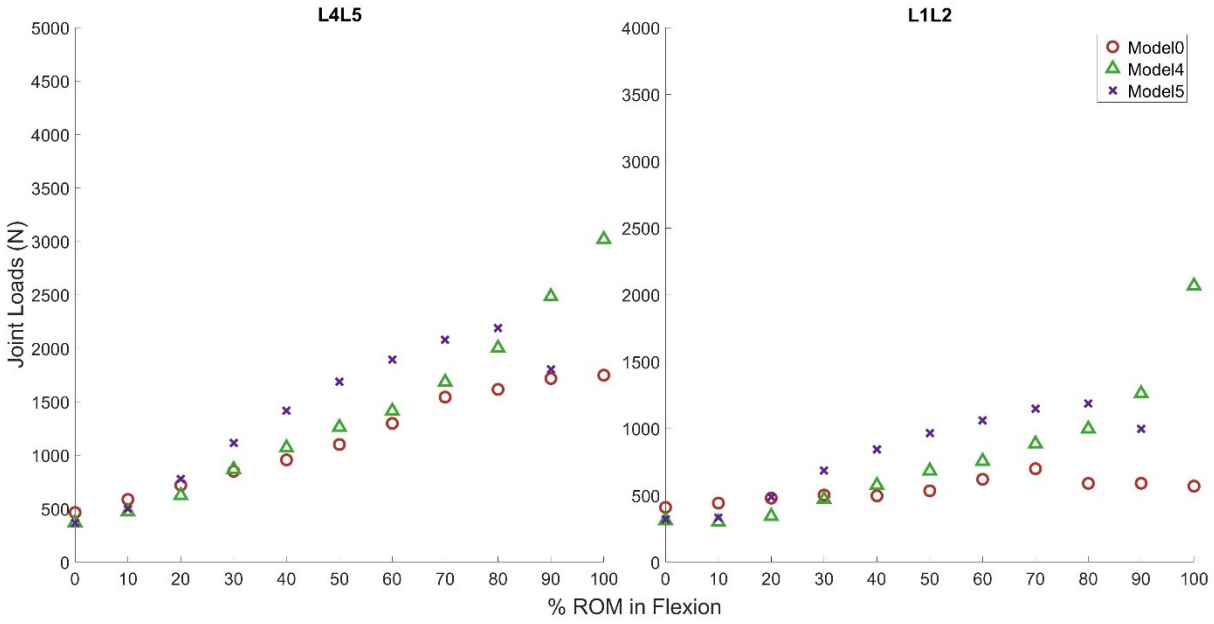

Figure 17: Joint compressive loads for L4L5 and L1L2 – model version 0, 4 and 5

A linear regression, illustrated in Figure 18, was performed between the joint loads of Model5 and Model0, and only for the 0 to 70% range of flexion. At both L4L5 and L1L2 joints, the joint loads in Model5 increased at higher rates than Model0 as the flexion angle increased. The coefficients a are larger than those for models 1, 2, and 4, but smaller than those of Model3, even though the rib actuators were not included in the model. Furthermore, like observations made for the other models, the relationship between the joint loads of Model5 and Model0 does not appear to be linear at the L1L2 joint, indicating that modifications made to the model had a greater impact at higher spinal levels.

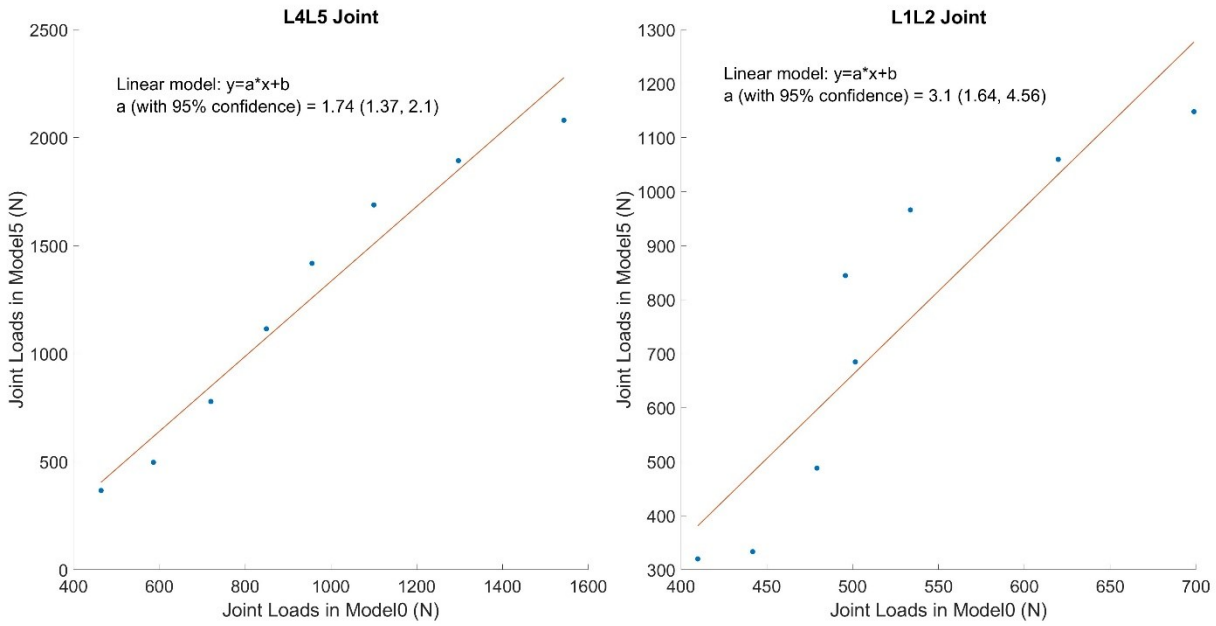

Figure 18: Linear regressions between Model5 and Model0

To evaluate the strength of the linear relationship between the compressive joint loads of Model5 and Model0, Pearson's correlation coefficient was estimated over 0 to 70% ROM. Very strong correlations were observed between the joint loads of the two models at both L4L5 and L1L2 levels, with $r = 0.98$ and $r = 0.90$, respectively. Once again, no comment can be made on the significance of the correlations, and lower correlations are observed at the L1L2 level due to the nonlinearity of the relationship between the two models at this joint.

The MAPD between Model5 and Model0 were computed to evaluate the effect of the modifications made to the model for the SCSO framework. Focusing on 0-70% ROM poses, the MAPD were 32.3% and 46.4% for the L4L5 and L1L2 joints, respectively. The differences in joint

loads between Model5 and Model0 are larger than those observed with models 1, 2, and 4, but substantially smaller than those observed with Model3.

4.2. Workflow Validation

4.2.1. Validation of the Co-Simulation Workflow – Version I

To validate the co-simulation workflow, the outputs, namely the IVJ kinematics and compressive loads, of simulations performed using the six scaled models were compared between the modeling platforms. Table 8 presents the maximum and mean absolute differences between the kinematics and compressive joint loads of the FE and MSK models using version I of the co-simulation workflow. Both kinematic and joint load differences increase with the spine flexion. The mean kinematic differences are all less than 1° and the maximum differences smaller than 2°. The mean joint load differences are all smaller than 30 N and the maximum differences smaller than 70 N.

Table 8: Maximum and mean absolute differences in kinematics and joint loads between modeling platforms, categorized by flexion pose – version I

Percent ROM in Flexion (%)	Kinematic Absolute Differences (°)		Joint Load Absolute Differences (N)	
	Max	Mean ± SD	Max	Mean ± SD
10	1.13	0.19 ± 0.28	41.00	7.32 ± 8.91
20	1.44	0.23 ± 0.32	41.41	9.30 ± 9.52
30	1.70	0.32 ± 0.36	52.79	13.69 ± 12.55
40	1.72	0.71 ± 0.46	65.88	23.48 ± 16.47

To better quantify the significance of these differences, Table 9 presents them as percent differences. Although the kinematic differences in Table 8 are always less than 2°, these differences often represent a large proportion of the rotation angles at each joint, which vary between 0° and 6° over all spinal levels and the 10 to 40% ROM simulated. This is observed in the maximum percent differences which are all greater than 100%. The percent differences in joint loads however are much smaller, where the maximum percent differences are less than 40% and the mean percent differences less than 15%. This is because the joint loads throughout the spine and through the ROM simulated reach values up to 1400 N. It is interesting to note that the absolute kinematic differences in Table 8 increase as the spine flexion increases, but the opposite is observed when

looking at the percent differences. This occurs because, although the absolute differences increase with flexion angle, the individual intervertebral angles also increase. Thus, the proportion of absolute differences to observed intervertebral angles become smaller as the spine flexion increases.

Table 9: Maximum and mean absolute percent differences in kinematics and joint loads between modeling platforms, categorized by flexion pose – version I

Percent ROM in Flexion (%)	Kinematic Absolute Percent Differences (%)		Joint Load Absolute Percent Differences (%)	
	Max	Mean ± SD	Max	Mean ± SD
10	416	54.4 ± 79.9	26.8	4.82 ± 6.13
20	180	32.9 ± 42.7	27.4	5.94 ± 6.72
30	150	29.3 ± 34.4	28.5	7.71 ± 8.42
40	163	41.5 ± 31.2	37.3	11.3 ± 10.5

The data shown in the previous tables often presents maximum differences which are largely outside the bounds of the SD, indicating potential outliers in the data. To identify whether peaks in differences occur at specific levels of the spine, the kinematic and joint load absolute percent differences were plotted for each intervertebral level in Figure 19 and Figure 20, respectively. The differences plotted represent the mean ± SD over all models, where each subplot is a different flexion pose. In Figure 19, differences between Ansys and OpenSim kinematics are near zero in the lumbar and lower thoracic spine, except for the 40% ROM pose, where differences are more significant throughout the spine. On the other hand, for all poses simulated, there are obvious peaks in kinematic differences at the T8T9, T9T10, and T1T2 levels which often surpass 100% differences. Peaks are also observed at the T5T6 and T6T7 levels in the 10% ROM poses. In Figure 20, joint load differences are negligible in the lumbar and low thoracic levels. In the upper thoracic spine, joint load differences are more significant, although less than 40% in all cases. No obvious peaks are observed in joint load differences in the thoracic spine. It should be noted that large ranges are presented for the SD, as these simulations were generated with six models varying in height in weight, resulting in a large variability of joint loads and differences observed between Ansys and OpenSim.

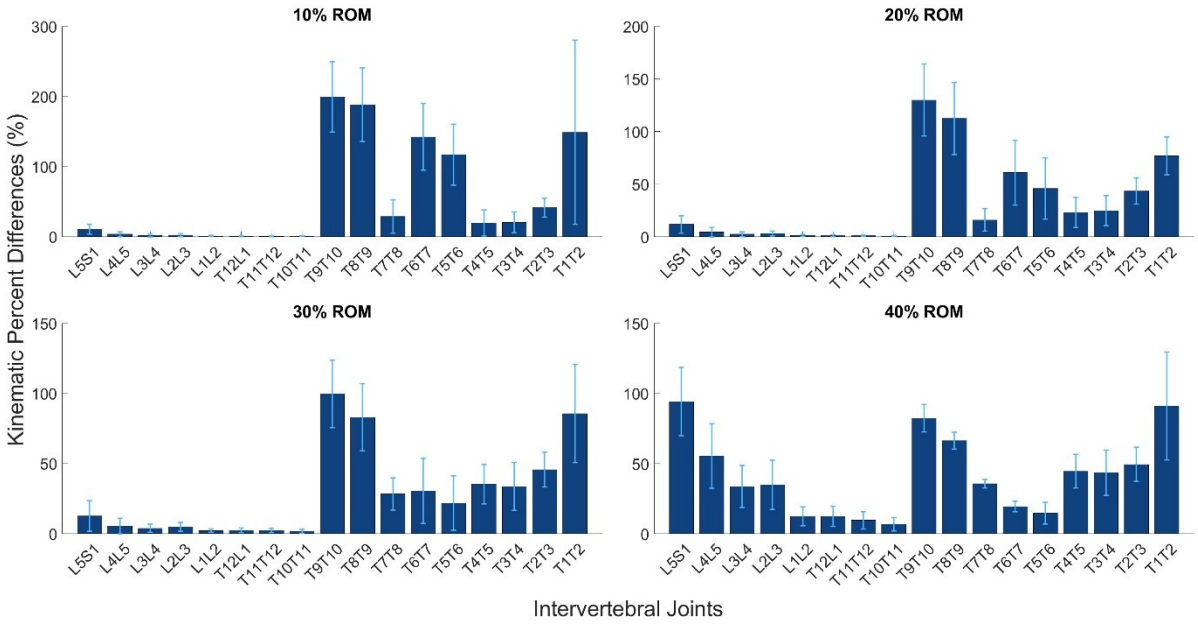

Figure 19: Mean kinematic percent differences categorized by IVJ – version I

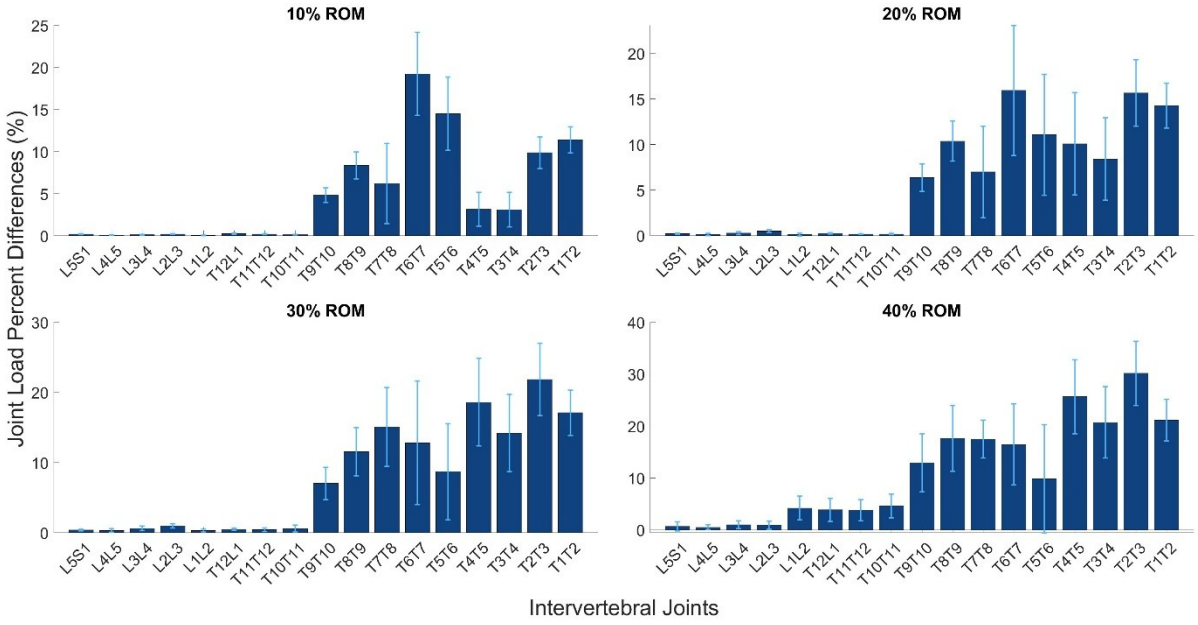

Figure 20: Mean joint load percent differences categorized by IVJ – version I

Finally, to evaluate the strength of the relationship between kinematics and joint loads simulated in Ansys and OpenSim, a correlation analysis was performed for both types of variables. The correlation analyses were performed over all scaled models, all IVJs, and all flexion poses

between 10% and 40% ROM, and are illustrated in Figure 21 and Figure 22. The intervertebral angles increase at each level as we move inferiorly within the spine and also increase as the total spine flexion increases. This results in a set of data points that is not normally distributed with a negative skew, as observed in the histogram of Figure 21. Note that the kinematics of Figure 21 are listed as negative values because of the definition of the axis systems in the model, where negative angles about the z-axis represent a rotation in the forward flexion direction. Since the data are non-normally distributed, Spearman's Rank Order Correlation Coefficient was estimated to perform this analysis. Strong significant correlations ($r > 0.7, p < 0.001$) were observed between the kinematics of both types of models.

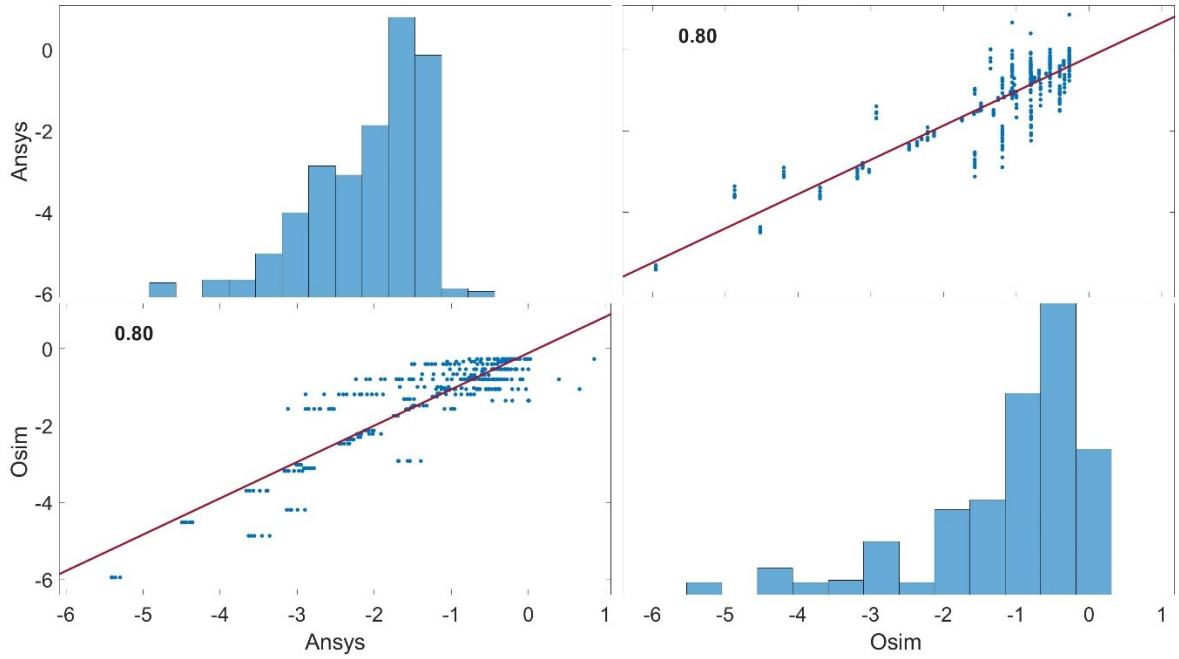

Figure 21: Spearman's Rank Correlation Coefficients between Ansys and OpenSim kinematics – version I

Similarly, the joint loads increase at each level as we move inferiorly throughout the spine and also increase as the total spine flexion increases. This also results in a non-normal distribution of data points, which can be seen in the histogram of Figure 22, with a positively skewed distribution. Since the data is non-normally distributed, Spearman's Rank Order Correlation Coefficient was estimated to perform this analysis. Very strong significant correlations ($r > 0.9, p < 0.001$) were observed between both types of models.

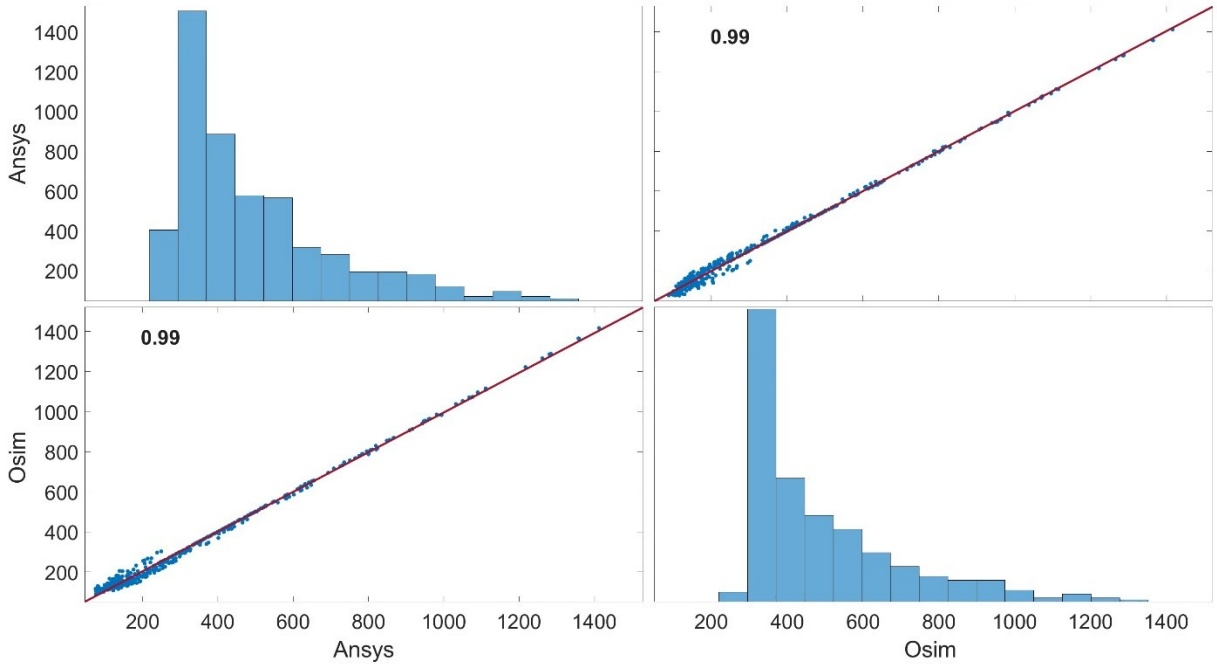

Figure 22: Spearman's Rank Correlation Coefficients between Ansys and OpenSim joint loads – version I

4.2.2. Validation of the Co-Simulation Workflow – Version II

As previously mentioned, all simulations were conducted by first selecting the smallest muscle proportionality constant (q) possible to reach simulation convergence in both the SCSO framework and in Ansys. Table 10 details the absolute differences in kinematics and joint loads between the FE and MSK modeling platforms, based on the minimum value of q required to simulate each static pose. The differences were calculated over all six model versions, IVJs, and flexion poses simulated, categorized by the value of q. In general, both the maximum and mean differences increase as the value of q increases, with the exception of the joint load differences when $q = 1$, which has larger differences than for $q = 2$.

Table 10: Maximum and mean absolute differences in kinematics and joint loads between modeling platforms, categorized by value of q

Muscle Proportionality Constant, q	**Kinematic Absolute Differences (°)**		**Joint Load Absolute Differences (N)**	
	Max	**Mean ± SD**	**Max**	**Mean ± SD**
0	1.71	0.27 ± 0.26	103.80	24.41 ± 20.93
0.5	3.33	0.52 ± 0.59	212.03	37.69 ± 38.33
1	4.63	0.70 ± 0.92	951.81	135.34 ± 179.22
2	7.33	1.20 ± 1.53	453.58	74.22 ± 91.60

To better quantify the significance of these differences, Table 11 details the absolute percent differences in kinematics and joint loads between the FE and MSK modeling platforms, based on the minimum value of q required to simulate each static pose. Although the kinematic differences in Table 10 are on average less than 2°, and maximum errors are less than 8°, these errors often represent a large proportion of the rotation angles at each joint, which vary between 0° and 11° over the 0 to 80% ROM range simulated. This is observed in the kinematic differences which are greater than 100% of the joint kinematics in many cases and greater than 1000% when $q = 1$ or $q = 2$. The percent differences in joint loads on the other hand are much smaller, because although differences reach up to several hundred Newtons, the joint loads in the spine are often upwards of 1000 N and can reach upwards of 3000 N in large flexion poses.

Table 11: Maximum and mean absolute percent differences in kinematics and joint loads between modeling platforms, categorized by value of q

Muscle Proportionality Constant, q	**Kinematic Percent Differences (%)**		**Joint Load Percent Differences (%)**	
	Max	**Mean ± SD**	**Max**	**Mean ± SD**
0	218	15.6 ± 21.8	30.4	4.73 ± 5.26
0.5	279	31.9 ± 42.5	50.0	5.28 ± 6.60
1	104 000	10 600 ± 21 300	60.9	8.05 ± 8.23
2	75 500	2 580 ± 10 700	114	11.4 ± 18.7

It is clear that the differences in both kinematics and joint loads increase as the value of q increases, hence model and simulation parameters of the MSK model are better reproduced in Ansys when $q = 0$. To evaluate these differences as the simulated pose increases in flexion, Table 12 details the absolute differences in kinematics and joint loads between the FE and MSK modeling platforms, for each flexion pose and when $q = 0$. Cells containing (-) are present when simulations could not be conducted with any scaled model with a q of zero for that flexion pose. Here, mean kinematic differences are greater at the 10% flexion pose, but otherwise range between 0.2° and 0.3°. Kinematic differences seem to decrease as the spine flexion increases towards the mid ROM but then increase as the flexion increases further. No obvious trend is observed in the joint load differences.

Table 12: Maximum and mean absolute differences in kinematics and joint loads between modeling platforms, when q is zero

Percent ROM (%)	Kinematic Absolute Differences (°)		Joint Load Absolute Differences (N)	
	Max	Mean ± SD	Max	Mean ± SD
0	-	-	-	-
10	1.36	0.41 ± 0.38	70.61	33.83 ± 22.12
20	1.16	0.29 ± 0.26	34.16	13.36 ± 10.72
30	1.71	0.28 ± 0.29	103.80	24.09 ± 21.82
40	0.61	0.20 ± 0.16	66.37	22.49 ± 17.20
50	0.80	0.24 ± 0.29	77.01	27.91 ± 22.02
60	1.29	0.28 ± 0.29	86.11	30.90 ± 25.30
70	-	-	-	-
80	-	-	-	-

Table 13 details the same information as Table 12, but the percent differences are presented. Here, the kinematic percent differences decrease as the flexion angle increases. This is in accordance with the observations made in Table 12, where the differences decreased from 10% to 40% of the ROM. Although differences increased slightly in the 50% and 60% ROM poses, these differences represent a smaller proportion of the actual kinematics, which translates in smaller percent differences. The opposite observation is made for the joint load differences, where the percent differences seem to increase as the flexion angle increases. However, this increase in percent differences is very small, as mean differences are always less than 10% of joint loads, and less than 5% for many flexion poses.

Table 13: Maximum and mean absolute percent differences in kinematics and joint loads between modeling platforms, when q is zero

Percent ROM (%)	Kinematic Absolute Percent Differences (%)		Joint Load Absolute Percent Differences (%)	
	Max	Mean ± SD	Max	Mean ± SD
0	-	-	-	-
10	218	64.0 ± 54.5	4.90	2.47 ± 1.40
20	60.2	22.9 ± 17.6	13.1	2.77 ± 3.61
30	46.3	14.1 ± 10.9	17.3	4.10 ± 3.64
40	18.3	8.18 ± 5.81	30.4	5.98 ± 6.82
50	15.4	7.59 ± 5.04	30.2	6.48 ± 7.18
60	18.2	6.68 ± 4.76	23.8	5.79 ± 5.38
70	-	-	-	-
80	-	-	-	-

Similarly to observations made during the validation of version I of the workflow, the data shown in the previous tables often presents maximum differences which are largely outside the bounds of the mean and SD differences, indicating potential outliers in the data. To identify whether these peaks in differences occur at specific levels of the spine, the kinematic and joint load percent differences were plotted for each intervertebral level in Figure 23 and Figure 24, respectively. The percent differences plotted represent the mean ± SD over all models, where each subplot is a different flexion pose simulated with $q = 0$. In Figure 23, we can see peaks in kinematic percent differences at L2L3 in the lumbar spine, and at T9T10, T8T9, T6T7, and T5T6 in the thoracic spine, although these peaks do not necessarily occur in all flexion poses. In Figure 24, the percent joint load differences are generally below 10%, and in some cases below 5%. We can see clear peaks in percent differences that surpass these thresholds at the T5T6 and T6T7 levels in the larger flexion poses. The peaks observed at T5T6, T6T7, T8T9, and T9T10 are consistent with those observed in the validation of version I of the workflow. Once again, it should be noted that large ranges are presented for the SD, as these simulations were generated with six models varying in height in weight, resulting in a large variability of muscle stiffnesses between models, joint loads and also large differences observed between Ansys and OpenSim.

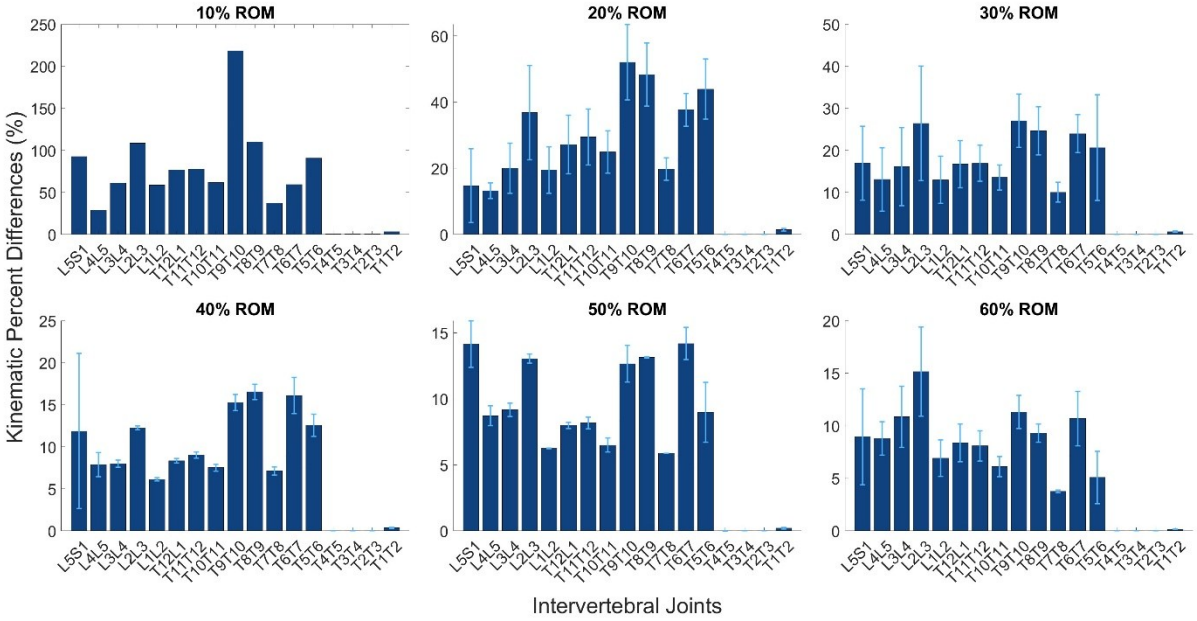

Figure 23: Mean kinematic percent differences categorized by IVJ when q=0 – version II

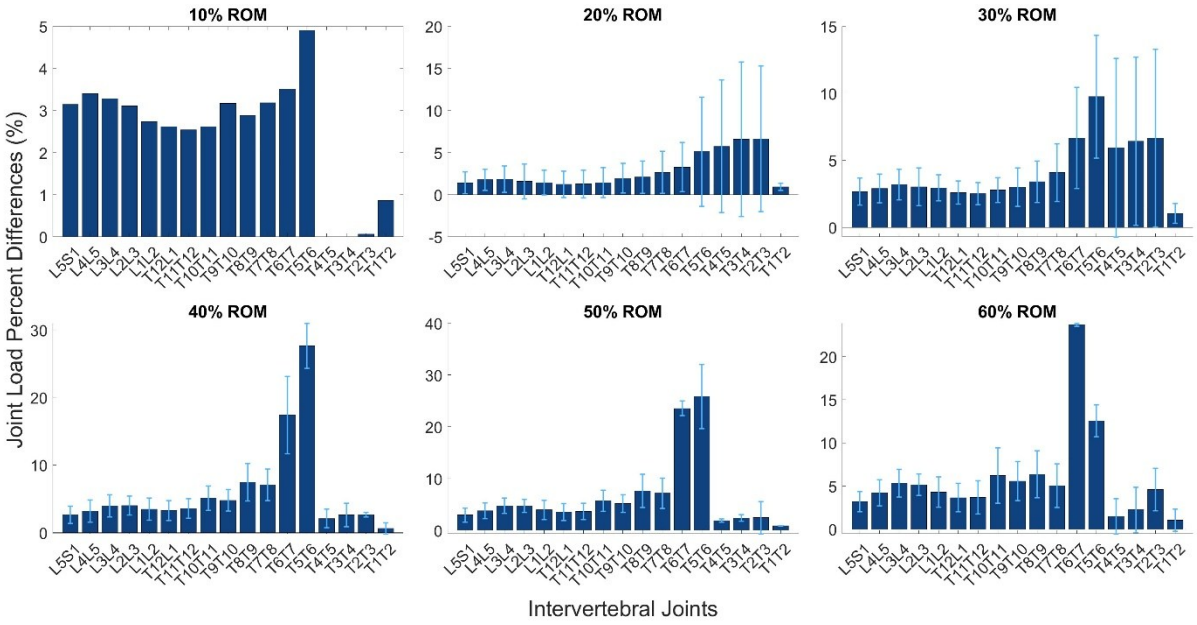

Figure 24: Mean joint load percent differences categorized by IVJ when q=0 – version II

Finally, to evaluate the strength of the relationship between kinematics and joint loads simulated in Ansys and those from the MSK model, a correlation analysis was performed for both types of variables. The correlation analysis was focused on simulations performed successfully with $q = 0$, and was evaluated over all scaled models, all IVJs, and all flexion poses. More simulations were successful for the 30% ROM flexion than the other flexion poses, which causes an uneven spread of data points representing the kinematics and joint loads. The kinematics and joint loads also vary throughout the spine. As a result, the data are not normally distributed, thus Spearman's Rank Order Correlation was performed for the analysis. Figure 25 illustrates the correlation between the kinematics obtained in Ansys and those from OpenSim. From the histograms, it is clear that the data are not normally distributed and are negatively skewed. Very strong significant correlations ($r > 0.9, p < 0.001$) were found between the kinematics of the two modeling platforms.

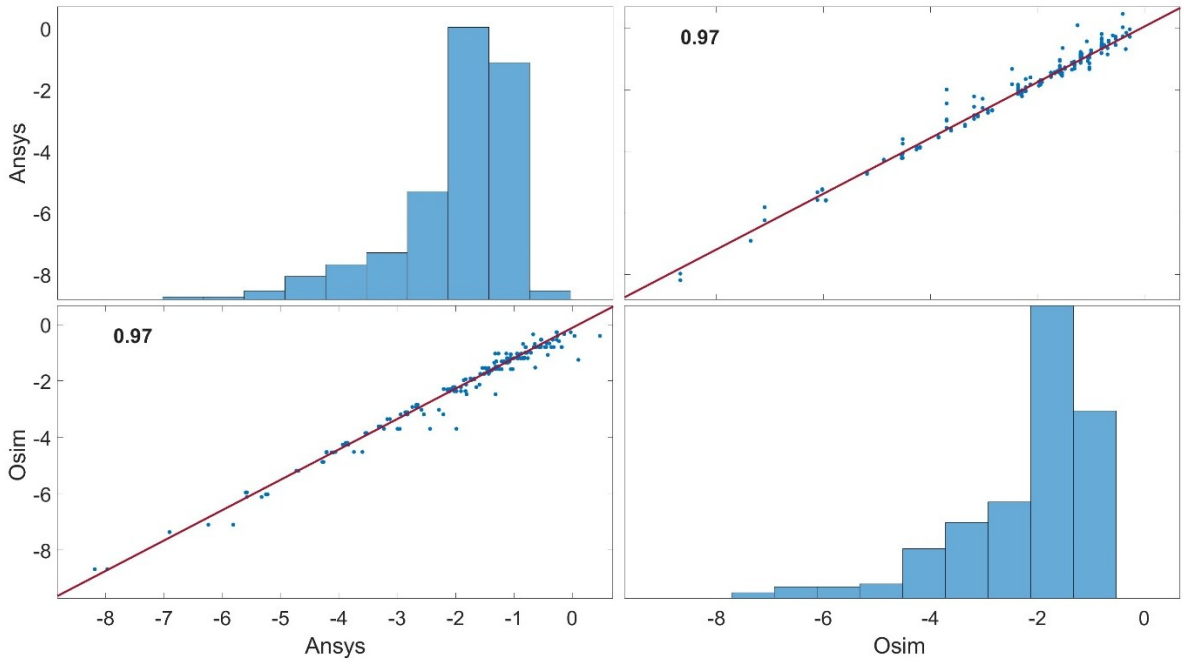

Figure 25: Spearman's Rank Correlation Coefficients between Ansys and OpenSim kinematics – version II

Figure 26 illustrates the correlation between the joint compressive loads in Ansys and those from OpenSim. Once again, the histograms show that the data are not normally distributed with a positive skew. Perfect correlations with a high level of significance ($r = 1, p < 0.001$) were found between the joint loads of the modeling platforms, which is a reflection of the negligible differences presented in Table 13.

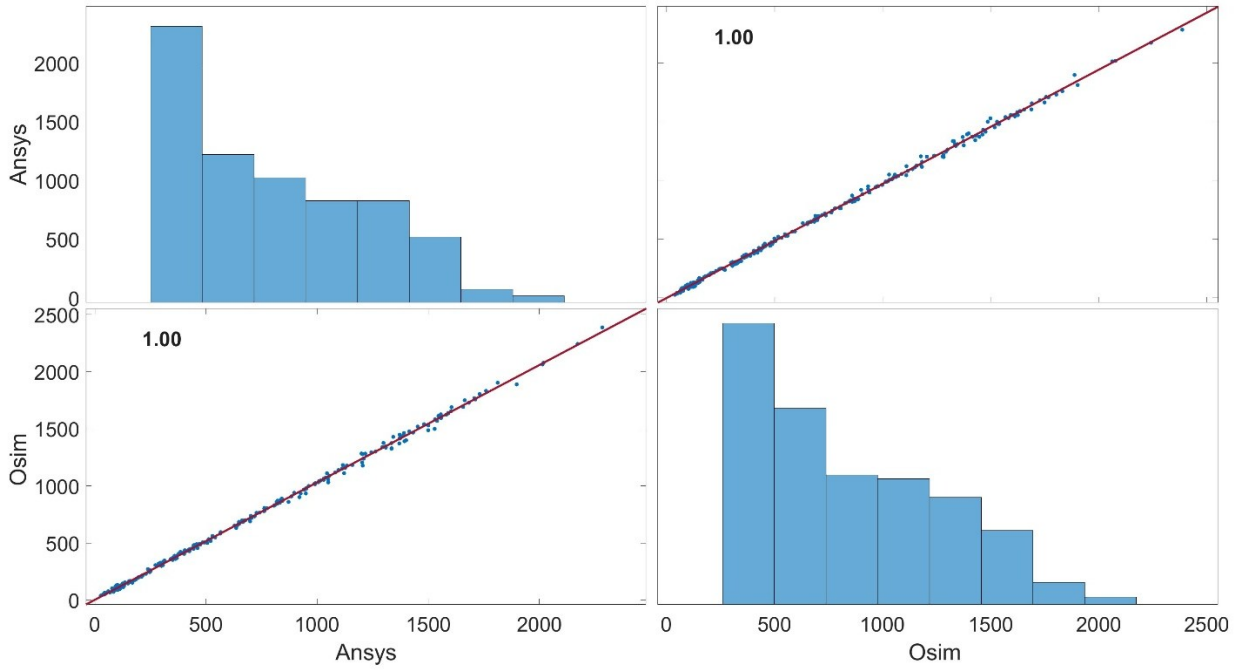

Figure 26: Spearman's Rank Correlation Coefficients between Ansys and OpenSim joint loads – version II

4.3. Simulation Performance

All simulations and analyses carried out for this project were done on a 2.30 GHz 12th Gen Intel Core i7-12700H laptop. The time required to perform any analyses within the OpenSim GUI or the API, including SO and JRA, took less than one minute. The time required to estimate muscle forces using the SCSO framework generally took between 5 and 10 minutes. It should be noted that the SCSO framework performs multiple analyses using the OpenSim API, such as several point kinematics analyses and a muscle analysis, followed by an optimization algorithm for computing muscle forces. That said, the computing time required to perform analyses using the SCSO framework is comparable to the time it would take to perform the same analyses directly in OpenSim.

All work done using the Ansys software was done through a virtual private network (VPN) to access the licenses provided by Numalogics Inc. This should be taken into account upon the consideration of computing times, as the VPN lowered the performance of the software. That said, the computing time required to generate the MSK model in Ansys using the automated

scripting workflow took up to several hours, depending on the number of muscles included in the model. For instance, the models used in version I of the co-simulation workflow included 306 musculotendon actuators. The time required to build an equivalent model in Ansys took between 2 and 3 hours. Loading different forces files to simulate a new static pose on an existing model took less than 2 minutes.

In version II of the co-simulation workflow, the models had 458 musculotendon actuators. Moreover, functions were added to the script for calculating the stiffness of each muscle spring. Generating a model in Ansys using version II of the workflow took between 3 and 4 hours. Loading different forces files and recalculating the muscle stiffnesses on an existing model took between 10 and 15 minutes. It should be noted that trial and error was required from the user to find the minimum value of q, the muscle proportionality constant, that would produce converging simulations in both the SCSO framework and in Ansys, and this time is not included in the computing time listed above.

Performing the scaling function of the scripting workflow in Ansys, to scale the generic model, took about 5 minutes.

Once the model was built and forces were applied to the model in Ansys, running the simulation itself and generating results took less than 1 minute for all models and for both versions of the simulation workflow.

5. DISCUSSION

The overarching objective of this project was to create a hybrid, or co-simulation, workflow to determine *in-vivo* loading conditions, namely muscle forces, that can be used to simulate functional ROM poses in a FE model of the whole spine. This workflow was created for the OpenSim and Ansys platforms and requires a combination of manual user manipulations and automated steps for the generation of matching MSK and FE models and for the execution of both types of simulations.

5.1. Sensitivity Analysis

The base model used to develop, test, verify, and validate the workflow was the MSK FATLS model. The original model had to be modified to simplify its representation in Ansys, to avoid convergence issues, and to make it compatible for use with the SCSO framework. Therefore, a sensitivity analysis was carried out to evaluate the sensitivity of the axial compressive loads at the IVJs to each model modification. This was necessary to determine whether the modifications brought to the model had significant impacts on model outputs that were of interest for the co-simulation workflow.

In performing SO analyses for the full ROM of the spine in flexion in the original model (Model0), it was noticed that the contribution of coordinate actuators started to increase at the 80% ROM pose and surpassed 10% of the total joint moments in the 90 and 100% poses. This is indicative that the musculotendon actuators in the model are not strong enough to satisfy model equilibrium constraints for those poses. In fact, in the validation studies performed by Bruno *et al*., they performed multiple static tasks ranging between neutral spine and 30° of flexion, but did not perform simulations for high trunk flexions [35]. In the validation study performed by Akhavanfar *et al.*, dynamic lifting tasks were simulated with high trunk flexion, but the exact range of spine flexion reached and contribution of coordinate actuators were not discussed [12]. Moreover, in both validation studies, the joint loads were investigated in the lumbar spine, but validation of the thoracic joint loads was very limited. Therefore, it is possible that the model would require adjustments so that it can be used to successfully perform full ROM tasks without the need for

coordinate actuators. In assuming that the model is not strong enough to satisfy equilibrium constraints in large ROM poses, it is reasonable to observe a large divergence in joint load predictions when modifications and simplifications were brought to the model.

The modifications brought to Model1 consisted of the removal of the upper limbs and of muscle groups attaching to the upper limbs. The linear regression analyses indicated that the joint loads predicted by this model increased with flexion angle 1.33 and 1.75 times faster than Model0 at the L4L5 and L1L2 joints, respectively. Moreover, the MAPD between the joint loads of the two models were 13.3 and 18.3%, at L4L5 and L1L2 respectively, where joint loads were smaller in Model1 at low flexion angles and greater at larger flexion angles. This can be explained by the added compression of the joints in low-flexion poses by the weight of the upper limbs. In the larger flexion poses, with the arms always vertically pointing towards the ground in Model0, the weight and muscle activity in the arms reduced the total compressive load on the lumbar spine. The arms were removed from the model as their modeling in Ansys was not necessary and would have produced a large computational burden. However, a simplified method for considering their weight on the trunk would be beneficial for more accuracy in joint load estimations.

In Model2, the intercostal muscles were removed. It was assumed that they would produce very little activity as the ribs were fixed with respect to the vertebrae, and so no intercostal movements could be produced. This hypothesis was confirmed by the small changes in linear regression coefficients and MAPD from those calculated with Model1.

Similarly, in Model3, the rib actuators were removed. Once again, because the ribs and sternum were fixed with respect to the vertebrae, it was hypothesized that the activity of the rib actuators would have little effect on the joint loads of the model. However, a significant increase in the joint loads was observed as the flexion angle increased in Model3, where joint loads increased more than five times faster than in Model0. This resulted in MAPD with Model0 that were greater than 100 and 200% at the L4L5 and L1L2 joints, respectively. Moreover, the SO analysis could not find converging solutions for poses greater than 60% of the ROM in flexion. For the simulated poses that did converge, high recruitment of the coordinate actuators was observed. The rib actuators were originally included in the model to mimic loads transmitted by costal cartilage through the ribcage, and their optimal forces were set to high values of 1000 N so that the SO algorithm would

favour their activation over the activation of muscles to support the ribcage [35]. In this version of the model, their role is unclear as the ribs have no DOF with respect to the vertebrae and the stiffening effect of the ribcage on the thoracic spine has been implicitly included in the bushing properties of the thoracic IVJs. It is possible that the forces produced by the rib actuators, between adjacent ribs, and between ribs and the sternum, were high enough to produce moments about the IVJs, contributing to the equilibrium of the model. In light of these results, the rib actuators were kept in the model for all future analyses.

In Model4, the motion of the abdomen was removed by fixing it with respect to the sacrum and all musculotendon actuator paths were reduced to origin and insertion points only. These modifications were required to reduce the computational burden of the model in Ansys and to avoid convergence issues. The linear regression coefficients and MAPD with Model0 are comparable to those of Model1 and Model2, indicating that these modifications had little effect on the joint loads.

Model5 was created so that the model would be compatible for use with the SCSO framework. Here, all coordinate and rib actuators had to be removed, which, as previously mentioned, caused the simulations to fail. To remedy this, the intercostal muscles were reintroduced into the model, which was successful in being able to produce converging simulations. Although the intercostal muscles were minimally activated and their removal produced very minimal change in the joint loads of Model2, it was hypothesized that their recruitment would increase when the rib actuators were not considered. Similarly, as these muscles attach to adjacent ribs which are fixed to the vertebrae, their activation is thought to produce moments about the IVJs which contribute to the model equilibrium. It is suspected that these muscles were not being recruited when the rib actuators were considered because the latter were assigned high optimal forces, making their recruitment more favourable than the recruitment of the intercostal muscles. The linear regression coefficient and MAPD with Model0 were significantly larger than for the other model versions, indicating that the modifications made to Model5 greatly influenced joint load predictions.

In sum, the correlation analyses showed very strong relationships between the joint loads of each modified model and Model0, although linear regressions and MAPDs indicated that some of the model modifications had significant impacts on the absolute values of the compressive joint

loads. The linear regression coefficients and the MAPD with Model0 were greater at the L1L2 joint for all models than at the L4L5 joint. This means that the modifications brought to the model produced greater changes in joint loads and joint load patterns in higher lumbar levels. The joint loads in the thoracic levels were not evaluated for this sensitivity analysis because those did not undergo as much validation, and so we have little information on their accuracy. The MAPD between Model1 and Model0 were greater than 10%, which has been recommended as the upper limit of acceptability [90]. Therefore, including the weight of the upper limbs in future developments of this project would be recommended for better joint load predictions. While the MAPD were higher than 10% in Model2 and Model4, which both also had upper limbs removed, the increase (or decrease) of MAPD from the values of Model1 are of less than 10%, indicating that the removal of intercostal muscles, fixing the abdomen, and simplifying the muscle lines of action did not significantly alter the joint load predictions. On the other hand, the increase in MAPD for Model5 was greater than 10%, meaning that this version of the model is not well suited for the evaluation of joint loads. Future developments of version II of the workflow should consider updating the SCSO framework to be able to consider actuators other than muscles in the model.

5.2. Workflow Version I

Using Model4 from the sensitivity analysis, version I of the co-simulation workflow was developed. Overall, the workflow consisted of recreating the FATLS model with the exact same structure and components in Ansys, and transferring loads calculated from OpenSim as loading conditions in Ansys. A few modeling choices were made to simplify this process. Firstly, the muscle fascicles were represented as uniaxial linear springs, with minimal stiffness, connecting the origin and insertion points of the muscles. In using springs to apply the muscle forces to the model, rather than simply applying them as force vectors [84, 91], regardless of potential differences in kinematics between the Ansys and OpenSim models, we are ensuring that the line of action of muscles is always directed along the path between origin and insertion points. Secondly, a decision was made to omit the action of the rib actuators in the Ansys model. From the sensitivity study of the joint loads, although it was hypothesized that the rib actuators produced moments about the IVJs, their role was not fully understood. Thus, their contributions to model kinematics were neglected in Ansys in hopes of simplifying the modeling process, getting a better

understanding of their role, and that simulation convergence could still be achieved without them. Note that the muscle forces transmitted to Ansys were those that were computed in OpenSim with the contribution of rib actuators. Thirdly, the gravity loads were separated into axial compressive force and joint moment components. Many co-simulation studies have reported that the BCs in the FE simulation included the kinematics of the spine in the deformed or flexed position in addition to the loading conditions extracted from MSK modeling methods [17, 81-82, 84]. Numalogics wanted a way to apply only loading conditions to the FE model in its undeformed state, namely in the neutral spine position. This was accomplished by decomposing the gravity loads into force and moment components. The moments produced by body masses in the neutral spine do not correspond to those in the flexed spine. Therefore, in applying moments, at each IVJ, that occur from gravity loads in the flexed configuration, these moments could perturb the model and cause it to flex forward until static equilibrium was reached with the applied muscle forces. The compressive components of the gravity loads were applied as FLs, using the current methodological approach used by Numalogics for the application of FLs. In general, the shear loads in the spine are much smaller than the compressive loads, and these were not of concern for Numalogics. Therefore, for the development and testing of the simulation workflow, at this time, the shear component of gravity loads was not modeled in Ansys.

5.3. Validation of Workflow – Version I

To validate version I of the co-simulation workflow, simulations of various flexion poses were produced for six scaled models. Flexion poses ranging between 10 and 40% of the ROM in flexion were successfully simulated. The 0% ROM, namely the neutral spine position, and flexion poses of 50% ROM and greater could not be simulated due to convergence issues in Ansys.

One of the limitations of the SO algorithm used in OpenSim is that it penalizes co-contraction, limiting the activation of antagonist and synergist muscles [13, 46]. In comparing model predictions with EMG measurements, it has been found that SO significantly underpredicts activation of the abdominal muscles [48, 59-60, 63, 92]. Moreover, the SO algorithm used in OpenSim does not consider stability constraints, which affects the prediction of co-activation. For instance, studies have found that small intersegmental muscles, such as the multifidus, are essential

for maintaining stability of the spine [57], along with activation of antagonistic abdominal muscles [55, 58-61]. These limitations of SO are thought to be large contributors to the convergence issues that were being encountered in Ansys.

More specifically, convergence issues were occurring at the neutral spine position, which has been shown to be a naturally unstable position, due to smaller muscle force demands and smaller stiffness of the joint structures [55]. Convergence issues were also occurring at large flexion poses, which contradicts the literature, where large flexion poses have been shown to be most stable [55, 57, 81]. This increase in stability is due to increased stiffness from the passive spinal structures in these poses and increased stiffness from the recruitment of muscles [55, 57]. Higher muscle recruitment in high flexion poses increases the compressive loads on the spine, which can be detrimental to spinal stability. However, experimental studies have shown that the functional spinal unit stiffness increases under increased compressive loads [93], inherently stabilizing the spine. The relationship between functional spinal unit stiffness and the magnitude of compressive loads havs not been incorporated into the passive stiffness definitions of the FATLS model, which could be part of the cause for these discrepancies with the literature.

Although many convergence issues were encountered while using this version of the co-simulation workflow, the latter could still be validated in the 10 to 40% ROM in flexion. For each simulation, the kinematics and axial compressive loads in the Ansys spine were compared to those in OpenSim. The magnitude of the compressive loads increased as the flexion angle increased, which resulted in larger differences occurring between models as the flexion angle increases as well. The mean percent differences were less than 10%, which is within the range of acceptability [90], except for the 40% ROM pose. Larger differences were observed in the 40% ROM pose as higher stiffnesses needed to be attributed to the muscle springs in Ansys for simulations to converge, which resulted in modeling discrepancies with OpenSim.

Upon observation of the kinematic differences, the absolute differences were, on average, less than 1° and always less than 2°. While these may seem like small differences, because each joint angle only varied between 0° and 6° in the range simulated, these sometimes resulted in percent differences that were greater than 100%. The percent differences, all being significantly greater

than 10%, indicate that the current modeling setup or simulation workflow is not adequate for accurately reproducing MSK simulations in OpenSim, with the FATLS model.

Since the maximum differences, for both joint loads and kinematics, were largely outside the bounds of the mean and SD ranges, the differences were observed at each independent spinal level to determine if specific areas of the spine were problematic. In doing so, it was found that the kinematic differences were minimal in the lumbar spine, and that large differences were observed in the thoracic spine specifically. The source of these differences may come in part from discrepancies in the modeling of the muscles between Ansys and OpenSim. Larger percent differences in the thoracic spine were also expected as the intervertebral angles during flexion are lower in the thoracic spine than in the lumbar spine, thus absolute differences translate into larger percent differences at these levels. However, it is most likely that these differences came from the lack of the action of rib actuators in Ansys. In performing SO analyses in OpenSim, convergence could not be reached when these were not considered along with coordinate actuators, but their true effect on the model was not fully understood. In Ansys however, simulation convergence could be obtained when these were omitted. In addition, no exponential increase in joint loads was observed in Ansys when omitting them, but a perfect match of model kinematics with OpenSim was not possible. It is likely that the muscles in the model are not strong enough to satisfy equilibrium constraints without the rib actuators. Therefore, in performing SO in OpenSim, without rib actuators, the algorithm would assign very high muscle activations, which resulted in large increases in joint loads as the spine flexion increased. It is now clear that, with the current configuration of the model, the rib actuators do in fact produce moments about the thoracic IVJs, and that the latter are necessary to equilibrate the spine in flexion, regardless of whether the rib cage has DOF or not.

The intervertebral rotations were smaller in Ansys than OpenSim at most levels, likely due to the attribution of stiffnesses to the muscles in Ansys, limiting the flexibility of the model. However, exceptions occurred at the T5T6, T6T7, T8T9, and T9T10 levels. At these levels, the Ansys model reached greater flexion angles than those in OpenSim. These levels also happen to be where some of the large peaks in kinematic differences were observed. The high flexion angles at these specific levels suggest that they are most dependent on the action of the rib actuators, and that the muscles surrounding these joints specifically may not be strong enough to satisfy equilibrium constraints.

Larger differences were also observed in the thoracic spine comparatively to the lumbar spine concerning the joint loads, however no specific joints were identified as being more problematic. Once again, these discrepancies could be due to the combined effects of missing rib actuators and stiffnesses attributed to muscle springs in Ansys. Further developments of version I should consider the modeling of the rib actuators in Ansys or should investigate ways to strengthen the model so that rib actuators may be omitted. For example, this could include the modification of joint stiffness properties at the thoracic levels to account for the additional stiffness otherwise provided by the rib actuators.

Lastly, to evaluate the strength of the relationship between the OpenSim and Ansys kinematics and joint loads, correlation analyses were performed over all IVJs, all flexion poses, and all scaled models. Strong significant correlations were found between both variables of the two modeling platforms. Indeed, some modeling choices, such as the exclusion of the rib actuators and the attribution of stiffnesses to the muscle springs in Ansys, created differences in joint loads and kinematics between the models. However, regardless of these sources of error, the workflow allowed us to produce simulations of static flexion tasks in a FE modeling platform, using *in-vivo* loading conditions, which predicted kinematics and joint loads with a strong relationship to those in the MSK model.

5.4. Workflow Version II

A big drawback from version I of the co-simulation workflow was the inability to simulate a wide ROM of poses, such as the neutral spine position and large flexion poses. SO penalizes co-contraction, limiting the activation of antagonist and synergist muscle groups which are essential for spinal stability. Therefore, although the SO algorithm computes muscle forces which satisfy equilibrium constraints, it does not ensure that the system is stable in the equilibrium position. This was hypothesized to be the cause of the convergence issues encountered in Ansys. To remedy this, a second version of the co-simulation workflow was developed so that we could compute muscle forces that satisfy both equilibrium and stability constraints. The SCSO framework developed by Akhavanfar *et al*. [63], which employs the simplified equation for stability derived by Potvin and Brown [62], was used in this version of the workflow. Model5 was used in this workflow, as

coordinate and rib actuators could not be accounted for when using the SCSO framework. Overall, the simulation workflow consisted of similar steps as version I of the workflow, in recreating the FATLS model with the exact same structure and components in Ansys, and transferring loads calculated from the SCSO framework and OpenSim as loading conditions in Ansys. In version II, muscle stiffnesses and their contribution to stability were calculated, and these same stiffnesses were assigned to the muscle springs in Ansys.

5.5. Validation of Workflow – Version II

To validate version II of the co-simulation workflow, simulations of various poses were performed for the six scaled models. While version I was limited to simulating poses ranging between 10 and 40% of the ROM in flexion, version II was able to produce simulations ranging between 0 and 80% of the ROM.

It was found that setting q to larger values increased the differences in kinematics and joint loads observed between the OpenSim and Ansys models. As previously mentioned, these increases in differences occurred because the muscle stiffnesses were computed for the flexed position in the SCSO framework, but they, along with muscle forces, were applied to the Ansys model in the neutral spine position. Therefore, in choosing larger values of q, the muscle stiffnesses increased, which inherently stiffened the spine so that it was not able to flex to the desired position. Because of this, trial and error was necessary to determine the smallest value of q that would produce converging simulations.

The smallest value of q for maintaining stability has been referred to as the critical q in the literature. Although the value of q for skeletal muscles has not yet been completely determined, with values ranging between 0.5 and 42 and a mean of 10 in the literature [56], many studies have examined the critical q for spine models. Gardner-Morse *et al.* used a model of the lumbar spine with 50 pairs of muscle fascicles and found a critical q of 6.92 for flexion and lateral bending tasks [58]. Arjmand and Shirazi-Adl used a kinematics-driven FE model of the lumbar spine with 56 muscle fascicles and found a critical q of 17 in standing when intra-abdominal pressure and abdominal co-activation were neglected and found a critical q of 8 when they were considered. In both cases, a critical q of 0 was found in flexion poses between 40 and 60° [94]. Lastly, in the

development of the SCSO framework, Akhavanfar *et al.* tested the workflow using a q of 3 and 5 and compared muscle activations with EMG measurements [63]. They found that assigning smaller values of q produced better agreement between model muscle activation patterns and EMG measurements for the co-activation of abdominal muscles. They determined that smaller values of q forced the algorithm to assign higher muscle activations to maintain stability, which triggered abdominal co-activation. In comparison to these studies, we found a critical q ranging between 0 and 2 for flexion poses of 0 to 80% ROM in forward flexion, depending on the scaled model used. Larger critical q values (values of 1 and 2) were necessary in all neutral standing poses and in some poses in the higher ROM in flexion, whereas most flexion poses in the mid ROM (10 to 50% ROM) were associated with smaller critical q values (values of 0 and 0.5). Hence, like these previous works, we found higher critical q values in standing comparatively to the critical q values for flexion poses. Poses that have a higher critical q represent poses that are less stable than poses with a critical q of zero, as this indicates that muscles are required to have more stiffness to maintain stability in these poses, based on the potential energy definition of stability. Overall, our values of critical q were smaller than those predicted by these other studies, which could be due to the very high number of muscle fascicles included in the model, naturally stiffening the spine and increasing its stability.

Contrarily, our results showed that the critical q slightly increased in large flexion poses (60 to 80% ROM), indicating less stability. Previous works have shown that the stability of the spine increases in large flexion because of increased stiffness from the passive joint properties at large flexion angles and because of the compression-dependent increase in stiffness [55]. The compression-dependent stiffness of the spinal units is not considered in the FATLS model, which could be a reason for these discrepancies with the literature. It is also possible that the tuning of the stiffness properties of the bushings in the model would be required to better replicate the increase in stiffness at high flexion angles. Moreover, we found that the critical q increased in the heavier and taller scaled models. Heavier models are subjected to larger compressive loads from gravity and taller models may be less stable due to higher external work applied on vertebral joints from the increased height of the bodies. The stiffness properties of the joint bushings are based on generic parameters and are not being scaled with model mass and height, which could explain why these models required larger values of q.

It should be noted that the poses in which higher values of q were required correspond to the same poses, namely neutral standing and large flexion poses, in which convergence issues were encountered in version I of the simulation workflow. This supports the hypothesis that convergence issues were occurring because the model was inherently unstable with the muscle stiffnesses and forces that were being applied to the model.

In producing simulations of flexion poses with values of q varying between 0 and 2, the differences between the kinematics and joint loads in the Ansys and OpenSim models were evaluated. Even in this low range of q values, it was evident that increasing its value caused large differences in kinematics and joint loads between the models. Overall, mean kinematic differences were less than 2°, however maximum differences reached over 7°. While the range of flexion poses was much larger in version II of the simulation workflow, these errors are larger than those observed in version I of the workflow. This is also evident in the percent differences, where these were over several thousand percent when q was 1 and 2. The percent differences in joint loads did increase with increasing q, however these differences were almost always less than 100%.

Since increasing the value of q produced large discrepancies in the Ansys model outputs compared to OpenSim, further data analysis was carried out by focusing on the simulations performed with a q of zero. In this case, the muscle stiffnesses were always zero, and so the model stability and equilibrium constraints were satisfied by the activation of muscles only, and it was possible to achieve matching simulation outputs between modeling platforms. In observing kinematic differences with a q of 0, we see that the differences were highest at 10% ROM, decreased as the flexion angle increased, and started to increase again at 50 and 60% ROM. An association can be made here between model instability and kinematic differences, where positions that have been shown to be less stable result in larger discrepancies between models. A possible explanation for these increases in differences is that at low values of q, when the model is less stable, the SCSO framework assigns higher muscle activations to the model [63]. The pairing of the OpenSim/SCSO framework and Ansys software can introduce sources of error from differences in tolerances attributed to model parameters and the order of operations performed. For example, in the SCSO framework, muscle forces are estimated such that model equilibrium is maintained for an input static flexion pose. In Ansys, those muscle forces are applied to the model and the flexion pose observed is a result of the application of the loading conditions to the model.

Therefore, number rounding, differences in tolerances, and small errors in the muscle forces output by the SCSO framework can reasonably produce slightly different kinematics in Ansys. Another source of error comes from slight differences in the definition of the Ansys and OpenSim models. For instance, in Ansys, muscle springs cannot have stiffnesses of zero, and in those cases, near zero stiffnesses are rather attributed to the muscles in Ansys. Therefore, with the prediction of high muscle forces from the SCSO framework, it is reasonable to also expect larger differences between the kinematics of the Ansys and OpenSim models.

Although the kinematic differences observed vary with flexion angle, the mean kinematic differences all remain within a small range of 0.2 to 0.3°, except for the 10% ROM pose. This reinforces the thought that with the high number of muscles included in the model, and with high muscle force values being transferred between the SCSO framework and Ansys, small discrepancies will always occur between model outputs. Moreover, because the absolute kinematic differences remain within this small range, this results in percent differences decreasing with increasing spine flexion angle. The 30 to 60% ROM poses presented MAPD less than 10%, which is within the range of acceptable differences [90], indicating that the workflow produces reliable model outputs in these poses.

In terms of the joint load differences, the MAPD are always less than 10%, and in some cases, less than 5%, which signifies that this workflow, with a q value of 0, produces highly accurate joint loads in Ansys in comparison to those in OpenSim.

Similarly to observations made in version I of the simulation workflow, the maximum differences, for both kinematics and joint loads, were often largely outside the bounds of the mean and SD ranges. In plotting the differences for each IVJ, peaks in kinematic differences occurred at multiple joints, namely L2L3, T9T10, T8T9, T6T7, and T5T6, whereas differences in the upper thoracic levels were negligible. Joint load differences presented peaks at the T6T7 and T5T6 joints as well. The peaks observed in the thoracic levels were at the same levels as the peak differences observed in version I of the simulation workflow. This reinforces the hypothesis that these specific joints may be less stable due to the lack of stiffness around these joints or that the muscles surrounding these joints are not strong enough.

To further validate the kinematic outputs of the simulation workflow, our kinematic differences were compared to those published by Khoddam-Khorasani *et al.* [17]. They developed a co-simulation workflow, where they simulated static poses up to the full ROM in flexion, using a model of the lumbar spine with 56 muscles. Their kinematic differences at each IVJ were less than 0.6°. They did not indicate the significance of these values in percent differences. The mean absolute differences in this workflow were mostly between 0.2 and 0.3°, with mean and SD ranges remaining below 0.6°. However, our maximum differences recorded were larger, but remained below 2°, which seems reasonable considering that our model features more DOF. We can conclude that this simulation workflow produces similar kinematic differences to those presented by Khoddam-Khorasani *et al.,* with the advantage that we are considering the kinematics of the entire thoracolumbar spine, a much larger number of muscles, and stability constraints.

Lastly, to evaluate the strength of the relationship between the OpenSim and Ansys kinematics and joint loads, correlation analyses were performed over all IVJs, all flexion poses, and all scaled models. Very strong significant correlations were found between the kinematics of the two modeling platforms, showing a stronger relationship with version II than version I of the workflow. Perfect significant correlations were found between the joint loads of the two modeling platforms, indicating that version II of the workflow, with a q of 0, is highly reliable for producing simulations of static poses using *in-vivo* loading conditions where the evaluation of joint loads is of interest.

5.6. Comparison of the Simulation Workflows

Both versions of the simulation workflow presented strengths and weaknesses. For instance, version II was more computationally expensive, with longer computation times required for performing the SCSO framework, for trial and error to find the critical q, and for the longer computation time required to build the model in Ansys because of the stiffness calculations and the higher number of muscles included. On the other hand, version I was very limited in the range of flexion poses that could be successfully simulated and generally presented larger kinematic and joint load differences between the Ansys and OpenSim models. On that note, correlations between the kinematics and joint loads of the Ansys and OpenSim models were much higher in version II of the workflow.

More specifically, in developing both versions of the workflow, it became clear that the consideration of stability constraints is essential for producing co-simulations of the full thoracolumbar spine with *in-vivo* loading conditions. The fact that stiffnesses had to be attributed to the muscle springs for simulations to converge in version I of the workflow indicates that the muscle forces predicted by the SO algorithm in OpenSim do not correspond to physiological muscle forces that would be required to maintain stability. Moreover, Akhavanfar *et al.* showed that the SCSO framework produced muscle activation patterns that better correlated to EMG measurements than the traditional SO algorithm at small values of q [63]. Lastly, the kinematic differences obtained using version II of the simulation workflow with a q of 0 were comparable to those found in the literature [17]. Therefore, it is my recommendation that version II of the simulation framework should be chosen when performing co-simulations of the thoracolumbar spine, using the FATLS model.

5.7. Strengths of the Simulation Workflow

The co-simulation workflow developed, along with the MSK model chosen for its development and validation, have many strengths. The FATLS model is currently one of the most detailed and biofidelic models of the thoracolumbar spine that has been published and validated. In using this model, this was the first study, according to this author's knowledge, that was able to successfully produce co-simulations using *in-vivo* loading conditions with a fully articulated thoracolumbar spine. All previous works modeled the lumbar spine only, or the lumbar spine with a lumped rigid thorax. In modeling the entirety of the thoracolumbar spine, we were able to account for the stiffening properties of the ribcage on the thoracic spine, to consider the motions of the thoracic spine, and to provide attachment points for all trunk muscle groups in physiological locations. Moreover, this model included the greatest number of musculotendon actuators of all published models used for co-simulation.

The workflow itself has many advantages as well. We found that, in producing co-simulations of the full thoracolumbar spine with *in-vivo* loading conditions, it was essential to consider stability constraints. This has not been consistently considered in the literature, with many groups still neglecting its importance in muscle force estimations [17, 83-84]. In considering stability

requirements, the workflow overcame the limitation of traditional SO algorithms which cannot account for co-activation, and this allowed us to simulate a large ROM of static poses without convergence issues.

In addition, the literature has shown that the application of *in vitro* loading conditions does not accurately reproduce physiological loading distributions in the spine when comparing IDP, compression, and shear loads throughout the spine with those resulting from muscle forces [7, 17]. In simulating functional ROM poses of the spine with muscle forces, we can better predict soft tissue stresses and deformations under physiological conditions.

Some groups have reported the need for iteratively modifying MSK stiffness properties to obtain matching kinematics between FE and MSK models due to differences in the modeling of soft tissue structures such as IVDs and ligaments [17]. The iteration procedure can be time consuming and doesn't necessarily always produce good results. To avoid this issue, the IVJs were modeled as bushings with identical stiffness properties in both the MSK and FE models. While this is not useful for simulating stresses and deformations in the IVDs, this setup will be very useful for Numalogics in their design optimization of medical devices. They currently have a model of the lumbar spine where the vertebrae are modeled as rigid bodies and the IVJs as bushings. Only instrumented vertebral bodies have elastic material properties for the simulation of contact stress between implant and bone and for the evaluation of stress distributions in the implants during functional spine movements [18]. With this workflow, Numalogics will be able to advance these analyses by modifying the material properties of vertebral bodies of interest and performing simulations with *in-vivo* loading conditions; something that could potentially influence the results of their analyses.

Another advantage of this workflow is that kinematics do not need to be considered as BCs in the FE model. Only the *in-vivo* loading conditions are applied to the model, which was a specified requisite for Numalogics and their analyses.

Lastly, the FATLS model was developed for OpenSim, an open-source software with in-depth documentation and resources. The OpenSim tools and resources are easily available to Numalogics. This software will allow them to perform various types of static simulations and will give them the potential to perform simulations with person-specific models, by scaling the generic

FATLS model and using experimental motion capture as input kinematics, in the event that this is needed. Similarly, through the creation of the automated scripting workflow for automating the model creation and scaling, and transfer of loading conditions from OpenSim to Ansys, this workflow will remain easy and efficient for them to use in their analyses.

5.8. Limitations

The model used also had many limitations. For instance, only the rotational DOFs were considered in the model and the stiffening effect of compressive loads were not considered. Wang *et al.* had modeled these in their definition of the IVJ stiffness properties [41], but they were not included in the validation study performed by Akhavanfar *et al.* because of difficulties in measuring translational kinematics of the spine using motion capture methods [12]. Also, the original FATLS model defined the muscles with curved lines of action or via points, which were modified to straight lines of action for the development of this workflow. Although the sensitivity analyses indicated that this modification had little impact on the joint loads in flexion poses, other studies have highlighted that the wrapping of the trunk extensor muscles influences joint loads, muscle force estimations, and stability levels [95]. Furthermore, the curved lines of action of the abdominal muscles and the activation of these muscles has been linked to intra-abdominal pressure, a mechanism shown to unload the spine and contribute to stability [96]. Another limitation includes the bushing stiffness properties, which were not currently scalable for taller/heavier models, and resulted in lower stability margins for these models. Moreover, the scaling of the model parameters assumed that bodies scale linearly, which may not be the most physiological representation of the varying total body height and mass in the population.

An important limitation of the model was that it was not strong enough to satisfy equilibrium constraints without the action of rib actuators in OpenSim. Because the stiffening effect of the ribcage has been included in the bushing definitions of the thoracic IVJs, the rib actuators should not have to be necessary to equilibrate the model. In addition, the original model was not strong enough to meet equilibrium constraints in the 90-100% ROM poses without contribution from the coordinate actuators. Therefore, care should be taken in the future to revise the properties of the model, such as muscle parameters and bushing stiffnesses at large flexion angles. The

identification of weaknesses at specific thoracic joints indicates that model weaknesses may occur around those levels specifically.

The SCSO framework had limitations of its own. Actuators other than muscles could not be considered in stability calculations. As a result, Model5 was used in version II of the workflow, and through the sensitivity analysis, it was found that this model predicted significantly different joint loads from Model0. In addition, the contribution of passive joint stiffness was not considered in the stability calculations. This did not prevent us from performing successful simulations in Ansys, as the consideration of passive joint stiffnesses would only increase the stability of the model. Future developments of the SCSO framework should focus on the implementation of passive joint stiffnesses in stability calculations and the consideration of various types of actuators. In addition, the SCSO framework was developed in MATLAB, which is not a tool that Numalogics has access to. For them to be able to use the framework in house, it would have to be converted to Python.

Although the SCSO framework was used to validate muscle activation patterns with EMG measurements using a simplified spine model [63], the muscle forces and joint loads computed with the FATLS model and the SCSO framework were not validated.

The co-simulation workflow developed also had limitations, the main one being that simulations cannot be performed with high values of q. Because the loading conditions are applied to the spine in its neutral state, high values of q stiffen the model to the point that it cannot flex to the desired positions. The simulation workflow is also limited in that it was validated by comparing kinematics and compressive joint loads at each level, between Ansys and OpenSim/SCSO, but the shear loads were not evaluated. Numalogics was not concerned about the shear loads in the model, as their current simulation methods do not account for shear loads at all. Therefore, to simplify the modeling process, shear from gravity loads were not considered, and so the comparison of shear loads in Ansys with those in OpenSim would have yielded significant differences. Lastly, the workflow was validated for flexion poses only. Future work should investigate the performance of the workflow in the other planes of motion.

6. CONCLUSION

6.1. Summary

This work was done in collaboration with Numalogics Inc., a Montreal-based company specializing in the use of FE models for computer modeling and simulation consulting services. In their current work with FE models of the spine, they commonly perform functional ROM movements to evaluate stress distributions in spinal instrumentation devices and to perform design optimization of these devices. Their current simulation methods consist of driving the model with *in vitro* loading conditions. Studies have shown that these *in vitro* loading conditions do not accurately represent the spinal load distributions produced by muscle forces. Therefore, they desire to assess whether these loading conditions are representative of *in-vivo* loading conditions in the evaluation of load distributions in spinal instrumentation devices, and whether this modeling choice has a significant impact on the conclusions drawn from their FE simulations. To be able to answer these questions, this work focused on the development of a co-simulation workflow, using matching MSK and FE models of the fully articulated thoracolumbar spine. With this workflow, *in-vivo* loading conditions could be applied to the FE model to simulate functional ROM static poses. More specifically, the overarching goal of this work was subdivided into three objectives.

The first objective was to replicate a validated MSK model of a fully articulated thoracolumbar spine in Ansys, the FE modeling software used by Numalogics. The FATLS model, selected for its high level of detail and the many validation studies carried out upon it, was modified to simplify its modeling in Ansys and to avoid convergence issues. The sensitivity of the simulation outputs, namely the compressive joint loads and kinematics, were evaluated for the modifications brought to the model. The model geometry was then imported into Ansys, and the structure of the FATLS model was replicated exactly. This included the definition of mass properties; joint positions, orientations, stiffnesses; joint types and DOF; and muscle stiffnesses and attachment point locations.

The second objective was to determine muscle forces and other BCs required to produce static simulations of spinal flexion in Ansys. To complete this objective, two versions of the simulation

workflow were developed. Version I consisted of performing a SO analysis in OpenSim using the MSK model to calculate muscle forces required to satisfy equilibrium constraints. Version II consisted of performing a SCSO analysis using a published MATLAB script to calculate muscle forces and stiffnesses required to satisfy equilibrium and stability constraints. In both versions of the simulation workflow, the forces and moments calculated from the MSK model were transferred to the FE model as loading conditions. These included muscle forces, FLs due to gravity loads, and joint torques representing moments produced by gravity loads and coordinate actuators in the simulated pose. In version II of the workflow, muscle stiffnesses were also assigned to the FE model based on a user-defined muscle proportionality constant, q, muscle forces, and muscle lengths.

The third objective was to validate the co-simulation workflows by comparing simulation outputs between the FE and MSK models, such as joint kinematics and compressive loads. This was essential to evaluate how well a MSK simulation can be reproduced in a FE model of the whole spine. This was accomplished by simulating static poses throughout the ROM of the spine in flexion with six scaled versions of the FATLS model. These simulations were performed for both versions of the co-simulation workflow, and the outputs between MSK and FE models were compared using absolute differences, absolute percent differences, and correlation analyses. Version I of the co-simulation workflow was not found to be adequate for producing FE simulations with *in-vivo* loading conditions, as many convergence issues were encountered, only a small ROM was successfully simulated, and large kinematic differences were observed. On the other hand, version II of the co-simulation framework was successfully validated for simulating flexion poses under *in-vivo* loading conditions. Negligible kinematic differences were observed in the 30-60% range of flexion, and negligible joint load differences were observed over the full ROM simulated. Very strong and perfect significant correlations were evaluated for both variables, respectively.

In sum, it was found that the consideration of stability constraints is essential to successfully perform simulations of the full thoracolumbar spine over a physiological ROM. Furthermore, through the sensitivity analysis and validation studies, it was found that the FATLS model is not adequate for simulating large flexion poses, as high contribution of coordinate actuators became necessary. Convergence issues were observed in OpenSim when the rib actuators were not

included in the model, even though the stiffening properties of the rib cage were implicitly included in the bushing properties of the thoracic vertebrae. More specifically, weaknesses were observed at specific thoracic IVJs, namely T9T0, T8T9, T6T7, and T5T6, where a revision of the model parameters was recommended for future developments.

In conclusion, this project focused on the development of a co-simulation workflow using a highly detailed and validated thoracolumbar spine model. This is the first study to perform a co-simulation workflow with a fully articulated thoracolumbar spine and with a comprehensive set of muscle groups and muscle fascicles. In developing this workflow, we have provided Numalogics with a framework for answering their research questions, like for example comparing joint loads or spinal implant stress distributions when using *in vitro* versus *in-vivo* loading conditions.

6.2. Future Work

The co-simulation workflow developed consisted of just the first step in the advancement of the simulation methodologies used by Numalogics. As highlighted in the text, there were many limitations to both the chosen model and the developed workflow that could be addressed in future work. For the FATLS model, it could be beneficial to model the six-DOF joints that were developed by Wang *et al.*, or simply include the compression-dependent stiffness properties in the joint bushings [41]. Identifying a way to define person-specific stiffness properties for the joint bushings could also be helpful in overcoming the decrease in stability that was observed in taller and heavier models. The curved lines of action of the muscles could be modeled in Ansys by using several springs connecting to each via point or attachment point. Furthermore, although explicitly modeling the upper limbs in Ansys would be computationally cumbersome, incorporating their weight on the trunk in a simplified manner would produce better joint loads in comparison to the original model. This could be done by applying the weight of the upper limbs at a single point with respect to the thorax. Lastly, as it was identified that the model has weaknesses in large flexion poses, specific thoracic joints, and when neglecting the contribution of the rib actuators, further investigation would be required to determine the source of these weaknesses, and to reinforce the model in these areas.

The SCSO framework was limited in that passive joint stiffnesses, coordinate actuators, and rib actuators could not be considered in the stability calculations. These should be implemented into the script in future developments. In addition, the framework was written for the OpenSim 3.3 API and in MATLAB. It would be beneficial to update the script to the most recent version of OpenSim and to convert it to Python so that it may be more easily accessible to Numalogics. While this framework was originally validated with a simple spine model and muscle activation patterns predicted were compared to EMG measurements, additional validation is warranted for its use with the FATLS model against both muscle activation patterns and joint loads.

Version II of the co-simulation framework was successful in performing simulations when q was set to 0, while increasing the value of q resulted in significant differences in model outputs. Although Numalogics specifically requested that the loading conditions be applied to the model in a neutral position, including model kinematics as BCs in addition to the loading conditions would help solve this problem. In applying kinematic BCs, all loading conditions would be applied to the model in the flexed position, and stiff muscles from large q values would only help to stabilize the model in this position, rather than creating discrepancies with the MSK model. Applying kinematic BCs would also allow us to consider the motion of the abdomen rather than fixing it with respect to the sacrum. Furthermore, in all simulations performed, the pelvis was fixed with respect to the ground. However, pelvis rotations contribute to the overall spine flexion during physiological movements and should be considered in future developments of this work.

Alternatively, to simulate flexion motions from the neutral spine position, Numalogics could employ a methodology similar to the one described by Honegger *et al.* [84], where both kinematics and loading conditions are applied at each instant in time to simulate a quasi-static movement from neutral to flexed positions. In this case, muscle stiffnesses would also have to be updated at each instant in time based on muscle forces and lengths.

Future work should also extend the validation of the workflow by modeling the shear components of the gravity loads and evaluating the total resulting shear loads with respect to those in the MSK model. Simulations should also be performed in the other planes of motion.

Lastly, Numalogics will be able to use this workflow to answer their research questions, by modifying the material properties of instrumented vertebrae, including instrumentation devices in

these vertebrae, and simulating functional ROM poses to evaluate the stress and load distributions throughout these medical devices in comparison to *in vitro* loading conditions.

REFERENCES

[1] I. Urits *et al.*, "Low Back Pain, a Comprehensive Review: Pathophysiology, Diagnosis, and Treatment," *Curr. Pain Headache Rep.*, vol. 23, no. 3, p. 23, Mar. 2019, doi: 10.1007/s11916-019-0757-1.

[2] K. Majid and E. Truumees, "Epidemiology and Natural History of Low Back Pain," *Semin. Spine Surg.*, vol. 20, no. 2, pp. 87–92, Jun. 2008, doi: 10.1053/j.semss.2008.02.003.

[3] T. Videman, M. C. Battié, L. E. Gibbons, K. Maravilla, H. Manninen, and J. Kaprio, "Associations Between Back Pain History and Lumbar MRI Findings," *Spine*, vol. 28, no. 6, pp. 582–588, Mar. 2003, doi: 10.1097/01.BRS.0000049905.44466.73.

[4] G. T. Desmoulin, V. Pradhan, and T. E. Milner, "Mechanical Aspects of Intervertebral Disc Injury and Implications on Biomechanics," *Spine*, vol. 45, no. 8, p. E457, Apr. 2020, doi: 10.1097/BRS.0000000000003291.

[5] N. Newell, J. Little, A. Christou, M. Adams, C. Adam, and S. Masouros, "Biomechanics of the Human Intervertebral Disc: A Review of Testing Techniques and Results," *J. Mech. Behav. Biomed. Mater.*, vol. 69, pp. 420–434, May 2017, doi: 10.1016/j.jmbbm.2017.01.037.

[6] F. Wang, F. Cai, R. Shi, X.-H. Wang, and X.-T. Wu, "Aging and Age Related Stresses: A Senescence Mechanism of Intervertebral Disc Degeneration," *Osteoarthritis Cartilage*, vol. 24, no. 3, pp. 398–408, Mar. 2016, doi: 10.1016/j.joca.2015.09.019.

[7] K.-S. Shih, P.-W. Weng, S.-C. Lin, Y.-T. Chen, C.-K. Cheng, and C.-H. Lee, "Biomechanical Comparison Between Concentrated, Follower, and Muscular Loads of the Lumbar Column," *Comput. Methods Programs Biomed.*, vol. 135, pp. 209–218, Oct. 2016, doi: 10.1016/j.cmpb.2016.07.021.

[8] A. Nachemson and J. M. Morris, "In-vivo Measurements of Intradiscal Pressure: Discometry, A Method for the Determination of Pressure in the Lower Lumbar Discs," *JBJS*, vol. 46, no. 5, p. 1077, Jul. 1964.

[9] K. Sato, S. Kikuchi, and T. Yonezawa, "In-vivo Intradiscal Pressure Measurement in Healthy Individuals and in Patients With Ongoing Back Problems," *Spine*, vol. 24, no. 23, p. 2468, Dec. 1999.

[10] H. J. Wilke, P. Neef, M. Caimi, T. Hoogland, and L. E. Claes, "New In-Vivo Measurements of Pressures in the Intervertebral Disc in Daily Life," *Spine*, vol. 24, no. 8, pp. 755–762, Apr. 1999, doi: 10.1097/00007632-199904150-00005.

[11] A. Rohlmann *et al.*, "Monitoring the Load on a Telemeterised Vertebral Body Replacement for a Period of Up to 65 months," *Eur. Spine J.*, vol. 22, no. 11, pp. 2575–2581, Nov. 2013, doi: 10.1007/s00586-013-3057-1.

[12] M. Akhavanfar, A. Mir-Orefice, T. K. Uchida, and R. B. Graham, "An Enhanced Spine Model Validated for Simulating Dynamic Lifting Tasks in OpenSim," *Ann. Biomed. Eng.*, vol. 52, no. 2, pp. 259–269, Feb. 2024, doi: 10.1007/s10439-023-03368-x.

[13] T. Lerchl, K. Nispel, T. Baum, J. Bodden, V. Senner, and J. S. Kirschke, "Multibody Models of the Thoracolumbar Spine: A Review on Applications, Limitations, and Challenges," *Bioengineering*, vol. 10, no. 2, Art. no. 2, Feb. 2023, doi: 10.3390/bioengineering10020202.

[14] C.-I. López Gualdrón, Bravo Ibarra, Edna-Rocío, Murillo Bohórquez, Andrea-Patricia, and I. and Garnica Bohórquez, "Present and Future for Technologies to Develop Patient-Specific Medical Devices: A Systematic Review Approach," *Med. Devices Evid. Res.*, vol. 12, pp. 253–273, Aug. 2019, doi: 10.2147/MDER.S215947.

[15] B. Khuyagbaatar, K. Kim, and Y. H. Kim, “Recent Developments in Finite Element Analysis of the Lumbar Spine,” *Int. J. Precis. Eng. Manuf.*, vol. 25, no. 2, pp. 487–496, Feb. 2024, doi: 10.1007/s12541-023-00866-9.
[16] K. Nispel, T. Lerchl, V. Senner, and J. S. Kirschke, “Recent Advances in Coupled MBS and FEM Models of the Spine—A Review,” *Bioengineering*, vol. 10, no. 3, Art. no. 3, Mar. 2023, doi: 10.3390/bioengineering10030315.
[17] P. Khoddam-Khorasani, N. Arjmand, and A. Shirazi-Adl, “Trunk Hybrid Passive–Active Musculoskeletal Modeling to Determine the Detailed T12–S1 Response Under In-vivo Loads,” *Ann. Biomed. Eng.*, vol. 46, no. 11, pp. 1830–1843, Nov. 2018, doi: 10.1007/s10439-018-2078-7.
[18] R. K. Eastlack *et al.*, “Finite Element Analysis Comparing a PEEK Posterior Fixation Device Versus Pedicle Screws for Lumbar Fusion,” *J. Orthop. Surg.*, vol. 18, no. 1, p. 855, Nov. 2023, doi: 10.1186/s13018-023-04349-5.
[19] M. Driscoll, J.-M. Mac-Thiong, H. Labelle, M. Slivka, S. Stad, and S. Parent, “Biomechanical Assessment of Reduction Forces Measured During Scoliotic Instrumentation Using Two Different Screw Designs,” *Spine Deform.*, vol. 1, no. 2, pp. 94–101, Mar. 2013, doi: 10.1016/j.jspd.2013.01.004.
[20] J. Clin *et al.*, “Biomechanical Comparison of the Load-Sharing Capacity of High and Low Implant Density Constructs With Three Types of Pedicle Screws for the Instrumentation of Adolescent Idiopathic Scoliosis,” *Spine Deform.*, vol. 7, no. 1, pp. 2–10, Jan. 2019, doi: 10.1016/j.jspd.2018.06.007.
[21] F. Galbusera, “Chapter 1 - The Spine: Its Evolution, Function, and Shape,” in *Biomechanics of the Spine*, F. Galbusera and H.-J. Wilke, Eds., Academic Press, 2018, pp. 3–9. doi: 10.1016/B978-0-12-812851-0.00001-X.
[22] R. Jonas and H.-J. Wilke, “Chapter 2 - The Cervical Spine,” in *Biomechanics of the Spine*, F. Galbusera and H.-J. Wilke, Eds., Academic Press, 2018, pp. 11–34. doi: 10.1016/B978-0-12-812851-0.00002-1.
[23] C. Liebsch and H.-J. Wilke, “Chapter 3 - Basic Biomechanics of the Thoracic Spine and Rib Cage,” in *Biomechanics of the Spine*, F. Galbusera and H.-J. Wilke, Eds., Academic Press, 2018, pp. 35–50. doi: 10.1016/B978-0-12-812851-0.00003-3.
[24] H.-J. Wilke and D. Volkheimer, “Chapter 4 - Basic Biomechanics of the Lumbar Spine,” in *Biomechanics of the Spine*, F. Galbusera and H.-J. Wilke, Eds., Academic Press, 2018, pp. 51–67. doi: 10.1016/B978-0-12-812851-0.00004-5.
[25] I. A. F. Stokes and M. Gardner-Morse, “A Database of Lumbar Spinal Mechanical Behavior for Validation of Spinal Analytical Models,” *J. Biomech.*, vol. 49, no. 5, pp. 780–785, Mar. 2016, doi: 10.1016/j.jbiomech.2016.01.035.
[26] M. M. Panjabi, T. R. Oxland, I. Yamamoto, and J. J. Crisco, “Mechanical Behavior of the Human Lumbar and Lumbosacral Spine as Shown by Three-Dimensional Load-Displacement Curves.,” *JBJS*, vol. 76, no. 3, p. 413, Mar. 1994.
[27] A. Malandrino, “Chapter 6 - Intervertebral Disc,” in *Biomechanics of the Spine*, F. Galbusera and H.-J. Wilke, Eds., Academic Press, 2018, pp. 89–103. doi: 10.1016/B978-0-12-812851-0.00006-9.
[28] “Cervical Spinal Joints,” Learn Muscles. Accessed: Jun. 27, 2025. [Online]. Available: https://learnmuscles.com/blog/2017/08/01/cervical-spinal-joints/

[29] T. Toumanidou, “Chapter 9 - Spinal Muscles,” in *Biomechanics of the Spine*, F. Galbusera and H.-J. Wilke, Eds., Academic Press, 2018, pp. 141–166. doi: 10.1016/B978-0-12-812851-0.00009-4.
[30] C. Muir, “The Anatomy Of Your Abdominal Muscles,” Caliber Fitness. Accessed: Jun. 27, 2025. [Online]. Available: https://caliberstrong.com/blog/abdominal-muscles/
[31] “Posterior Triangle of the Neck - Subdivisions - TeachMeAnatomy.” Accessed: Jun. 27, 2025. [Online]. Available: https://teachmeanatomy.info/neck/areas/posterior-triangle/
[32] “Longus colli muscle,” *Wikipedia*. May 02, 2024. Accessed: Jun. 27, 2025. [Online]. Available: https://en.wikipedia.org/w/index.php?title=Longus_colli_muscle&oldid=1221883297
[33] M. Christophy, N. A. Faruk Senan, J. C. Lotz, and O. M. O’Reilly, “A Musculoskeletal Model for the Lumbar Spine,” *Biomech. Model. Mechanobiol.*, vol. 11, no. 1, pp. 19–34, Jan. 2012, doi: 10.1007/s10237-011-0290-6.
[34] K.-S. Han, T. Zander, W. R. Taylor, and A. Rohlmann, “An Enhanced and Validated Generic Thoraco-Lumbar Spine Model for Prediction of Muscle Forces,” *Med. Eng. Phys.*, vol. 34, no. 6, pp. 709–716, Jul. 2012, doi: 10.1016/j.medengphy.2011.09.014.
[35] A. G. Bruno, M. L. Bouxsein, and D. E. Anderson, “Development and Validation of a Musculoskeletal Model of the Fully Articulated Thoracolumbar Spine and Rib Cage,” *J. Biomech. Eng.*, vol. 137, no. 8, p. 081003, Aug. 2015, doi: 10.1115/1.4030408.
[36] M. E. Raabe and A. M. W. Chaudhari, “An Investigation of Jogging Biomechanics using the Full-Body Lumbar Spine Model: Model Development and Validation,” *J. Biomech.*, vol. 49, no. 7, pp. 1238–1243, May 2016, doi: 10.1016/j.jbiomech.2016.02.046.
[37] C. D. Favier, M. E. Finnegan, R. A. Quest, L. Honeyfield, A. H. McGregor, and A. T. M. Phillips, “An Open-Source Musculoskeletal Model of the Lumbar Spine and Lower Limbs: A Validation for Movements of the Lumbar Spine,” *Comput. Methods Biomech. Biomed. Engin.*, vol. 24, no. 12, pp. 1310–1325, Oct. 2021, doi: 10.1080/10255842.2021.1886284.
[38] M. Senteler, Weisse, Bernhard, Rothenfluh, Dominique A., and J. G. and Snedeker, “Intervertebral Reaction Force Prediction Using an Enhanced Assembly of OpenSim Models,” *Comput. Methods Biomech. Biomed. Engin.*, vol. 19, no. 5, pp. 538–548, Apr. 2016, doi: 10.1080/10255842.2015.1043906.
[39] X. Meng, A. G. Bruno, B. Cheng, W. Wang, M. L. Bouxsein, and D. E. Anderson, “Incorporating Six Degree-of-Freedom Intervertebral Joint Stiffness in a Lumbar Spine Musculoskeletal Model-Method and Performance in Flexed Postures,” *J. Biomech. Eng.*, vol. 137, no. 10, p. 101008, Oct. 2015, doi: 10.1115/1.4031417.
[40] D. Ignasiak, S. Dendorfer, and S. J. Ferguson, “Thoracolumbar Spine Model with Articulated Ribcage for the Prediction of Dynamic Spinal Loading,” *J. Biomech.*, vol. 49, no. 6, pp. 959–966, Apr. 2016, doi: 10.1016/j.jbiomech.2015.10.010.
[41] W. Wang, D. Wang, F. De Groote, L. Scheys, and I. Jonkers, “Implementation of Physiological Functional Spinal Units in a Rigid-Body Model of the Thoracolumbar Spine,” *J. Biomech.*, vol. 98, p. 109437, Jan. 2020, doi: 10.1016/j.jbiomech.2019.109437.
[42] A. V. Hill, “The Heat of Shortening and the Dynamic Constants of Muscle,” *Proc. R. Soc. Lond. Ser. B - Biol. Sci.*, vol. 126, no. 843, pp. 136–195, Jan. 1997, doi: 10.1098/rspb.1938.0050.
[43] F. E. Zajac, “Muscle and Tendon: Properties, Models, Scaling, and Application to Biomechanics and Motor Control,” *Crit. Rev. Biomed. Eng.*, vol. 17, no. 4, pp. 359–411, 1989.

[44] T. K. Uchida, S. L. Delp, and D. Delp, *Biomechanics of Movement: The Science of Sports, Robotics, and Rehabilitation*. Cambridge, United States: MIT Press, 2021. Accessed: Mar. 31, 2025. [Online]. Available: http://ebookcentral.proquest.com/lib/ottawa/detail.action?docID=6434343

[45] S. L. Delp *et al.*, "OpenSim: Open-Source Software to Create and Analyze Dynamic Simulations of Movement," *IEEE Trans. Biomed. Eng.*, vol. 54, no. 11, pp. 1940–1950, Nov. 2007, doi: 10.1109/TBME.2007.901024.

[46] M. Dreischarf, A. Shirazi-Adl, N. Arjmand, A. Rohlmann, and H. Schmidt, "Estimation of Loads on Human Lumbar Spine: A Review of In-Vivo and Computational Model Studies," *J. Biomech.*, vol. 49, no. 6, pp. 833–845, Apr. 2016, doi: 10.1016/j.jbiomech.2015.12.038.

[47] N. Arjmand and A. Shirazi-Adl, "Sensitivity of Kinematics-Based Model Predictions to Optimization Criteria in Static Lifting Tasks," *Med. Eng. Phys.*, vol. 28, no. 6, pp. 504–514, Jul. 2006, doi: 10.1016/j.medengphy.2005.10.001.

[48] E. Beaucage-Gauvreau *et al.*, "Validation of an OpenSim Full-Body Model with Detailed Lumbar Spine for Estimating Lower Lumbar Spine Loads During Symmetric and Asymmetric Lifting Tasks," *Comput. Methods Biomech. Biomed. Engin.*, vol. 22, no. 5, pp. 451–464, Apr. 2019, doi: 10.1080/10255842.2018.1564819.

[49] D. Ignasiak, S. J. Ferguson, and N. Arjmand, "A Rigid Thorax Assumption Affects Model Loading Predictions at the Upper but Not Lower Lumbar Levels," *J. Biomech.*, vol. 49, no. 13, pp. 3074–3078, Sep. 2016, doi: 10.1016/j.jbiomech.2016.07.006.

[50] A. G. Bruno *et al.*, "Incorporation of CT-Based Measurements of Trunk Anatomy into Subject-Specific Musculoskeletal Models of the Spine Influences Vertebral Loading predictions," *J. Orthop. Res.*, vol. 35, no. 10, pp. 2164–2173, 2017, doi: 10.1002/jor.23524.

[51] S. Schmid, K. A. Burkhart, B. T. Allaire, D. Grindle, and D. E. Anderson, "Musculoskeletal Full-Body Models Including a Detailed Thoracolumbar Spine for Children and Adolescents Aged 6–18 Years," *J. Biomech.*, vol. 102, p. 109305, Mar. 2020, doi: 10.1016/j.jbiomech.2019.07.049.

[52] J. J. Banks, M. M. Alemi, B. T. Allaire, A. C. Lynch, M. L. Bouxsein, and D. E. Anderson, "Using Static Postures to Estimate Spinal Loading During Dynamic Lifts with Participant-Specific Thoracolumbar Musculoskeletal Models," *Appl. Ergon.*, vol. 106, p. 103869, Jan. 2023, doi: 10.1016/j.apergo.2022.103869.

[53] J. A. Actis, J. D. Honegger, D. H. Gates, A. J. Petrella, L. A. Nolasco, and A. K. Silverman, "Validation of Lumbar Spine Loading from a Musculoskeletal Model Including the Lower Limbs and Lumbar Spine," *J. Biomech.*, vol. 68, pp. 107–114, Feb. 2018, doi: 10.1016/j.jbiomech.2017.12.001.

[54] A. Bergmark, "Stability of the Lumbar Spine," *Acta Orthop.*, pp. 1–54, Jan. 1989, doi: 10.3109/17453678909154177.

[55] F. Ghezelbash, A. Shirazi-Adl, M. Sharifi, N. Arjmand, and B. Bazrgari, "Chapter 4 - Computational Stability of Human Musculoskeletal Systems," in *Digital Human Modeling and Medicine*, G. Paul and M. Hamdy Doweidar, Eds., Academic Press, 2023, pp. 85–105. doi: 10.1016/B978-0-12-823913-1.00025-7.

[56] J. J. Crisco and M. M. Panjabi, "The Intersegmental and Multisegmental Muscles of the Lumbar Spine. A Biomechanical Model Comparing Lateral Stabilizing Potential," *Spine*, vol. 16, no. 7, pp. 793–799, Jul. 1991, doi: 10.1097/00007632-199107000-00018.

[57] J. Cholewicki and S. McGill, “Mechanical Stability of the In-Vivo Lumbar Spine: Implications for Injury and Chronic Low Back Pain,” *Clin. Biomech.*, vol. 11, no. 1, pp. 1–15, Jan. 1996, doi: 10.1016/0268-0033(95)00035-6.
[58] M. G. Gardner-Morse and I. A. F. Stokes, “The Effects of Abdominal Muscle Coactivation on Lumbar Spine Stability,” *Spine*, vol. 23, no. 1, p. 86, Jan. 1998.
[59] S. H. M. Brown and J. R. Potvin, “Constraining Spine Stability Levels in an Optimization Model Leads to the Prediction of Trunk Muscle Cocontraction and Improved Spine Compression Force Estimates,” *J. Biomech.*, vol. 38, no. 4, pp. 745–754, Apr. 2005, doi: 10.1016/j.jbiomech.2004.05.011.
[60] M. Hajihosseinali, N. Arjmand, A. Shirazi-Adl, F. Farahmand, and M. S. Ghiasi, “A Novel Stability and Kinematics-Driven Trunk Biomechanical Model to Estimate Muscle and Spinal Forces,” *Med. Eng. Phys.*, vol. 36, no. 10, pp. 1296–1304, Oct. 2014, doi: 10.1016/j.medengphy.2014.07.009.
[61] K. P. Granata and S. E. Wilson, “Trunk Posture and Spinal Stability,” *Clin. Biomech.*, vol. 16, no. 8, pp. 650–659, Oct. 2001, doi: 10.1016/S0268-0033(01)00064-X.
[62] J. R. Potvin and S. H. M. Brown, “An Equation to Calculate Individual Muscle Contributions to Joint Stability,” *J. Biomech.*, vol. 38, no. 5, pp. 973–980, May 2005, doi: 10.1016/j.jbiomech.2004.06.004.
[63] M. H. Akhavanfar, S. C. E. Brandon, S. H. M. Brown, and R. B. Graham, “Development of a Novel MATLAB-Based Framework for Implementing Mechanical Joint Stability Constraints within OpenSim Musculoskeletal Models,” *J. Biomech.*, vol. 91, pp. 61–68, Jun. 2019, doi: 10.1016/j.jbiomech.2019.05.007.
[64] J. M. Barrett *et al.*, “Head Supported Mass, Moment of Inertia, Neck Loads and Stability: A Simulation Study,” *J. Biomech.*, vol. 146, p. 111416, Jan. 2023, doi: 10.1016/j.jbiomech.2022.111416.
[65] A. Welch-Phillips, D. Gibbons, D. P. Ahern, and J. S. Butler, “What Is Finite Element Analysis?,” *Clin. Spine Surg.*, vol. 33, no. 8, pp. 323–324, Oct. 2020, doi: 10.1097/BSD.0000000000001050.
[66] P. A. Kramer, A. G. Hammerberg, and A. D. Sylvester, “Modeling the Spine Using Finite Element Models: Considerations and Cautions,” in *Spinal Evolution: Morphology, Function, and Pathology of the Spine in Hominoid Evolution*, E. Been, A. Gómez-Olivencia, and P. Ann Kramer, Eds., Cham: Springer International Publishing, 2019, pp. 387–400. doi: 10.1007/978-3-030-19349-2_17.
[67] V. Sciortino, S. Pasta, T. Ingrassia, and D. Cerniglia, “On the Finite Element Modeling of the Lumbar Spine: A Schematic Review,” *Appl. Sci.*, vol. 13, no. 2, Art. no. 2, Jan. 2023, doi: 10.3390/app13020958.
[68] H.-J. Wilke, K. Wenger, and L. Claes, “Testing Criteria for Spinal Implants: Recommendations for the Standardization of In Vitro Stability Testing of Spinal Implants,” *Eur. Spine J.*, vol. 7, no. 2, pp. 148–154, May 1998, doi: 10.1007/s005860050045.
[69] S. Naoum, A. V. Vasiliadis, C. Koutserimpas, N. Mylonakis, M. Kotsapas, and K. Katakalos, “Finite Element Method for the Evaluation of the Human Spine: A Literature Overview,” *J. Funct. Biomater.*, vol. 12, no. 3, Art. no. 3, Sep. 2021, doi: 10.3390/jfb12030043.
[70] A. G. Patwardhan, R. M. Havey, K. P. Meade, B. Lee, and B. Dunlap, “A Follower Load Increases the Load-Carrying Capacity of the Lumbar Spine in Compression,” *Spine*, vol. 24, no. 10, p. 1003, May 1999.

[71] A. Rohlmann, T. Zander, M. Rao, and G. Bergmann, “Applying a Follower Load Delivers Realistic Results for Simulating Standing,” *J. Biomech.*, vol. 42, no. 10, pp. 1520–1526, Jul. 2009, doi: 10.1016/j.jbiomech.2009.03.048.
[72] K. Kim, Y. H. Kim, and S. Lee, “Increase of Load-Carrying Capacity Under Follower Load Generated by Trunk Muscles in Lumbar Spine,” *Proc. Inst. Mech. Eng. Part H*, vol. 221, no. 3, pp. 229–235, Mar. 2007, doi: 10.1243/09544119JEIM229.
[73] K. Kim and Y. H. Kim, “Role of Trunk Muscles in Generating Follower Load in the Lumbar Spine of Neutral Standing Posture,” *J. Biomech. Eng.*, vol. 130, no. 041005, May 2008, doi: 10.1115/1.2907739.
[74] K.-S. Han, A. Rohlmann, S.-J. Yang, B. S. Kim, and T.-H. Lim, “Spinal Muscles can Create Compressive Follower Loads in the Lumbar Spine in a Neutral Standing Posture,” *Med. Eng. Phys.*, vol. 33, no. 4, pp. 472–478, May 2011, doi: 10.1016/j.medengphy.2010.11.014.
[75] M. Driscoll, J.-M. Mac-Thiong, H. Labelle, and S. Parent, “Development of a Detailed Volumetric Finite Element Model of the Spine to Simulate Surgical Correction of Spinal Deformities,” *BioMed Res. Int.*, vol. 2013, p. 931741, 2013, doi: 10.1155/2013/931741.
[76] E. Taleghani *et al.*, “Finite Element Assessment of a Disc-Replacement Implant for Treating Scoliotic Deformity,” *Clin. Biomech. Bristol Avon*, vol. 84, p. 105326, Apr. 2021, doi: 10.1016/j.clinbiomech.2021.105326.
[77] D. J. Polga *et al.*, “Measurement of In-vivo Intradiscal Pressure in Healthy Thoracic Intervertebral Discs,” *Spine*, vol. 29, no. 12, p. 1320, Jun. 2004, doi: 10.1097/01.BRS.0000127179.13271.78.
[78] J. Henao, Aubin, Carl-Éric, Labelle, Hubert, and P.-J. and Arnoux, “Patient-Specific Finite Element Model of the Spine and Spinal Cord to Assess the Neurological Impact of Scoliosis Correction: Preliminary Application on Two Cases With and Without Intraoperative Neurological Complications,” *Comput. Methods Biomech. Biomed. Engin.*, vol. 19, no. 8, pp. 901–910, Jun. 2016, doi: 10.1080/10255842.2015.1075010.
[79] A. Kiefer, A. Shirazi-Adl, and M. Parnianpour, “Synergy of the Human Spine in Neutral Postures,” *Eur. Spine J.*, vol. 7, no. 6, pp. 471–479, Dec. 1998, doi: 10.1007/s005860050110.
[80] A. Shirazi-Adl, S. Sadouk, M. Parnianpour, D. Pop, and M. El-Rich, “Muscle Force Evaluation and the Role of Posture in Human Lumbar Spine Under Compression,” *Eur. Spine J.*, vol. 11, no. 6, pp. 519–526, Dec. 2002, doi: 10.1007/s00586-002-0397-7.
[81] N. Arjmand and A. Shirazi-Adl, “Biomechanics of Changes in Lumbar Posture in Static Lifting,” *Spine*, vol. 30, no. 23, p. 2637, Dec. 2005, doi: 10.1097/01.brs.0000187907.02910.4f.
[82] F. Azari, N. Arjmand, A. Shirazi-Adl, and T. Rahimi-Moghaddam, “A Combined Passive and Active Musculoskeletal Model Study to Estimate L4-L5 Load Sharing,” *J. Biomech.*, vol. 70, pp. 157–165, Mar. 2018, doi: 10.1016/j.jbiomech.2017.04.026.
[83] M. A. Rajaee, N. Arjmand, and A. Shirazi-Adl, “A Novel Coupled Musculoskeletal Finite Element Model of the Spine – Critical Evaluation of Trunk Models in Some Tasks,” *J. Biomech.*, vol. 119, p. 110331, Apr. 2021, doi: 10.1016/j.jbiomech.2021.110331.
[84] J. D. Honegger, J. A. Actis, D. H. Gates, A. K. Silverman, A. H. Munson, and A. J. Petrella, “Development of a Multiscale Model of the Human Lumbar Spine for Investigation of Tissue Loads in People With and Without a Transtibial Amputation During Sit-To-Stand,” *Biomech. Model. Mechanobiol.*, vol. 20, no. 1, pp. 339–358, Feb. 2021, doi: 10.1007/s10237-020-01389-2.

[85] M. Panico, T. Bassani, T. M. T. Villa, and F. Galbusera, “The Simulation of Muscles Forces Increases the Stresses in Lumbar Fixation Implants with Respect to Pure Moment Loading,” *Front. Bioeng. Biotechnol.*, vol. 9, Nov. 2021, doi: 10.3389/fbioe.2021.745703.
[86] D. G. Thelen, “Adjustment of Muscle Mechanics Model Parameters to Simulate Dynamic Contractions in Older Adults,” *J. Biomech. Eng.*, vol. 125, no. 1, pp. 70–77, Feb. 2003, doi: 10.1115/1.1531112.
[87] J. L. Hicks, T. K. Uchida, A. Seth, A. Rajagopal, and S. L. Delp, “Is My Model Good Enough? Best Practices for Verification and Validation of Musculoskeletal Models and Simulations of Movement,” *J. Biomech. Eng.*, vol. 137, no. 2, p. 020905, Feb. 2015, doi: 10.1115/1.4029304.
[88] V. F. Cassola, F. M. Milian, R. Kramer, C. A. B. de Oliveira Lira, and H. J. Khoury, “Standing Adult Human Phantoms Based on 10th, 50th and 90th Mass and Height Percentiles of Male and Female Caucasian Populations,” *Phys. Med. Biol.*, vol. 56, no. 13, p. 3749, May 2011, doi: 10.1088/0031-9155/56/13/002.
[89] P. Schober, C. Boer, and L. A. Schwarte, “Correlation Coefficients: Appropriate Use and Interpretation,” *Anesth. Analg.*, vol. 126, no. 5, p. 1763, May 2018, doi: 10.1213/ANE.0000000000002864.
[90] D. G. Mayer and D. G. Butler, “Statistical Validation,” *Ecol. Model.*, vol. 68, no. 1, pp. 21–32, Jul. 1993, doi: 10.1016/0304-3800(93)90105-2.
[91] T. Liu, K. Khalaf, S. Naserkhaki, and M. El-Rich, “Load-Sharing in the Lumbosacral Spine in Neutral Standing & Flexed Postures – A Combined Finite Element and Inverse Static Study,” *J. Biomech.*, vol. 70, pp. 43–50, Mar. 2018, doi: 10.1016/j.jbiomech.2017.10.033.
[92] M. M. Alemi, J. J. Banks, A. C. Lynch, B. T. Allaire, M. L. Bouxsein, and D. E. Anderson, “EMG Validation of a Subject-Specific Thoracolumbar Spine Musculoskeletal Model During Dynamic Activities in Older Adults,” *Ann. Biomed. Eng.*, vol. 51, no. 10, pp. 2313–2322, Oct. 2023, doi: 10.1007/s10439-023-03273-3.
[93] A. G. Patwardhan *et al.*, “Effect of Compressive Follower Preload on the Flexion–Extension Response of the Human Lumbar Spine,” *J. Orthop. Res.*, vol. 21, no. 3, pp. 540–546, 2003, doi: 10.1016/S0736-0266(02)00202-4.
[94] N. Arjmand and A. Shirazi-Adl, “Role of Intra-Abdominal Pressure in the Unloading and Stabilization of the Human Spine During Static Lifting Tasks,” *Eur. Spine J.*, vol. 15, no. 8, pp. 1265–1275, Aug. 2006, doi: 10.1007/s00586-005-0012-9.
[95] N. Arjmand, A. Shirazi-Adl, and B. Bazrgari, “Wrapping of Trunk Thoracic Extensor Muscles Influences Muscle Forces and Spinal Loads in Lifting Tasks,” *Clin. Biomech. Bristol Avon*, vol. 21, no. 7, pp. 668–675, Aug. 2006, doi: 10.1016/j.clinbiomech.2006.03.006.
[96] I. A. F. Stokes, M. G. Gardner-Morse, and S. M. Henry, “Intra-Abdominal Pressure and Abdominal Wall Muscular Function: Spinal Unloading Mechanism,” *Clin. Biomech.*, vol. 25, no. 9, pp. 859–866, Nov. 2010, doi: 10.1016/j.clinbiomech.2010.06.018.

Appendix A – FATLS Model Properties – Version I

The model used for version I of the simulation workflow had a total of 56 bodies, 51 rotational DOF, and 306 musculotendon actuators (Figure A.1). The bodies included consisted of the pelvis, sacrum, 5 lumbar vertebrae, 12 thoracic vertebrae, a lumped body for the head and neck, the sternum, the 12 pairs of ribs, and 11 bodies representing the abdomen. The rotational DOF of the model consisted of 3 rotational DOF for each of the 17 IVJs. The musculotendon actuators consisted of several fascicles representing all of the major muscle groups surrounding the spine. These included the psoas major, the erector spinae (iliocostalis, longissimus thoracis pars thoracis, and longissimus thoracis pars laborum), the abdominals (rectus abdominus, internal obliques, and external obliques), the multifidus, the quadratus laborum, and neck muscles (cervical erector spinae, cervical multifidus, splenius, scalenus, longus colli, semispinalis, and sternocleidomastoid). Lastly, the model included force actuators called rib actuators, which apply forces between adjacent ribs and between the ribs and the sternum to replicate the forces transmitted by costal cartilage.

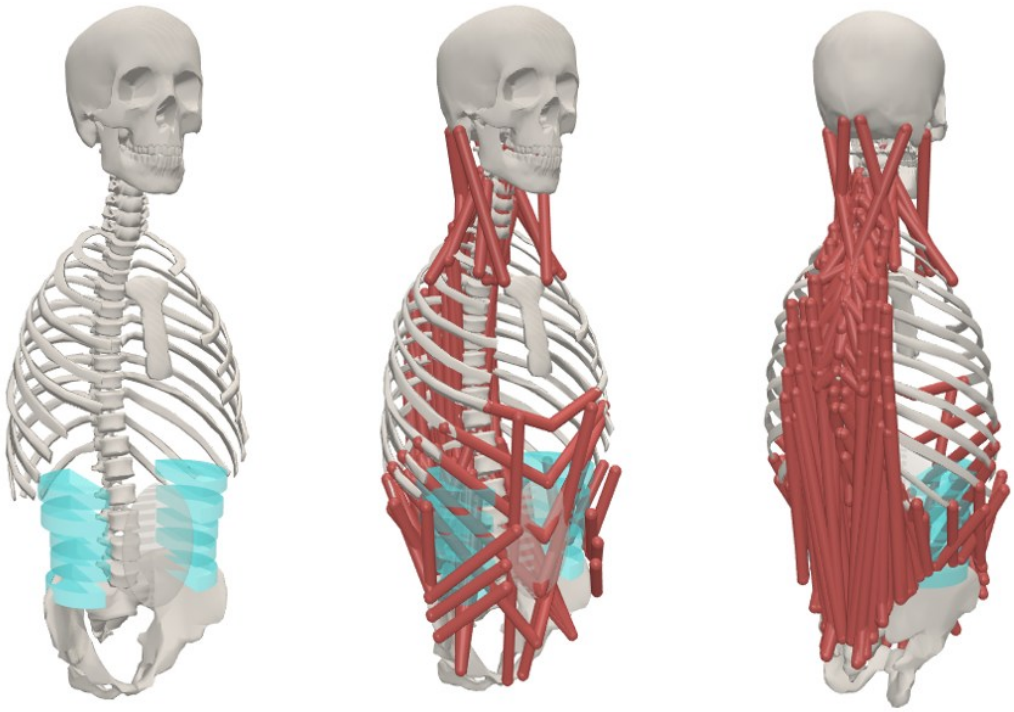

Figure A.1: Illustrations of the FATLS model used in version I of the workflow, featuring the bodies (left), the anterior muscles (middle), and the posterior muscles (right).

Appendix B – Motion Files

Table B.1: Intervertebral rotations for each static flexion pose between 0 and 100% ROM, where negative angles represent a forward flexion angle

		Intervertebral Rotation Angle (°)					
		0% ROM	**10% ROM**	**20% ROM**	**30% ROM**	**40% ROM**	**50% ROM**
IVJ	**L5S1**	0	-0.347	-0.687	-1.027	-1.353	-1.673
	L4L5	0	-0.74952	-1.48392	-2.21832	-2.92248	-3.61368
	L3L4	0	-1.0757	-2.1297	-3.1837	-4.1943	-5.1863
	L2L3	0	-1.2492	-2.4732	-3.6972	-4.8708	-6.0228
	L1L2	0	-1.5268	-3.0228	-4.5188	-5.9532	-7.3612
	T12L1	0	-0.7981	-1.5801	-2.3621	-3.1119	-3.8479
	T11T12	0	-0.7981	-1.5801	-2.3621	-3.1119	-3.8479
	T10T11	0	-0.5899	-1.1679	-1.7459	-2.3001	-2.8441
	T9T10	0	-0.40252	-0.79692	-1.19132	-1.56948	-1.94068
	T8T9	0	-0.40252	-0.79692	-1.19132	-1.56948	-1.94068
	T7T8	0	-0.40252	-0.79692	-1.19132	-1.56948	-1.94068
	T6T7	0	-0.33659	-0.66639	-0.99619	-1.31241	-1.62281
	T5T6	0	-0.27066	-0.53586	-0.80106	-1.05534	-1.30494
	T4T5	0	-0.27066	-0.53586	-0.80106	-1.05534	-1.30494
	T3T4	0	-0.27066	-0.53586	-0.80106	-1.05534	-1.30494
	T2T3	0	-0.27066	-0.53586	-0.80106	-1.05534	-1.30494
	T1T2	0	-0.27066	-0.53586	-0.80106	-1.05534	-1.30494

		Intervertebral Rotation Angle (°)				
		60% ROM	**70% ROM**	**80% ROM**	**90% ROM**	**100% ROM**
IVJ	**L5S1**	-1.972	-2.251	-2.496	-2.686	-2.808
	L4L5	-4.25952	-4.86216	-5.39136	-5.80176	-6.06528
	L3L4	-6.1132	-6.9781	-7.7376	-8.3266	-8.7048
	L2L3	-7.0992	-8.1036	-8.9856	-9.6696	-10.1088
	L1L2	-8.6768	-9.9044	-10.9824	-11.8184	-12.3552
	T12L1	-4.5356	-5.1773	-5.7408	-6.1778	-6.4584
	T11T12	-4.5356	-5.1773	-5.7408	-6.1778	-6.4584
	T10T11	-3.3524	-3.8267	-4.2432	-4.5662	-4.7736
	T9T10	-2.28752	-2.61116	-2.89536	-3.11576	-3.25728
	T8T9	-2.28752	-2.61116	-2.89536	-3.11576	-3.25728
	T7T8	-2.28752	-2.61116	-2.89536	-3.11576	-3.25728
	T6T7	-1.91284	-2.18347	-2.42112	-2.60542	-2.72376
	T5T6	-1.53816	-1.75578	-1.94688	-2.09508	-2.19024
	T4T5	-1.53816	-1.75578	-1.94688	-2.09508	-2.19024
	T3T4	-1.53816	-1.75578	-1.94688	-2.09508	-2.19024
	T2T3	-1.53816	-1.75578	-1.94688	-2.09508	-2.19024
	T1T2	-1.53816	-1.75578	-1.94688	-2.09508	-2.19024

Appendix C – Derivation of the Equation for Joint Moments in Ansys

In the co-simulation workflow, pure moment loads are applied at each IVJ, about the z-axis, representing the combined action of torques created by the mass properties of the bodies located above each joint, and coordinate actuators, when applicable.

To obtain the joint torques produced by mass properties, the script requires the ID results that are output from the SO or SCSO frameworks. The ID Tool in OpenSim estimates the net generalized forces (forces or torques) that produce the movement described in the motion file. With the FATLS model, the IVJs only have DOF in rotation, and only simulations of forward flexion, which are movements occurring in the sagittal plane, were simulated for this project. Therefore, only the ID results in rotation about the z-axis were of interest. Furthermore, all poses simulated were static, hence the equation of motion about the z-axis of a joint in rotation is of the following form:

$$\sum M = 0 \qquad \text{(Eq. C.1)}$$

where $\sum M$ is the sum of moments about a given joint. The moments acting on each joint are moments from passive stiffnesses, namely the joint bushings (M_{joint}), moments from gravity ($M_{gravity}$) and external moments ($M_{external}$), such as those produced by muscle forces and reserve actuators (Eq. C.2). The ID Tool explicitly calculates the external moments from muscle forces and reserve actuators, as the other moments are already known from information in the model file (Eq. C.3).

$$\sum M = 0 = M_{gravity} + M_{joint} + M_{external} \qquad \text{(Eq. C.2)}$$

$$M_{external} = ID\ (inverse\ dynamics\ result) \qquad \text{(Eq. C.3)}$$

The moments produced by gravity at a given joint can therefore be determined from the ID results and the moments produced by the joint bushings, which are obtained from the forces file output by the SO solver in OpenSim:

$$M_{gravity} = -ID - M_{joint} \quad \text{(Eq. C.4)}$$

Lastly, the moments produced by gravity can be combined with the torques produced by coordinate actuators (obtained from the forces file output by the SO solver in OpenSim) as a single resulting moment that is applied to each joint in the Ansys model ($M_{applied}$):

$$M_{applied} = M_{gravity} + M_{reserveAct} \quad \text{(Eq. C.5)}$$

$$M_{applied} = -ID - M_{joint} + M_{reserveAct} \quad \text{(Eq. C.6)}$$

In Ansys, M_{joint} is explicitly modeled through the definition of joint stiffnesses, and muscle forces are directly applied to the model as well. Thus, the torques acting at each joint are applied to the Ansys model to match those of the OpenSim model.

Appendix D – Detailed Schematic of Simulation Steps

Figure D.1 presents a schematic of the simulation steps performed in version I. In step 1, a SO framework is employed to estimate muscle forces required to satisfy equilibrium equations for a static flexion pose in a MSK model, using OpenSim. Gravity loads from body masses are also computed for the given static pose. In steps 2 and 3, the geometry of the model is defined in Ansys, followed by the definition of an identical model structure to the OpenSim model. This implies that the two models have identical geometry, joint definitions, stiffness properties, and muscle representations. In Ansys, the muscles are modeled as linear springs connecting the origin and insertion points. In step 4, outputs from the SO framework are used to define the loading conditions applied to the Ansys model. The loading conditions consist of the muscle forces, joint moments (from gravity loads and from coordinate actuators), and FLs, which are the axial compressive load components of the gravity loads. These loading conditions are applied to the model in a neutral position. In step 5, the FE simulation is performed. In applying the loading conditions simultaneously, the joint moments corresponding to the gravity loads in the flexed configuration are what drive the model displacement until static equilibrium is reached. Because the Ansys and OpenSim models are identical, the static equilibrium pose simulated in Ansys should correspond to the static flexion pose simulated in OpenSim in the SO framework.

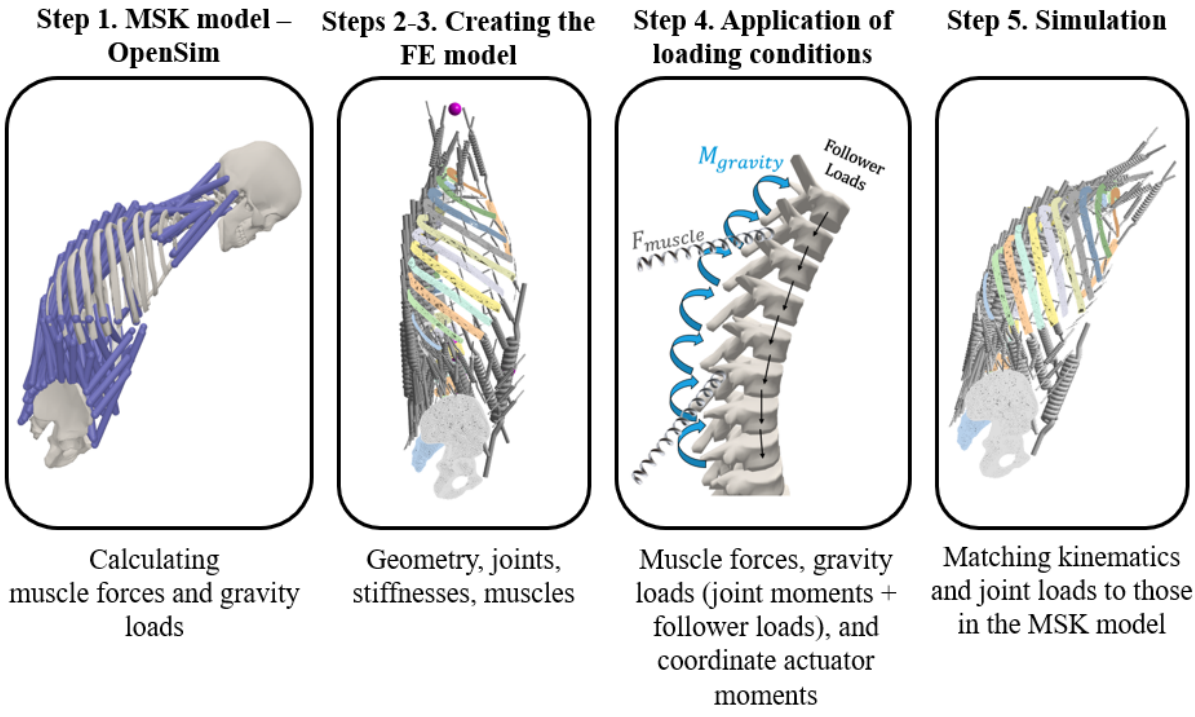

Figure D.1: Detailed schematic of the simulation steps for version I. Step 1: Calculation of muscle forces and gravity loads. Steps 2-3: Definition of an identical model geometry and structure in Ansys. Step 4: Application of the loading conditions to the Ansys model. Step 5: Performing the simulation.

Appendix E – FATLS Model Properties – Version II

The model used for version II of the simulation workflow had a total of 56 bodies, 51 rotational DOF, and 458 musculotendon actuators (Figure E.1). The bodies and rotational DOF included in the model are identical to those presented in Appendix A. The musculotendon actuators included those listed in Appendix A, in addition to the internal and external intercostal muscles. For version II of the simulation workflow, the rib actuators mentioned in Appendix A were removed from the model.

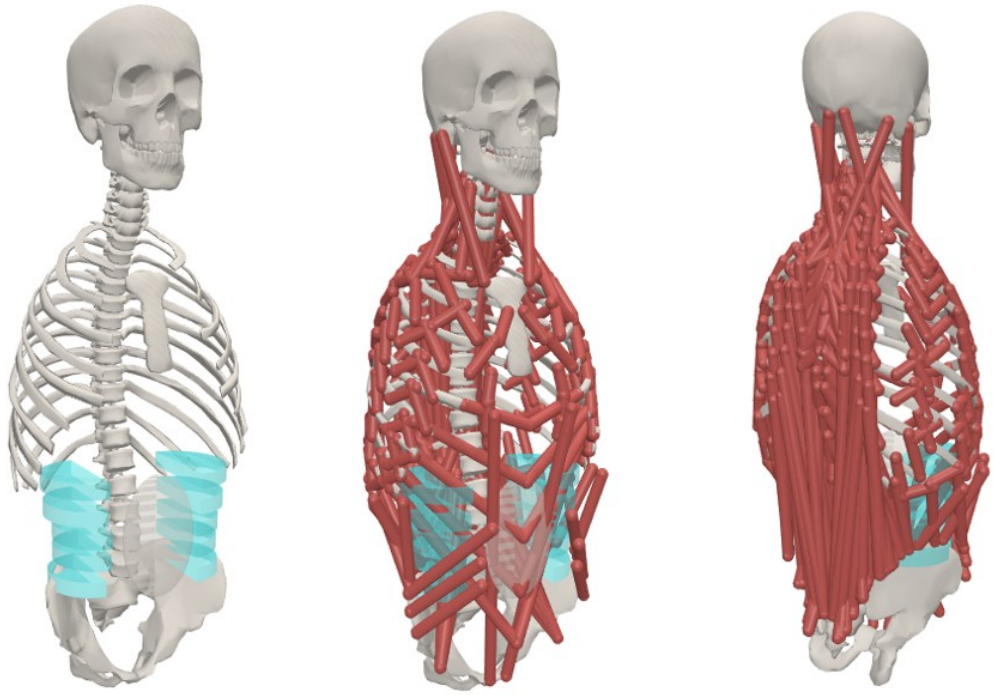

Figure E.1: Illustrations of the FATLS model used in version II of the workflow, featuring the bodies (left), the anterior muscles (middle), and the posterior muscles (right).

Appendix F – Automated Scaling of the Model Geometry in Ansys

In OpenSim, the Scale Tool can be used to scale a generic model to fit a specific individual, based on manual scaling factors or on marker data from laboratory experiments. The geometry that was imported in Ansys SpaceClaim is the geometry of the generic FATLS model. To produce co-simulations using a scaled model, it is necessary to scale the geometry in SpaceClaim as well. A function was added to the automated scripting workflow used in the FE modeling framework to scale the model when it is required to do so. The following paragraphs will elaborate on the steps that are taken to scale the model geometry in SpaceClaim using the scripting workflow.

When a model is scaled in OpenSim, the model file will contain information on its scaling. First, the model file states the scaling factors that were used to scale the geometry of each body in the x, y, and z directions. Second, the positions of the joints and of the COM of each body are adjusted from those in the generic model file. Third, the geometry representing each body is repositioned to reflect changes in joint centers and body COM positions. It should be noted that the COMs of the bodies defined in the model file do not necessarily correspond to the centroids of the geometries representing said bodies. For instance, in the FATLS model, the mass properties of the ribcage were partitioned between the vertebral bodies and sacrum, hence the COM of each vertebra is situated anterior to its geometrical body. This means that the positions of the body COMs in the scaled model file cannot be used to reposition the geometry in SpaceClaim. Instead, we must consider that the centroid of the geometry representing a body, expressed in the CS of the parent joint, is proportional to the scaling factors for that body. For example, the position of the centroid of the geometry used to illustrate T11, expressed in the CS of the joint T11T12, will be proportional to the scaling factors of T11 in x, y, and z.

When building a scaled version of the FATLS model in Ansys, information from the generic model is required, such as the definitions of the joint CSs. In Workbench, the user must set up two Static Structural Analysis Systems. The first one is used to perform the Read Geometry and Joints functions of the script (see Chapter 3.1.4), so that all joint CSs are defined for the generic model. In the second analysis system, the user must load the generic model geometry from SpaceClaim and run the model building script, as described in Chapter 3.1.4, with the scaled model file as an input. The Read Geometry and Joints functions are run, where the CSs of the joints for the scaled

model are defined. Then, a Geometry Update function is performed, which scales the SpaceClaim geometry according to information from both the generic model and the scaled model file, through a series of steps. The steps followed by the Geometry Update function will be explained with the scaling of the T11 geometry as an example.

From the generic model that was defined in the first Static Structural Analysis System, the script extracts the global transformations of each joint CS.

$$Generic\ IV\ Joint_g = \begin{bmatrix} | & | & | & P_x \\ X & Y & Z & P_y \\ | & | & | & P_z \\ 0 & 0 & 0 & 1 \end{bmatrix} \quad \text{(Eq. F.1)}$$

where columns 1 to 3 are the direction vectors of the x, y, and z axes of the joint CS, and column 4 (rows 1 to 3) is the (x, y, z) coordinates of the origin of the joint CS. The fourth row of the transformation matrix is set to (0, 0, 0, 1). The subscript *g* indicates that the CS is expressed in the global space. Taking the T11T12 joint as an example, its transformation matrix is defined, in the global reference system, and in metres, as

$$Generic\ T11T12_g = \begin{bmatrix} 0.96126 & -0.27563 & 0 & -0.041897 \\ 0.27563 & 0.96126 & 0 & 0.30846 \\ 0 & 0 & 1 & 0 \\ 0 & 0 & 0 & 1 \end{bmatrix} \quad \text{(Eq. F.2)}$$

From the generic model geometry defined in SpaceClaim, the script extracts the global position of the geometry centroid for T11 as

$$Generic\ T11_g = \begin{bmatrix} -0.05526 \\ 0.31872 \\ 0 \\ 1 \end{bmatrix} \quad \text{(Eq. F.3)}$$

where the first 3 rows are the x, y, and z coordinates of the centroid. To find the position of the T11 centroid expressed in the CS of the T11T12 joint, the script multiplies the inverse of $Generic\ T11T12_g$ with $Generic\ T11_g$:

$$Generic\ T11_l = \begin{bmatrix} 0.96126 & -0.27563 & 0 & -0.041897 \\ 0.27563 & 0.96126 & 0 & 0.30846 \\ 0 & 0 & 1 & 0 \\ 0 & 0 & 0 & 1 \end{bmatrix}^{-1} \begin{bmatrix} -0.05526 \\ 0.31872 \\ 0 \\ 1 \end{bmatrix} = \begin{bmatrix} -0.01 \\ 0.0135 \\ 0 \\ 1 \end{bmatrix}$$

(Eq. F.4)

where the subscript l is for "local" definition of the centroid coordinates, and the position of the T11 centroid in the T11T12 CS is $(-0.01, 0.0135, 0)$.

From the scaled model file, the script extracts the scaling factors for each body. For T11, the scaling factors in x, y, and z are

$$SF_{T11} = (1.022054, 1.076546, 1.19907)$$

The position of the T11 centroid, expressed in the T11T12 joint CS, is proportional to the scaling factors of T11. Therefore, by performing a dot product of the position of the T11 centroid in the T11T12 frame with the T11 scaling factors, we obtain

$$Scaled\ T11_l = \begin{bmatrix} -0.01 \\ 0.0135 \\ 0 \\ 1 \end{bmatrix} \cdot \begin{bmatrix} 1.022054 \\ 1.076546 \\ 1.19907 \\ 1 \end{bmatrix} = \begin{bmatrix} -0.01 \\ 0.0146 \\ 0 \\ 1 \end{bmatrix} \qquad \text{(Eq. F.5)}$$

where $Scaled\ T11_l$ is the position of the T11 centroid, expressed in the T11T12 joint of the scaled model.

Finally, the position of the scaled T11 centroid must be expressed in the global space so that the geometry of the vertebra may be repositioned correctly in space. Because, at this point, the script has already performed the Joints function for the scaled model, the joint CSs have already been defined. The transformation matrix for the T11T12 joint of the scaled model is defined as

$$Scaled\ T11T12_g = \begin{bmatrix} 0.96126 & -0.27563 & 0 & -0.066454 \\ 0.27563 & 0.96126 & 0 & 0.33447 \\ 0 & 0 & 1 & 0 \\ 0 & 0 & 0 & 1 \end{bmatrix} \qquad \text{(Eq. F.6)}$$

To find the global position of the T11 centroid, the script multiplies $Scaled\ T11T12_g$ with $Scaled\ T11_l$:

$$Scaled\ T11_g = \begin{bmatrix} 0.96126 & -0.27563 & 0 & -0.066454 \\ 0.27563 & 0.96126 & 0 & 0.33447 \\ 0 & 0 & 1 & 0 \\ 0 & 0 & 0 & 1 \end{bmatrix} \begin{bmatrix} -0.01 \\ 0.0146 \\ 0 \\ 1 \end{bmatrix} = \begin{bmatrix} -0.0801 \\ 0.3457 \\ 0 \\ 1 \end{bmatrix}$$

(Eq. F.7)

Therefore, the centroid of the T11 geometry must be repositioned to $(-0.0801, 0.3457, 0)\ m$.

The script performs these transformations for all the geometries included in the model, namely the pelvis, sacrum, vertebrae, ribs, and sternum. The updated SpaceClaim geometry is reloaded in Ansys Mechanical, replacing the generic model geometry. From this point on, the script execution is performed as was explained in Chapter 3.1.4, for the rest of the model definition and for performing simulations.